**Universidade de Brasília**

**Instituto de Geociências**

**Programa de Pós-Graduação em Geologia**

**Geologia Regional**

TESE DE DOUTORADO Nº 173

# EVOLUTION OF PARALLEL TO SUB-PARALLEL GRABENS USING ANALOGUE AND NUMERICAL MODELLING: EXAMPLE OF THE PIMENTA BUENO AND COLORADO GRABENS, PARECIS BASIN, BRAZIL

Magda Estrela Oliveira Rodrigues

Orientador:

Prof. Dr. George Sand Araújo Leão de França

Co-orientadores:

Prof. Dr. Reinhardt Adolfo Fuck

Prof. Dr. João Casal Duarte (FCUL)

Março, 2021

Ficha catalográfica elaborada automaticamente,
com os dados fornecidos pelo(a) autor(a)

RR696e

Rodrigues, Magda Estrela Oliveira
Evolution of parallel to sub-parallel grabens using analogue and numerical modelling: example of the Pimenta Bueno and Colorado grabens, Parecis Basin, Brazil / Magda Estrela Oliveira Rodrigues; orientador George Sand Araújo Leão de França; co-orientador Reinhardt Adolfo Fuck. -- Brasília, 2021.
164 p.

Tese (Doutorado - Doutorado em Geologia) -- Universidade de Brasília, 2021.

1. Analogue modelling. 2. Numerical modelling. 3. Initial stages of rifting. 4. Parecis Basin. 5. Parallel rifts. I. França, George Sand Araújo Leão de, orient. II. Fuck, Reinhardt Adolfo, co-orient. III. Título.

**Universidade de Brasília**

**Instituto de Geociências**

**Programa de Pós-Graduação em Geologia**

**Geologia Regional**

TESE DE DOUTORADO Nº 173

# EVOLUTION OF PARALLEL TO SUB-PARALLEL GRABENS USING ANALOGUE AND NUMERICAL MODELLING: EXAMPLE OF THE PIMENTA BUENO AND COLORADO GRABENS, PARECIS BASIN, BRAZIL

Magda Estrela Oliveira Rodrigues

Banca Examinadora:

Prof. Dr. George Sand Leão Araújo de França (orientador)

Prof. Dr. Victor Sacek – USP (titular externo)

Prof. Dr. Francisco Hilario Bezerra – UFRN (titular externo)

Prof. Dr. Elder Yokoyama – UnB (titular interno)

Março, 2021

**Universidade de Brasília**

**Instituto de Geociências**

**Programa de Pós-Graduação em Geologia**

**Geologia Regional**

TESE DE DOUTORADO Nº 173

# EVOLUTION OF PARALLEL TO SUB-PARALLEL GRABENS USING ANALOGUE AND NUMERICAL MODELLING: EXAMPLE OF THE PIMENTA BUENO AND COLORADO GRABENS, PARECIS BASIN, BRAZIL

Autora:

Magda Estrela Oliveira Rodrigues

Tese apresentada ao Programa de Pós-graduação em Geologia do Instituto de Geociências da Universidade de Brasília – UnB para obtenção do título de Doutor em Geologia.

Área de concentração: Geologia Regional

Banca Examinadora:

Prof. Dr. George Sand Leão Araújo de França (orientador)

Prof. Dr. Victor Sacek – USP (titular externo)

Prof. Dr. Francisco Hilario Bezerra – UFRN (titular externo)

Prof. Dr. Elder Yokoyama – UnB (titular interno)

Março, 2021

*“Isn't it splendid to think of all the things there are to find out about?*

*It just makes me glad to be alive - it's such an interesting world.*

*It wouldn't be half so interesting if we know all about everything, would it?*

*There'd be no scope for imagination then, would there?”*

*In Anne of Green Gables, by Lucy Maud Montgomery*

# ABSTRACT

Extensional structures such as rift systems, have been widely studied in the context of sedimentary basins. The study of structural traps in exploratory basins, by the oil industry, allowed the development of techniques such as analogue and numerical modelling. The aim of this study was to understand the initial stages of rifting in the context of an intracratonic basin, inspired by the example of the evolution of the Pimenta Bueno and Colorado grabens of the Parecis Basin, centre-west Brazil. These structures seem to have been developed from inherited structures from a previous orogenic event. Analogue and numerical modelling experiments were developed to study the initial stages of continental rifting, focusing on the formation of two parallel to sub-parallel rifts developed by the reactivation of inherited structures.

In the analogue modelling experiments, we used a sandbox apparatus to understand what the conditions in which two grabens were mutually interfered, and what were the resulting deformational patterns. Two sets of experiments were performed (set 1 and 2). In both sets the distance and geometry of two basal velocity discontinuities (VDs) was varied to represent reactivated inherited structures. In all experiments, a total extension of 3 cm (scaling to 12 km in nature) was applied to a 3 cm thick sand pack. In the 1$^{st}$ set of experiments (P-experiments), we systematically varied the distance between the VDs. In the other set (O and TJ experiments), we varied the angles between the VDs using different configurations. As a result, when the VDs were initially close (< 2 cm) the resulting grabens interfered while if the spacing between VDs is > 2cm, the grabens did not mutually interfere and developed independently. The prescription of VDs to the base of the sand pack always led to the formation of asymmetric grabens, except when the VDs were initially in contact. In the experiments with conjugate “triple-junction” grabens, the extension was shared between two independent asymmetric grabens when the VDs were at a certain distance from each other, and the formation of a wide graben when they became closer or intersected. In this case, the grabens were symmetric or asymmetric depending on the initial geometric configuration of the velocity discontinuities.

The numerical models were developed with the Underworld code to understand the effects of varying both the distance between inherited structures (seeds) and the assumed continental-crust rheological profiles (Crème Brûlée” vs. “Jelly Sandwich”). Three series of 2D numerical models were developed, where these variables were systematically varied. With these models, we discussed to what extent the twin rifts mutually interfered and whether one of the rifts

became dominant over the other. The results show that either the existence and distance of seeds nor the rheological crustal structure can individually explain the mechanics of early rifting geometries. The rifting patterns were recognized only when these effects were considered together. Also, it was observed that double riffing is expected when only one seed is present in the crust, or in the cases where there were no inherited weaknesses.

**Keywords:** Analogue modelling; Numerical modelling; Initial stages of rifting; Parecis Basin; Parallel rifts.

# RESUMO

As estruturas extensionais, como os sistemas de rifte, são amplamente estudadas no contexto de bacias sedimentares. Na indústria do petróleo o estudo de armadilhas estruturais em bacias de exploração permitiu o desenvolvimento e avanço de técnicas como a modelagem análoga e numérica. O objetivo deste estudo foi entender a evolução dos estágios iniciais de rifteamento em contexto de bacias intracratônicas, inspirado no exemplo da evolução dos grabens Pimenta Bueno e Colorado da Bacia dos Parecis, no centro-oeste do Brasil. O desenvolvimento dessas estruturas aparenta ter sido induzido por estruturas reativadas de um evento orogênico anterior. Foram realizados modelos análogos e numéricos para estudar os estágios iniciais de rifteamento continental, mais especificamente, a formação de dois riftes paralelos a sub-paralelos como consequência da reativação de estruturas herdadas.

Nos experimentos de modelagem análoga foi utilizado um aparato do tipo caixa de areia para entender em que condições os dois grabens interferem e quais os padrões de deformação resultantes. Foram executados dois *sets* experimentais (*set* 1 e 2). Em ambos se variaram a distância e geometria das *velocity discontinuities* (VDs), representando as estruturas herdadas reativadas. Em todos os experimentos foram prescritos 3 cm de extensão total (escalados na Natureza como 12 km) a um pacote de areia de 3 cm. No primeiro *set* (experimentos P) a distância entre as VDs foi variada sistematicamente. No segundo *set* (experimentos O e TJ) foram testadas diferentes configurações com a variação dos ângulos entre as VDs. Como resultado, quando as VDs estavam inicialmente próximas (< 2 cm), os grabens interferiram, e quando as VDs estavam mais distantes (> 2 cm), os grabens desenvolveram-se independentemente. A colocação das VDs na base do pacote de areia originou sempre grabens assimétricos, exceto quando as VDs estavam inicialmente em contato. Nos experimentos com os grabens conjugados em junção tríplice, a extensão foi partilhada entre dois grabens assimétricos e independentes quando as VDs estavam a uma certa distância uma da outra, e ocorreu formação de um graben largo e simétrico quando as VDs estavam próximas ou se intersectavam. Nesse caso, os grabens formados são simétricos ou assimétricos, dependendo da configuração geométrica inicial das VDs.

Os modelos numéricos foram desenvolvidos com o código *Underworld* para estudar os efeitos de variar tanto a distância entre as estruturas herdadas *(seeds)* como os perfis reológicos assumidos para a crosta continental (Crème Brûlée" vs. "Jelly Sandwich"). Foram

desenvolvidos três *sets* de experimentos onde esses parâmetros foram variados. Com base nesses modelos, discutimos até que ponto os riftes paralelos interferem, e se um dos riftes prevalece sob o outro. Os resultados mostraram que somente a existência de *seeds* ou dos perfis reológicos assumidos para a crosta continental, não conseguem explicar a mecânica das geometrias de início de rifteamento. Os padrões de rifteamento são somente reconhecidos quando estes fatores são considerados em conjunto. Além disso verifica-se que o rifteamento duplo é esperado quando uma só *seed* está presente na crosta, ou também quando não existe nenhuma heterogeneidade.

**Palavras-chave:** Modelagem análoga, Modelagem numérica, Estágios iniciais de rifteamento, Bacia dos Parecis, Riftes paralelos.

# AGRADECIMENTOS

Ao final deste capítulo alguns agradecimentos devem ser realizados a todas as pessoas e entidades que tornaram este projeto de pesquisa possível. Sou muito grata a todos e a todas as oportunidades que tive durante este percurso.

Inicialmente gostaria de agradecer aos meus orientadores.

Ao Professor Dr. George Sand França pela oportunidade em embarcar neste projeto de pesquisa, por todos os ensinamentos, confiança, encorajamento e apoio para a realização deste trabalho e para a minha formação como pesquisadora. Gostaria de agradecer por sempre encorajar a cooperação científica com outros pesquisadores, a participação em eventos científicos, e por sempre me ensinar tanto a mim como a todos os seus alunos, a importância da divulgação científica em tempos tão desafiantes para a ciência.

Ao Professor Dr. Reinhardt Adolfo Fuck, pela oportunidade, ensinamentos e apoio durante a pesquisa. As discussões sobre a geologia da Bacia dos Parecis foram essenciais para o desenvolvimento dos modelos análogos e numéricos.

Ao Professor Dr. João Duarte por ter aceitado em participar deste projeto de pesquisa e por me receber na Faculdade de Ciências da Universidade de Lisboa para a realização dos experimentos em modelagem análoga. Gostaria de agradecer por toda a ajuda e apoio para a realização do projeto e por me ter encorajado para o desenvolvimento dos modelos numéricos. Além disso, gostaria de agradecer todo o apoio por parte de toda a sua equipe de pesquisa e por toda a disponibilidade para discutir e conversar sobre os trabalhos. Essa cooperação sem dúvida foi essencial para o projeto e sou muito grata por isso!

Ao Programa de Pós-Graduação em Geologia, ao Instituto de Geociências e Universidade de Brasília pela oportunidade de poder ter ingressado no curso de Doutorado e ao Observatório Sismológico e todos os seus funcionários e Professores pela infraestrutura e todos os recursos disponibilizados para a realização da pesquisa.

Gostaria de agradecer à FAPDF e à CAPES pela bolsa de estudos de Doutorado. O presente trabalho foi realizado com apoio da Coordenação de Aperfeiçoamento de Pessoal de Nível Superior - Brasil (*CAPES*) - Código de Financiamento 001.

Ao Projeto de pesquisa Projeto Parecis (CNPq 456560/2014-9), “Estudos tectônicos da Bacia dos Parecis” e ao INCT-ET Estudos Tectônicos (CNPq, CAPES, FAPDF) pelo apoio financeiro para a realização do projeto, deslocações ao laboratório e na participação de eventos científicos.

Ao meu colega e amigo Afonso Gomes por me ter ajudado e realizado juntamente comigo todos os experimentos laboratoriais e por me ter dado todo o suporte na realização dos modelos numéricos, figuras e vídeos. Obrigada por toda a disponibilidade para me ajudar e discutir sobre os trabalhos. Sou extremamente grata por toda a ajuda e apoio!

Ao Professor Dr. Filipe Rosas, por também ter embarcado neste projeto e por todo apoio e conhecimento sobre a modelagem análoga e numérica. Obrigada por toda a disponibilidade e ajuda para o desenvolvimento dos trabalhos de modelagem análoga e numérica.

Ao colega e amigo Jaime Almeida por toda a disponibilidade e conhecimento partilhados sobre a modelagem numérica.

Gostaria de agradecer também a Ilísio Boaventura e Nuno Carmo pelo suporte e ajuda nos trabalhos laboratoriais.

Ao Professor Dr. Fernando César por me ter recebido no Laboratório de Modelamento Estrutural na UFRN para a realização dos experimentos iniciais desta pesquisa, por me ajudar no planeamento desses experimentos e na discussão dos resultados. Agradeço também a Marilia Venâncio e Ricardo Rodrigues pela ajuda no laboratório.

Gostaria de agradecer aos Professores do Programa de Pós-Graduação em Geologia, em especial às Professoras Dra. Rejane Cicerelli e Dra. Susanne Maciel. Ao Professor Dr. Elder Yokoyama por ter possibilitado a cooperação com os Professores da Faculdade de Ciências da Universidade de Lisboa.

Aos meus colegas e amigos do Observatório Sismológico Diogo Albuquerque, Cristobal Quispe e Chris Fianco, pela amizade e sempre boas discussões sobre as Geociências. A Eveline Sayão por toda a amizade, conversas e apoio, obrigada!

Aos meus amigos, por sempre estarem lá, mesmo longe ou perto, Ingrid Maciel, Isabel Sá, Manuel Reis, Nadja Ferraz e Gabriela Pereira.

Por fim, à minha família, ao Lucas, o meu companheiro da vida, aos meus pais, Paula e Eduardo e ao meu irmão Hugo por sempre me apoiarem! Amo-vos!

Muito obrigada a todos!

# TABLE OF CONTENTS

# LIST OF FIGURES

## CHAPTER 1

**CHAPTER 2**

**CHAPTER 3**



**CHAPTER 4**

**CHAPTER 5**

with a markedly symmetric configuration; B3: symmetric crustal break-up. C - RII-10 model (two rifting-seeds, 10 km apart). C1-C2: early (extensional) strain nucleation above both nearby seeds and formation of two (tectonically interfering) main grabens; C3: crustal (relatively wider) break-up is achieved through only one of the grabens, while the other is abandoned. An overall symmetric geometry is nevertheless preserved. D - RII-14 model (two rifting-seeds, 50 km apart). D1: early development of two individual, symmetric, main grabens, nucleated above each of the distant seeds; D2: one of the grabens begins to shut down while the other evolves to become a symmetric rift; D3: symmetric, single-rift, crustal break-up. All insets depict the (line drawing) interpretation of the main structures above the viscosity output, and the corresponding strain-rate output overlain by the velocity field. Yellow arrows: sites of strong (extensional) strain localization, rifting and eventual crustal break-up. White arrows: sites of rift waning and shutdown……...p.85

Figure 4. "Thick-Jelly Sandwich" RIII model results. A – RIII-15 (absence of rifting-seeds). A1: bulk extensional strain is accommodated by a pervasive delocalized fault pattern in the strong portion of the upper crust (UC), and by viscous homogenous stretching in the weak middle-crust layer. No faults/shear zones are localized in the strong top segment of the lower crust (LC); A2: continued fault localization in the strong UC renders a relatively larger distance between faults/shear zones (less pervasive distribution); A3: rifting is localized in the UC only at a relatively late stage. The underlying strong top portion of the LC is only mildly perturbed. B - RIII-16 model (single rifting-seed). B1: early extensional-strain nucleation above the LC rifting-seed marked by the formation of two UC main grabens. Note that the grabens are aligned atop each of the flanks of the seed-related LC rift; B2: strain localization in the previously formed UC grabens results in the formation of two main UC rifts. Simultaneously, the seed-related LC rift undergoes significant bulging and widening; B3: relative narrow crustal break-up configuration, expressing a significant amount of decoupling in the way through which extensional-strain is accommodated above and below the middle-crust weak layer. C - RIII-17 model (two rifting-seeds, 10 km apart). C1 to C3: evolution similar to the one depicted in B (RIII-16 model). The two closed seeds interfere and coalesce, exerting a rheological control on the evolving rift configuration similar to the one observed for the single rifting-seed case above. D - RIII-21 model (two rifting-seeds, 50 km apart). D1: early development of two UC graben-like structures above each of the two LC seed-related rifts; D2: the previously formed pairs of UC grabens evolve into well-defined rift structures, although only one in each pair eventually evolves to render UC break-up (while the other wanes and shuts down); D3: final, wide,

# LIST OF TABLES

## CHAPTER 1



## CHAPTER 2



## CHAPTER 4



## CHAPTER 5

# CHAPTER 1. INTRODUCTION

## 1.1. Presentation

In this document, are presented the results of the author's research on the early stages of rifting using the techniques of analogue and numerical modelling inspired by the development of the sub-parallel grabens of Pimenta Bueno and Colorado of the Parecis Basin. The research was developed in the Observatório Sismológico - Instituto de Geociências (SIS-IG), within the scope of the Programa de Pós-Graduação em Geologia (PPG) of the Universidade de Brasília (UnB). The laboratory experiments were developed in the Laboratório de Tectonofísica e Tectônica Experimental (LATTEX) of the Faculdade de Ciências da Universidade de Lisboa (FCUL) and Laboratório de Modelamento Estrutural (LME) of the Departamento de Geologia of the Universidade Federal do Rio Grande do Norte (UFRN) in collaboration with Dr. João Duarte, MSc. Afonso Gomes, Dr. Filipe Rosas and Dr. Fernando Alves da Silva. The numerical models were developed in collaboration with Dr. João Duarte, Dr. Filipe Rosas, MSc. Afonso Gomes and MSc. Jaime Almeida from FCUL.

This thesis is divided into six chapters, including two scientific papers (chapters 4 and 5). In this chapter, the geological problem approached during this research is introduced by explaining the motivations, aims of the study and a brief description on the methodology used for the development of the models. The different hypotheses for the geological-tectonic framework of the area of study (Parecis Basin) are described in chapter 2. Chapter 3 presents the state of the art of the techniques used in this study – analogue and numerical modelling, outlining their history and development. In the next chapter (Chapter 4) are the results from the analogue modelling experiments, displaying the 1$^{st}$ scientific paper, in order to understand the development of parallel, oblique and triple-junction grabens/rifts and correlate these with the initial development of the Parecis Basin and other similar structures. Chapter 5 contains the 2$^{nd}$ scientific paper and the results of the numerical modelling experiments developed with the Underworld code. In chapter 6 are the final considerations of this research.

## 1.2. Motivation

Geological and geophysical information, such as field work, gravity, seismic and seismological surveys, can be complemented by experimental laboratory and computational models using analogue and numerical modelling techniques. With these models, it is possible to study the nucleation, evolution, and tectonics of a determined geological structure (McClay et al., 2001).

Analogue and numerical modelling are tools that revealed to be especially important for simulating and understanding the development of geological structures. Through laboratory experiments in sandbox apparatus and computational experiments it is possible to conduct studies on the tectonic evolution of a geological area or a specific geological structure.

These techniques can be applied to the different areas of the geosciences, such as structural geology, tectonics, sedimentary processes, igneous intrusions, and salt tectonics. The application of these techniques to the study of sedimentary basins and to the oil industry allowed the development of new tools with the aim to extract the maximum of information of a determined structural model. Such structures are important to be studied through modelling to understand how they formed and developed, such as, for example hydrocarbon traps.

Using these techniques and inspired by the initial stages of development of two parallel grabens in the Parecis Basin – Pimenta Bueno and Colorado, it is possible to elaborate analogue and numerical models to understand how these specific and similar structures have developed. With these models, the most initial stages of continental rifting and the formation of parallel and sub-parallel grabens can be discussed, including comparing the results with the natural analogues. The analogue models are developed at a laboratory scale and the numerical models by using an open-source modelling code. In both cases, the models obey the relations of scale between the natural prototype (Parecis Basin and adjacent structures) and the analogue and numerical models, set by Hubbert (1937).

This research is included in the Universal-CNPq project "*Estudos tectônicos sobre a Bacia dos Parecis"*, coordinated by Professor Dr. George Sand França with the participation of Professor Dr. Reinhardt Fuck.

## 1.3. Parecis Basin

The Parecis Basin is located in Mato Grosso and Rondônia states in the centre-west of Brazil, with an area of approximately 500,000 km$^2$ (Siqueira, 1989; Fig. 1.1.). Although considered as a new frontier hydrocarbon exploration basin (Haeser, 2013), there are several hypotheses for its tectonic-stratigraphic evolution. Authors as Siqueira (1989), Braga and Siqueira (1996), Silva et al. (2003), Bahia et al. (2006, 2007) and Bahia (2007) consider the basin evolution as being of the IF/IS type (IF – interior rift – interior fracture produced by extension; IS – interior sag – interior depression caused by vertical movement), as in the Kingston et al. (1983) classification. On the other hand, recent research (e.g. Haeser, 2013; Haeser et al., 2014; Vasconcelos et al., 2014; Loureiro, 2016; Loureiro et al., 2017) consider that the basin includes a foreland component related to the Neoproterozoic Paraguay Fold Belt, therefore presenting a distinct stratigraphy from the previously established one. Although several studies (mainly geophysical) have been carried out to understand the basin's development, more geological data are still needed to better correlate the Parecis Basin infill with the Paraguay Belt stratigraphy (Santos and Flexor, 2013).

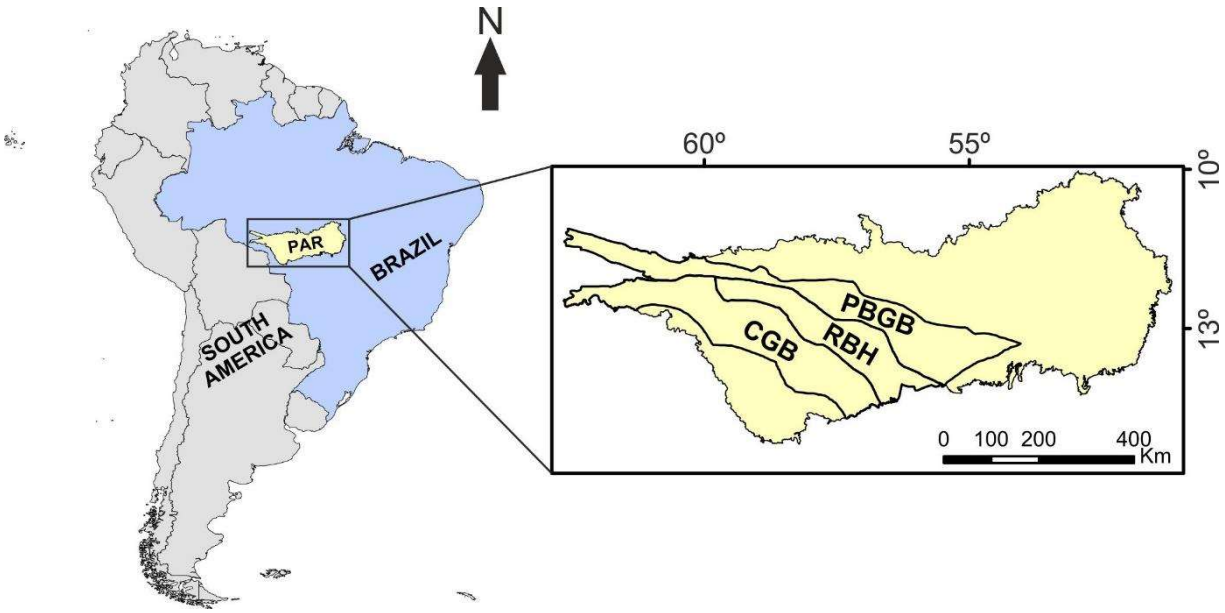


**Figure 1.1.** Location map of Parecis Basin. PAR – Parecis Basin; CGB – Colorado Graben; PBGB – Pimenta Bueno Graben; RBH – Rio Branco High. Source: shapefiles from Serviço Geológico do Brasil (CPRM).

## 1.4. Aim of the work

The aim of this research is to understand the influence of inherited structures in the initial stages of development of parallel and sub-parallel rifts in the context of continental rifting, inspired by the example of the Pimenta Bueno and Colorado grabens of the Parecis Basin, by using the techniques of analogue and numerical modelling. Other objectives of this research are:

- The assemblage of the analogue and numerical models by integrating the published results, discussions and interpretations of the natural analogue that inspired this research;
- Understanding the influence of varying the distance and geometry of inherited structures (analogue model velocity discontinuities, VDs, and numerical modelling seeds) and their influence on the development of parallel, oblique and triple-junction grabens;
- In the analogue models, understand what are the conditions in which two nearby forming grabens interfere and what are the resulting deformational patterns;
- Understanding how symmetric and asymmetric graben geometries are developed;
- In the numerical models, understand the effects of varying both the distance between the inherited structures (seeds) and the assumed rheological profiles;
- Appling and comparing the obtained models not only to the Colorado and Pimenta Bueno grabens, but also to other similar structures.

## 1.5. Methodology

In this research, the techniques of analogue and numerical modelling were used to investigate the initial stages of continental rifting by the reactivation of inherited structures. Both techniques were used to understand different aspects of rift distance and geometry (in the analogue models) and the effect of distance and rheology in the numerical models. The state of the art of these techniques is presented in Chapter 3 and the detailed methodologies are described in Chapters 4 and 5.

For assembling the analogue and numerical models, published geological/geophysical data on the Parecis Basin were used, more specifically, the reinterpretation of the Bahia et al. (2007) tectonic evolution by Loureiro (2016, Fig. 1.2), where the formation and development of the sub-parallel Colorado and Pimenta Bueno grabens is represented; the proposed depths for the basin grabens depocenters by the geophysical interpretations of Faria (2015) of ~12 km, and the proposed crustal thickness by receiver function studies in the Parecis Basin (~40 km) of Assumpção et al. (2013) and Albuquerque et al. (2017).

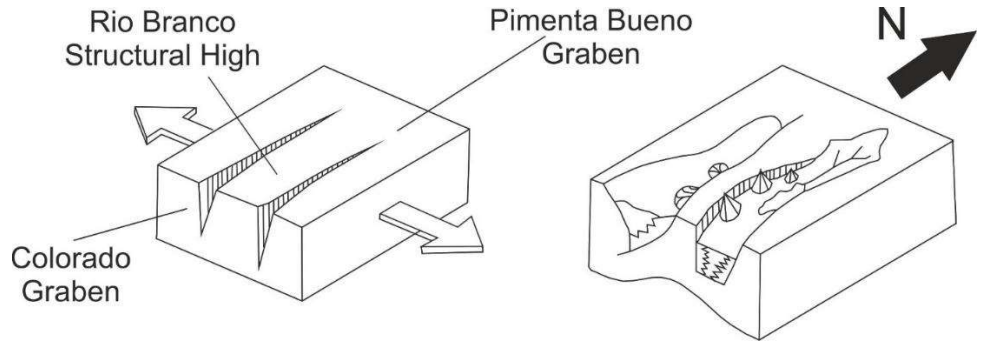


**Figure 1.2.** Initial stages of rifting of the Parecis Basin with the formation of the sub-parallel grabens of Colorado and Pimenta Bueno (Modified from Loureiro, 2016).

### 1.5.1. Analogue modelling experiments

In this research, we studied two sets of analogue modelling experiments (table 1.1). In the first set of experiments, the distance between two basal velocity discontinuities (VDs) was systematically varied. In the second set, different angles and modes of intersection between two VDs were tested. The VDs were used to represent inherited structures from previous orogenic events that when reactivated induce a preferential place where the new structures may develop. In the experimental setup, the VDs were represented by two sheets of sandpaper attached to the lateral moving walls, with different configurations (Fig. 1.3). These moved over the base of the box, also covered by a fixed sandpaper sheet to maintain a constant coefficient of friction all along the base of the experimental box. The lateral moving walls were attached to two stepping motors moving at a constant velocity of ~1.44 cm/h. The sandbox was filled with a 3 cm thick sand cake composed of alternating layers of coloured and natural (uncoloured) sand. The sand was sieved over the box using a mobile elongated funnel running over lateral rails. In these models, we did not use syntectonic sedimentation as to avoid interfering with the experiment

and to clearly mark the structures formed on the surface of the experiment. In our experiments, we used natural and coloured quartz sand. Quartz sand is a good analogue for upper crustal rocks and it has been commonly used as an analogue for natural brittle materials (e.g. Vendeville et al., 1987; McClay, 1990; Schellart, 2000; Schreurs et al., 2006).

In the first set of experiments, we systematically varied the distance between two parallel VDs from 0 to 5 cm, in steps of 1 cm, corresponding to experiments P-00, P-01, P-02, P-03, P-04 and P-05 (see general configuration in Fig. 1.4A). In a second set, we tested further four initial VD's configurations: two oblique (O) and two triple-junction (TJ) geometries (Fig. 1.4B, C, D and E).

**Table 1.1.** Summary of the analogue modelling experiments performed in this study.

| | Experiment | Initial spacing between VDs | Angle between VDs | Scaled initial distance between VDs |
|---|---|---|---|---|
| 1st set | P-00 | 0 cm | 0º | 0 km |
| | P-01 | 1 cm | 0º | 4 km |
| | P-02 | 2 cm | 0º | 8 km |
| | P-03 | 3 cm | 0º | 12 km |
| | P-04 | 4 cm | 0º | 16 km |
| | P-05 | 5 cm | 0º | 20 km |
| 2nd set | O-01 | variable between 0 to 4 cm | ~6º | variable between 0 to 16 km |
| | O-02 | variable between 1 to 5 cm | ~6º | variable between 4 to 20 km |
| | O-02a | variable between 1 to 5 cm | ~6º | variable between 4 and 20 km |
| | TJ-01 | variable | 60º | variable |
| | TJ-02 | variable | 60º | variable |

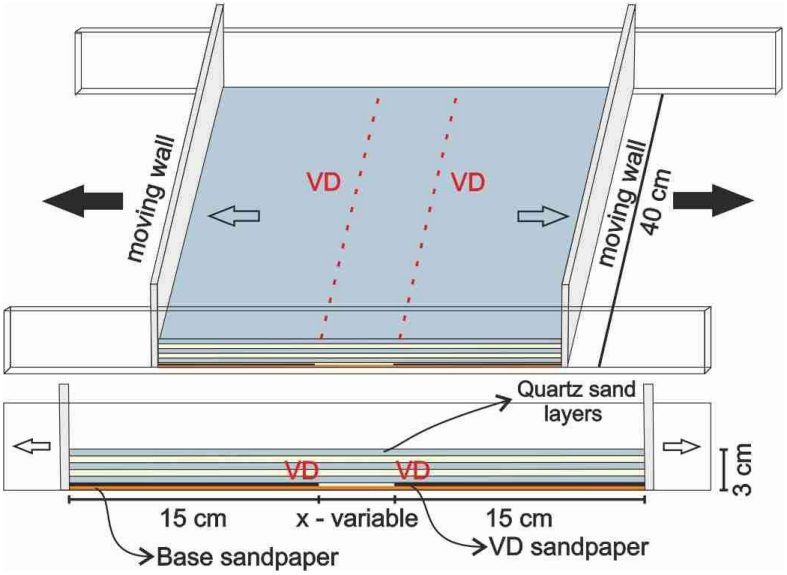


**Figure 1.3.** Initial configuration of the sandbox apparatus used in this study. The coloured layers represent quartz sand (natural and coloured). Each layer had a thickness of approximately 0.5 cm and the total thickness of the package was 3 cm. Note the variable position of the basal velocity discontinuities (VDs). Sandpaper sheet thickness is exaggerated for illustration purposes.

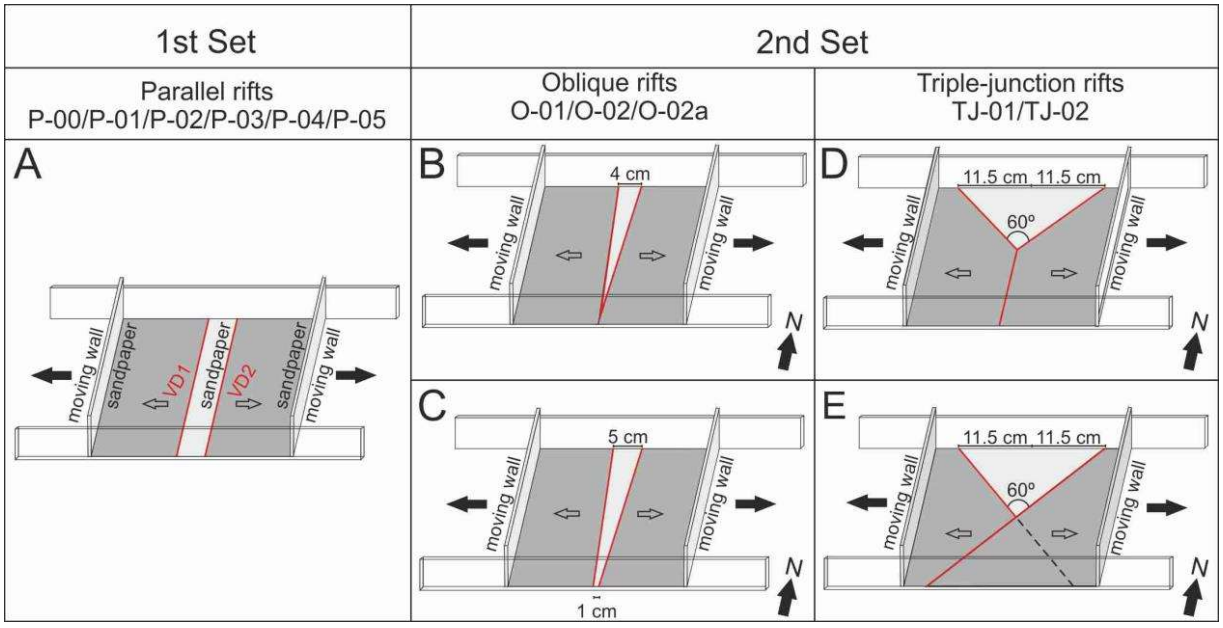


**Figure 1.4.** Configuration of all the experiments performed in this study. A. Configuration of the 1st set of experiments (P-00, P-01, P-02, P-03, P-04, and P-05), with the spacing of the VDs varying between 0 and 5 cm in steps of 1 cm. B. O-01. The VDs were placed at an angle (~6º) with their distance varying continuously between 0 and 4 cm. C. O-02 and O-02a. The VDs were placed at an angle (~6º) with their distance varying continuously between 1 and 5 cm. D. TJ-01. The configuration between the VDs varies along-strike; they are placed parallel (orthogonal to the extension) in the southern part of the box and diverge with an angle of 60º towards the northern boundary. E. TJ-02. The VDs make an angle of 60º between them (and in relation to the moving walls), intersecting at the centre of the box. Note that in the southern part of the box one of the VDs is covered by the sandpaper attached to the other wall, and thus does not affect the sand cake. Note that this configuration causes the migration of the "triple-point" to the south as the experiment unfolds.

### 1.5.2. Numerical modelling experiments

The numerical models were developed with the Underworld code (Moresi et al., 2003, 2017, 2018), an open-source geodynamical modular computational framework which uses particle-in-cell (PIC) and finite element methods, allowing for the parallel computation of thermo-mechanical tectonic problems (Moresi et al., 2017, 2018).

We have performed a total of 21 numerical modelling experiments (Table 1.2), in which we varied the distance between two rift-seeding weak zones for three different rheological structures of the crust (RI, RII and RIII), according to the following specifications:

a) The first rheological profile (RI, Fig. 1.5A, Table 1.2) comprises a 10 km thick upper-crust (UC) and a 30 km thick lower-crust (LC). Both the UC and the LC have a visco-plastic rheology, with a Patrice-Arrhenius non-Newtonian viscosity. However, while the UC was set to accommodate plastic yielding (following a Drucker-Prager criterion), the LC was set to deform only viscously, simulating a Strong UC and a Weak LC in compliance with a "Crème Brûlée" rheological profile;
b) The second rheological profile (RII, Fig. 1.5B, Table 1.2) has a layer thickness similar to RI, but in this case the LC also has a Drucker-Prager plastic yielding. The resulting (non-linear, thermal dependent) strength-depth configuration comprised an interbedded thin weak layer (~1.5 km thick) between the strong upper and lower crusts, conforming with a "Thin-Jelly Sandwich" rheological configuration;
c) The third rheological profile (RIII, Fig. 1.5C, Table 1.2) has a 20 km thick UC and a 20 km thick LC. In this case both the UC and the LC have the same rheological characteristics as RII, which render an overall crustal "Thick Jelly Sandwich" rheological profile (see Fig. 1C).

For each rheological profile, the distance between the two seeds was systematically varied between 10 and 50 km (with increments of 10 km). For each set, we have also tested the cases without and with only one seed.

**Table 1.2.** Summary of the numerical models developed in this study.

| SET | EXPERIMENTAL MODEL | CRUSTAL STRENGTH PROFILE | | Number of weaknesses | Distance between weaknesses |
|---|---|---|---|---|---|
| | | UPPER CRUST | LOWER CRUST | | |
| RI | 1 | "*Crème Brûlée*" | | 0 | - |
| | 2 | | | 1 | - |
| | 3 | Strong (10 km thick) | Very weak (no yielding criteria, 30 km thick) | 2 | 10 km |
| | 4 | | | 2 | 20 km |
| | 5 | | | 2 | 30 km |
| | 6 | | | 2 | 40 km |
| | 7 | | | 2 | 50 km |
| RII | 8 | *"Thin-Jelly Sandwich"* | | 0 | - |
| | 9 | | | 1 | - |
| | 10 | Strong top (8.5 km thick) + Weak thin bottom (1.5 km thick) | Strong top (10 km thick) + Weak bottom (20 km thick) | 2 | 10 km |
| | 11 | | | 2 | 20 km |
| | 12 | | | 2 | 30 km |
| | 13 | | | 2 | 40 km |
| | 14 | | | 2 | 50 km |
| RIII | 15 | *"Thick-Jelly Sandwich"* | | 0 | - |
| | 16 | | | 1 | - |
| | 17 | Strong top (10 km thick) + Weak bottom (10 km thick) | Strong top (10 km thick) + Weak bottom (10 km thick) | 2 | 10 km |
| | 18 | | | 2 | 20 km |
| | 19 | | | 2 | 30 km |
| | 20 | | | 2 | 40 km |
| | 21 | | | 2 | 50 km |

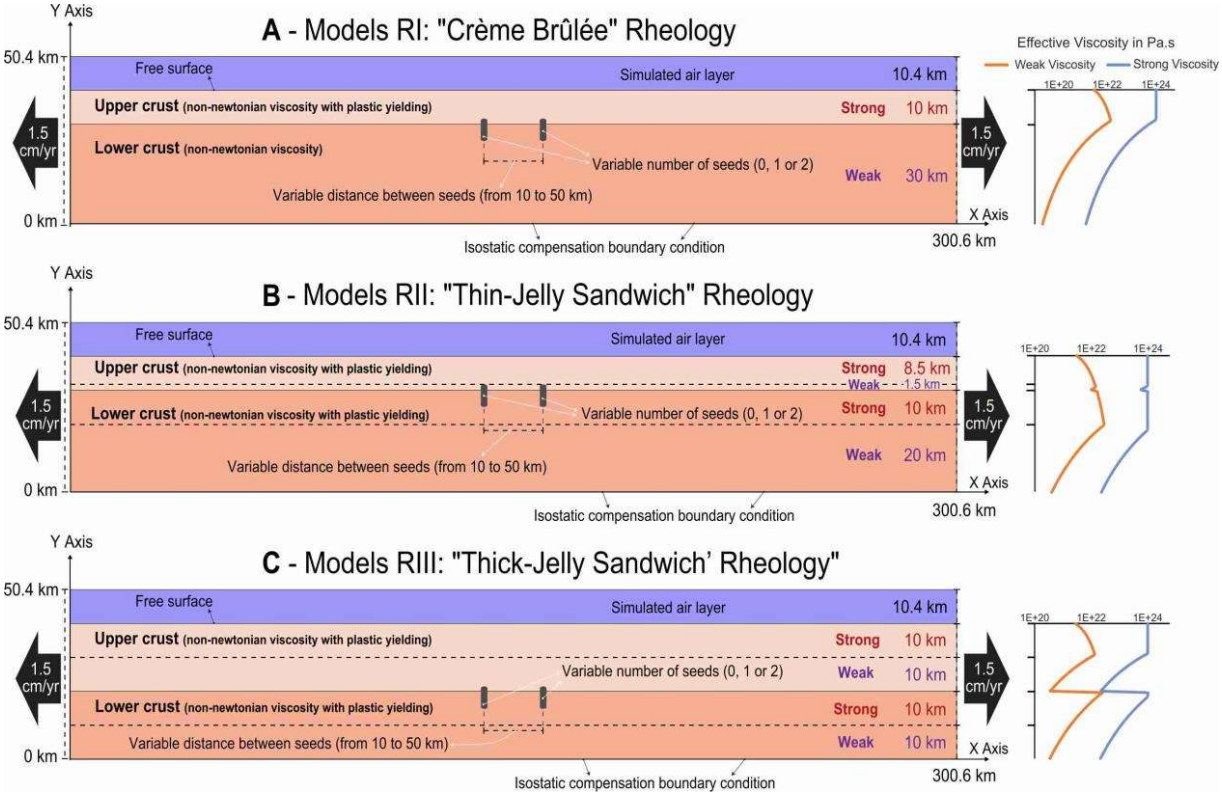


**Figure 1.5.** Model setup for the three (RI, RII and RIII) groups of carried-out numerical experiments. All models have the same (300.6 x 50.4 km) domain dimensions, the same boundary conditions**,** and the same number of (0, 1 or 2) rift-seeding weaknesses, set at the same (10 to 50 km) range of tested distances. A – "Crème Brulée" RI model setup: both a 10 km thick upper crust (UC) and a 30 km thick lower crust (LC) were ascribed non-Newtonian, thermal-dependent, viscous rheologies (Patrice-Arrhenius viscosity). However, the upper crust was additionally set to be able to yield plastically (Drucker-Prager criterion). B – "Thin-Jelly Sandwich" RII model setup: the upper and lower crust have the same thicknesses as in RI, but a plastic yielding criterion was additionally ascribed to the LC in this case. C – "Thick-Jelly Sandwich" RIII model setup: as in RII, non-Newtonian viscosity and plastic yielding were ascribed to both the upper and lower crust, although in this case both these units were set to have a thickness of 20 km. In the Effective Viscosity charts, the strong viscosity (in the colour blue) assumes the default strain rate of $10^{-17}s^{-1}$, and corresponds to the crustal profile in a region away from the seeds in the final stages of the model, after the localization of the deformation along discrete shear zones; the weak viscosity (in the colour orange) assumes a strain rate of $10^{-15}s^{-1}$, corresponding to the early stages of deformation, when deformation is more homogeneous.

# CHAPTER 2. NATURAL ANALOGUE: PARECIS BASIN, TECTONIC FRAMEWORK AND REGIONAL GEOLOGY

The Parecis Basin is located in the centre-west of Brazil and is part of the South American Platform. This platform was defined by Almeida et al. (2000) as the continental part of the crust that remained stable, with a small amount of deformation in the last orogenic events – the Caribbean and Andean orogeneses. The basement of the platform was amalgamated during the Brasiliano/Pan African Orogeny (900-500 Ma) as part of the Gondwana supercontinent (Almeida et al., 2000). The sediment covers date to the Phanerozoic and were mostly developed since the Ordovician as part of the Gondwana and Pangea supercontinent evolution (Schobbenhaus and Brito Neves, 2003).

Brazil was divided into structural provinces by (Almeida et al., 1977, 1981) and over the years several additions and changes to this configuration occurred due to new geochronological, geological and geophysical data. In the study area of this research the Parecis Basin, the Amazonian Craton and the Paraguay Fold Belt can be highlighted.

The geological and tectonic history of the Parecis Basin is quite controversial. At first, this basin was identified as a Palaeozoic intracratonic basin by several authors (e.g. Siqueira, 1989; Braga and Siqueira, 1996; Silva et al., 2003; Bahia et al., 2006, 2007; Bahia, 2007). However, recently, new data, interpretations and analysis provided a new hypothesis for this basin's tectono-stratigraphic evolution. In this new hypothesis, the initial stages of development of the basin are dated to the Neoproterozoic, long before the age suggested in the previous hypothesis (Haeser, 2013; Haeser et al., 2014; Vasconcelos et al., 2014; Alvarenga et al., 2016; Loureiro, 2016; Vidotti et al., 2016; Loureiro et al., 2017; Vilela et al., 2020).

Although this research is focused on the early stages of development of the basin, in this chapter, a synthesis of the geological and tectono-stratigraphic evolution of the Parecis Basin is presented, as well as the adjacent areas which are considered the basin's basement – the Amazonian Craton and the Paraguay Fold Belt.

## 2.1. Adjacent basement structures

### 2.1.1. Amazonian Craton

The Amazonian Craton is one of the larger and less known cratons of the world (Tassinari et al., 2000) and one of the major tectonic units of South America, with ~5,600,000 km$^2$ (Santos, 2003). The craton is divided into two Precambrian shields – Central Brazil Shield and the Guianas Shield, separated by the Phanerozoic Solimões and Amazon basins (Tassinari et al., 2000). The craton's western limit is difficult to establish because it is separated from the Andean belt by an extensive Cenozoic cover - the Colombian Llanos, the Venezuelan Llanos and the Paraguay-Bolivian Chaco (Santos, 2003). The craton's extension to the west is indicated by Greenvillian fragments in the Oriental Cordillera (e.g. Garzón and Santa Marta, Kroonenberg, 1982; Priem et al., 1989).

In the Brazilian territory, the Amazonian Craton underlies an area of about 4,400,000 km$^2$ and is limited by the Araguaia belt (Baixo Araguaia Supergroup) to the east and by the Paraguay belt, comprising the Cuiabá, Corumbá and Alto Paraguai groups to the south and southeast (Tassinari et al., 2000; Santos, 2003). The concept of craton was here applied regarding the rocks developed in the Brasiliano Orogeny, representing a pre-Brasiliano stabilized area (Santos et al., 2000). The Amazonian Craton is partially covered by Phanerozoic sedimentary basins as the ones of Parnaíba (east), Xingu and Alto Tapajós (south), Parecis (southeast), Solimões (west), Tacutu (north) and Amazon (center, Santos, 2003).

The Amazonian Craton (Almeida, 1978) followed the previous classification of shield (Barbosa and Andrade Ramos, 1959) and platform (Ferreira, 1969; Suszczynski, 1970; Amaral, 1974). While this area is complex, there are two main models for the subdivision of this structure: the geophysical-structural and the geochronological.

The geophysical-structural model was proposed by Hasui et al. (1984) and Costa and Hasui (1997) and considers the Amazonian Craton as a mosaic of twelve blocks or paleo plates with granite-greenstone characteristics and with Archean to Paleoproterozoic ages. These blocks are surrounded by nineteen collisional belts or shear belts, also with ages between the Archean and the Paleoproterozoic, and reactivated in the Phanerozoic. This model was based on geophysical data such as the gravity map of South America and the magnetic map of Brazil in addition to

structural data. In this model, only Himalayan collision type processes (continent-continent) were considered. Costa and Hasui (1997) suggest several areas that may consist of granulitic rocks, located in the shear zones between blocks, which would indicate the existence of high-grade terrains related to collision processes.

The geochronological model had several contributions over the years. Initially proposed by Amaral (1974), this model divides the craton into geochronological provinces based on the Rb-Sr radiometric age method that were produced by the Amazonian Radar Project. Amaral (1974) divided the craton into three geochronological provinces: Amazônia Oriental, Amazônia Central and Amazônia Ocidental (Fig. 2.1A). Cordani et al. (1979) followed the proposal of Amaral (1974), changed some of the province's names and added an additional province – the Rondoniana Province (1400–1100 Ma, Fig. 2.1B). With this model was possible to realize the existence of an ancient core that formed the craton – the Amazônia Central Province (Archean or Paleoproterozoic) surrounded by fold belts formed in the Paleoproterozoic. However, due to the low reliability of the Rb-Sr radiometric age method, the values disagreed with the regional stratigraphic framework and had to be amended (Santos, 2003). Teixeira et al. (1989) considered the previous model and classified only Amazônia Central as a province, and the others as fold belts. These authors presented some changes, including separating the Rondoniana Fold Belt from the Sunsás Fold Belt (1200-900 Ma, Fig. 2.1C). Tassinari et al. (1996) and Tassinari and Macambira (1999), based on Rb-Sr and U-Pb radiometric ages, adopted the province nomenclature and modified the limits and age intervals of the previous models, creating a new province between Rio Negro-Juruena and Amazônia Central – the Ventuari-Tapajós Province (1900–1800 Ma, Fig. 2.1D). Santos et al. (2000) and Santos (2003) made several reinterpretations of the provinces based on data from U-Pb and Sm-Nd radiometric age data and geological mapping results (Fig. 2.1E). Tassinari and Macambira (2004) based on Sr, Pb and Nd radiometric ages divided the craton in six geochronological provinces.

More recent studies, as the ones of Scandolara et al. (2017) and Tavares et al. (2018) propose new interpretations for the geotectonic evolution of different parts of the Amazonian Craton. Tavares et al. (2018) studied the Carajás Province region, suggesting the superposition of three compressional-extensional cycles for the orogenic and sedimentary events. This proposal is consistent with other studies of Archean cratonic nuclei, where the Archean-Paleoproterozoic deformation could be explained by processes related to plate tectonics. Scandolara et al. (2017) propose an accretionary orogenic belt in the southwestern part of the

Amazonian Craton (bordering the Parecis Basin) – the Juruena accretionary orogen. This orogen was originated by the interaction of the Jamari and Juruena terranes (Scandolara et al., 2017). The study was based on geological mapping, geochemical and geochronological data, which confirm the connection of these terrains. This structure does not have the same general trend as the previously proposed geochronological provinces.

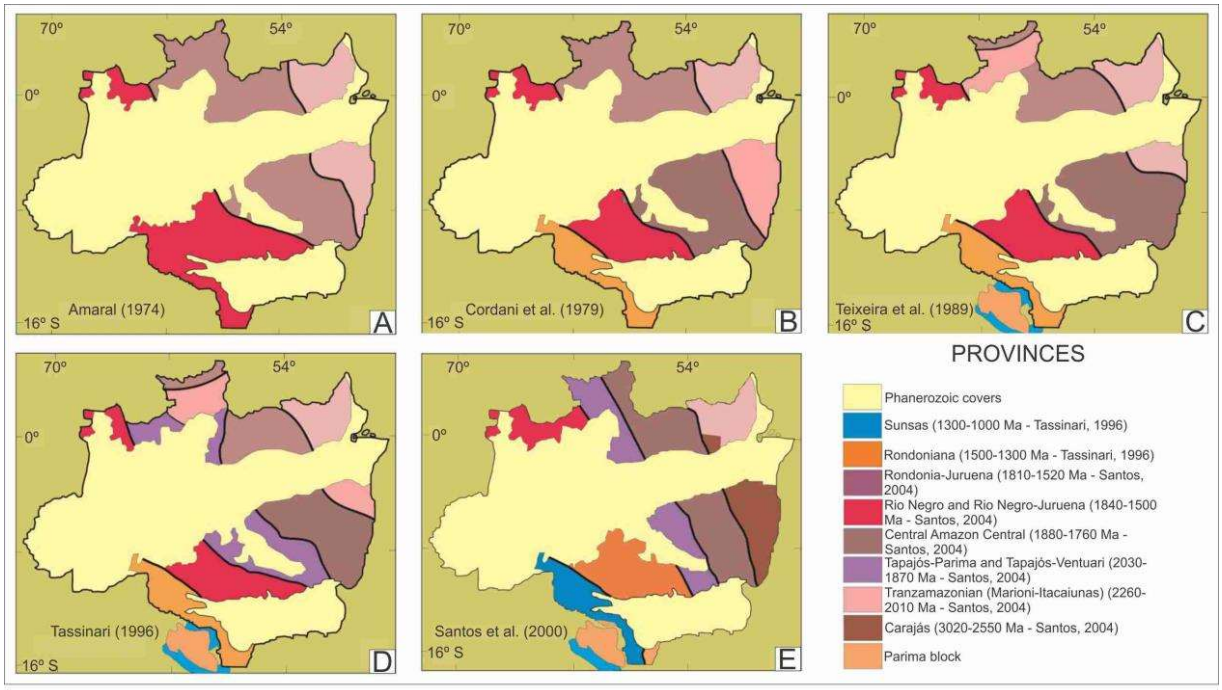


**Figure 2.1.** Evolution of the geochronological models for the Amazonian Craton. A. Model from Amaral (1974). B. Model from Cordani et al. (1979). C. Model from Teixeira et al. (1989). D. Model from Tassinari (1996). E. Model from Santos et al. (2000). Figure modified from Faria (2015), adapted from Santos (2003).

### 2.1.2. Paraguay Fold Belt

The Paraguay Fold Belt is located along the south-southeast margin of the Amazonian Craton and the east margin of the Rio Apa Block (Dantas et al., 2009). The fold belt consists of metasedimentary rocks that progressively change towards the craton to sedimentary covers. These are contemporary in part, structurally rippled, faulted and not metamorphosed (Alvarenga and Trompette, 1993). The sedimentary section presents a thick sequence of glacial-marine, turbiditic, carbonate and siliciclastic sedimentary rocks, which form a passive margin (Alvarenga and Trompette, 1993). The fold belt is approximately 1500 km long and ~300 km

wide (Souza, 2015). It extends from the Rio das Mortes area (Mato Grosso - MT) passing through the Cuiabá area (MT), where there is an inflection to the N-S direction, extending to Corumbá and Serra da Bodoquema (Mato Grosso do Sul – MS, Silva, 2007). This section was folded and metamorphosed (greenschist facies) during the Brasiliano Orogeny and intruded by late- to post-tectonic granites (end of Neoproterozoic/beginning of Cambrian, Alvarenga et al., 2000).

Almeida (1984) divided the Paraguay fold belt and the adjacent part of the Amazonian Craton into three structural zones, which were defined and characterized as: i) sedimentary platform covers; ii) external folded zone (minor or no metamorphism); iii) internal zone (metamorphosed with granitic intrusions). A large portion of the rocks of the internal zone is masked by the post-Ordovician sedimentary basin covers of Paraná, Parecis and Pantanal basins (Alvarenga and Trompette, 1993).

Alvarenga and Trompette (1993) included the lithostratipgraphic units (from the Neoproterozoic to Cambrian) in three large associations: lower unit (glacial-turbiditic), central unit (carbonate) and upper unit (detritic).

There is controversy concerning the Paraguay Fold Belt stratigraphy. There are several proposals for the stratigraphic column, more precisely in the transition between the internal and external structural zones of the fold belt (Alvarenga, 1984). Two of these proposals are:

1. Two large structural and stratigraphic units, the older composed of folded and metamorphosed rocks of the Cuiabá Group (internal zone) and the rocks of the Diamantino, Raizama, Araras, Puga and Bauxi Formations, representing the external part of the fold belt and the cratonic cover (Figueiredo and Olivatti, 1974; Ribeiro Filho and Figueiredo, 1974; Ribeiro Filho et al., 1975; Nogueira and Oliveira, 1978; Corrêa et al., 1979; Oliva et al., 1979; Schobbenhaus Filho and Oliva, 1979; Schobbenhaus Filho et al., 1981, 1984; Araújo et al., 1982; Barros et al., 1982; Del'Arco et al., 1982; Almeida, 1984);
2. Puga and Bauxi Formations, which are the partially contemporary deposits of the sedimentary rocks that form the lower part of the cratonic platform covers, the external zone of the belt and the Cuiabá Group, consisting of metasedimentary rocks of the internal zone of the fold belt (Almeida, 1964, 1965, 1974; Alvarenga, 1985, 1988; Alvarenga and Trompette, 1988, 1992).

The northern portion of the Paraguay Belt presents four lithostratigraphic successions that include from the oldest to the newest: fine-grained metasedimentary rocks of the Cuiabá Group;

glacial diamictite-tubidite of the Cuiabá Group and Puga Formation; metacarbonates of the Araras Group and metasedimentary epiclastic rocks of the Alto Paraguay Group (Alvarenga and Trompette, 1993; Alvarenga et al., 2004). Table 2.1 shows the lithostratigraphic nomenclature of the units that form the Paraguay Belt (Dantas et al., 2009), highlighting the formations and groups that can also be observed in the Parecis Basin.

**Table 2.1.** Neoproterozoic lithostratigraphic nomenclature of the Paraguay Fold Belt. In bold are the formations and groups that also occur in the Parecis Basin (from Dantas et al., 2009).

| **PERIOD** | **NORTHERN PARAGUAY FOLD BELT** | | | |
|---|---|---|---|---|
| | **LITHOSTRATIGRAPHIC SUCCESSION** | **GROUP** | **FORMATION** | **LITHOLOGY** |
| Edicardian | Upper | **Alto Paraguai** | **Diamantino** | Arkosic siltite and sandstone |
| | | | **Raizama** | Sandstone |
| | Carbonate | **Araras** | Nobres | Dolostone and sandy dolostone |
| | | | Guia | Limestone and mudstone |
| | | | Mirassol d'Oeste | Cap-dolostone |
| Cryogenian | Glacial diamictite-turbidite (~635 Ma) | | **Puga** | Diamictite |
| | | Cuiabá | Undivided | Diamictite, conglomerate, sandstone and fine-grained rock |
| | Lower | | Lower | *Graphite Phyllite* |

## 2.2. Parecis Basin

The Parecis Basin, also known as Parecis/Alto Xingu Basin, covers an area of approximately 500,000 km$^2$ of Rondônia and Mato Grosso (Fig. 1.1) in the centre-west of Brazil (Siqueira, 1989). It is considered as a new frontier of exploration for hydrocarbon resources and has been of interest to the oil industry. However, its geological history, tectonic evolution and stratigraphy are widely discussed.

Siqueira (1989) compiled the results obtained in several geological campaigns, analysed, and discussed the stratigraphy and tectonic evolution of the Parecis Basin correlating it to other Brazilian intracratonic basins. In his study, the Parecis Basin was classified as interior fracture (IF)/ interior sag (IS), according to the Kingston et al. (1983) basin classification. The IF phase, dated to the Silurian, comprises the development of rifts that later, in the Carboniferous-Permian, turned to sag characteristics – IS phase (Siqueira, 1989). The basin was divided into three distinct areas according to their structural-stratigraphic organization: Rondônia Tectonic Trench (western area) characterized by two well defined grabens – Pimenta Bueno and Colorado grabens; the Parecis Gravity Low (central area), represented by a -40 mgal anomaly; and the Alto Xingu Depression (eastern area, Siqueira, 1989). Two depositional transgressive-regressive cycles, separated by a regional unconformity, took place in the Palaeozoic (Siqueira, 1989). The first cycle includes the deposition of the Ponta Grossa, Pimenta Bueno and Fazenda da Casa Branca formations (Siqueira, 1989). The second cycle comprises the basaltic flows of Anari and Tapirapuã formations (dated to the Jurassic), after which the sediments of the Parecis Formation were deposited (Siqueira, 1989).

Using gravity and magnetic data, Braga and Siqueira (1996) established the structural limits of the basin's basement. These results were then analysed by (Bahia et al., 2006, 2007) and Bahia (2007) to review the stratigraphy and the tectonic-sedimentary evolution of the Parecis Basin, based on Siqueira (1989).

An integration of the tectonic-sedimentary evolution of the basin was made in the work of Bahia et al. (2006). Their stratigraphic column of the Parecis Basin (Fig. 2.2) presents the sedimentary units with the same nomenclature used in previous contributions (Siqueira, 1989; Bahia and Pedreira, 1996; Bahia et al., 1996). In some of the time intervals, absence of sedimentary deposits is indicated by unconformities, evidencing sedimentation hiatuses (Bahia et al., 2006). The sedimentation started in the Neo-Ordovician, during the rift phase of the basin, when the Cacoal Formation was deposited (Rondônia Tectonic Trench), representing the continental portion of the sedimentary sequence of the basin (Bahia et al., 2006). The Devonian Furnas Formation is represented by costal sediments deposited in the Alto Xingu Depression, followed by the Ponta Grossa Formation of marine sediments (Bahia et al., 2006). During the transitional Carboniferous-Permian rift/sag phase climate changes occurred when the glaciogenic Pimenta Bueno and the periglaciogenic Fazenda da Casa Branca formations were deposited (Bahia et al., 2006). Before the deposition of the Parecis Group, extensional events triggered the Mesozoic Anari and Tapirapuã basaltic flows (Bahia et al., 2006). More recent

studies on the stratigraphic framework of the Cretaceous in the Parecis Basin (Batezelli and Ladeira, 2016; Rubert et al., 2017, 2019) also follow this hypothesis and bring new insights and proposals for the stratigraphic chart of the basin (Fig. 2.2).

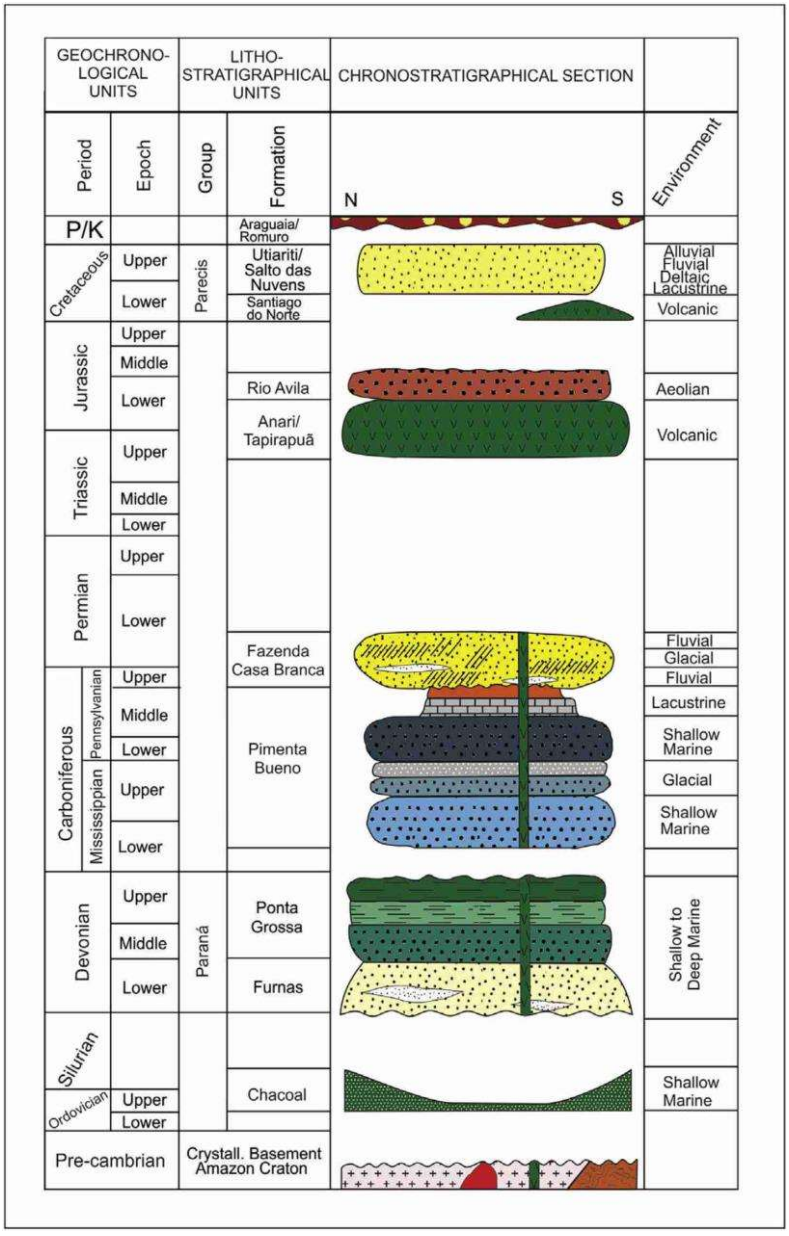


**Figure 2.2.** Stratigraphic chart of the Parecis Basin (from Rubert et al., 2017, modified from Bahia et al., 2006).

Bahia et al. (2007) were the first authors that aimed to record the tectono-sedimentary evolution of the Parecis Basin with geophysical data. Analysis of the gravity map made it possible to obtain the geometric signature of the main faults of the basin, as well as the structures of the geophysical domains and location of the main basin depocenters. Bahia et al.

(2007) concluded that the basin was formed by extensional processes in the Amazonian Craton area, originating the Pimenta Bueno and Colorado grabens that were infilled with continental and marine sedimentary sequences. These authors also agreed with the previously proposed evolution by Siqueira (1989) – interior fracture/interior sag. Figure 2.3 shows the proposed tectonic evolution (Bahia et al., 2007). The first stage of development (Fig. 2.3A) – the rift phase, is marked by N-S extensional forces forming the Pimenta Bueno and Colorado grabens. During the rift phase, there was the sedimentary infill of the grabens with the Cacoal and Pimenta Bueno formations (Fig. 2.3B). After this, the sag phase happened through regional subsidence and the Fazenda da Casa Branca, Rio Ávila, Anari and Parecis formations were deposited (Fig. 2.3C).

The work of Faria (2015) also used geophysical gravimetric and magnetic data to define the structure of the Parecis Basin, refining its tectonic domains and estimating the grabens depths to ~12 km (Fig. 2.4).

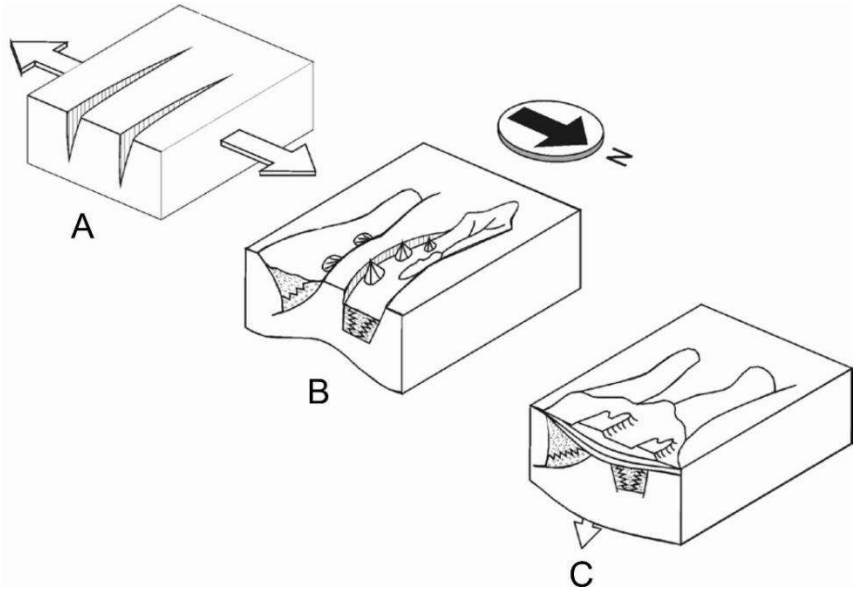


**Figure 2.3.** Diagrams illustrating the evolution of the Parecis Basin western portion. A. Rift phase – extension in the SW sector of the Amazonian Craton forming the Pimenta Bueno and Colorado grabens. B. Deposition of the Cacoal and Pimenta Bueno formations in the grabens. C. Sag phase – regional subsidence and deposition of the Fazenda da Casa Branca, Rio Ávila, Anari and Parecis formations (from Bahia et al., 2007).

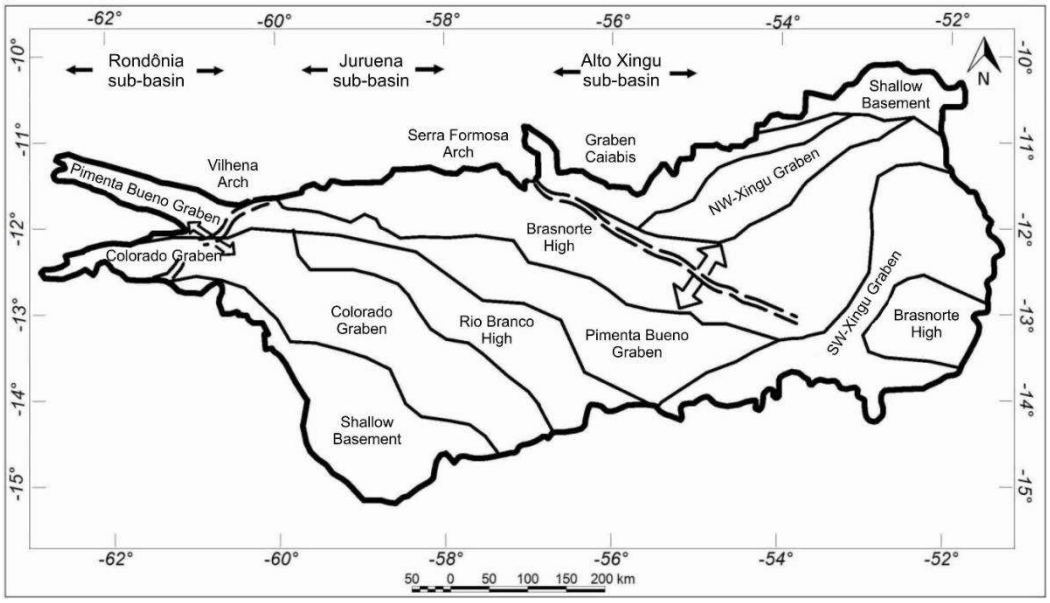


**Figure 2.4.** Tectonic-geophysical domains of the Parecis Basin (from Faria, 2015).

More recently, authors as Haeser et al. (2014), Vasconcelos et al. (2014), Alvarenga et al. (2016), Loureiro (2016), Vidotti et al. (2016), Loureiro et al. (2017) proposed a new hypothesis for the evolution of the Parecis Basin. Data of isotopic stratigraphy, new wells, new interpretations of seismic lines and integration of gravity and magnetic data showed a much older history than previously established, initiated in the Neoproterozoic and not in the Palaeozoic.

Vasconcelos et al. (2014) did a stratigraphic revision of the basin through new studies of the regional framework, reinterpretation of the lithostratigraphy of wells and new seismic lines, concluding that the pre-Cretaceous sequences in subsurface are folded, correlating them to the Neoproterozoic folded sequences of the Paraguay Fold Belt.

Haeser et al. (2014) proposed a stratigraphic revision for the Parecis Basin (Fig. 2.5), discussing the implications for the oil exploration. The authors emphasise that this basin is in an incipient stage of exploration, but that the existence of hydrocarbon systems is still speculative. Based on seismic sections, possible reservoir rocks and generating rocks were suggested. Haeser et al. (2014) suggested the possibility of accumulations related to structural traps formed in the Neoproterozoic or in compressive events that generated the Paraguay Fold Belt.

Loureiro (2016) and Loureiro et al. (2017) provided the geologic-tectonic characterization of the Parecis Basin by integrating gravity and magnetic methods with seismic data aiming to

understand the sedimentation recorded in the basin. These authors believe that the sedimentation was associated to tectonic processes of continental scale, such as the Rodinia Supercontinent break-up, the Neoproterozoic Brasiliano Orogeny, and the formation of part of the Andes Orogenic Fold belt in the Palaeozoic (Loureiro, 2016). The basin infill would have been controlled by the structural highs and lows and the W-E trending grabens. Loureiro (2016) inferred that the Neoproterozoic sedimentation in the basin occurred in three relevant tectonic events: a rift phase, a thermal subsidence and flexural phase (deposition of the Puga Formation, Araras Group and Serra Azul Formation), followed by a compressive phase generating foreland basins – beginning of the Brasiliano Orogeny and formation of the Paraguay, Araguaia and Brasília fold belts (Fig. 2.6). Some dense bodies found in the gravity models were interpreted as basic and ultrabasic rocks, that are probably related to previous subduction processes occurred in the Mesoproterozoic (Loureiro, 2016).

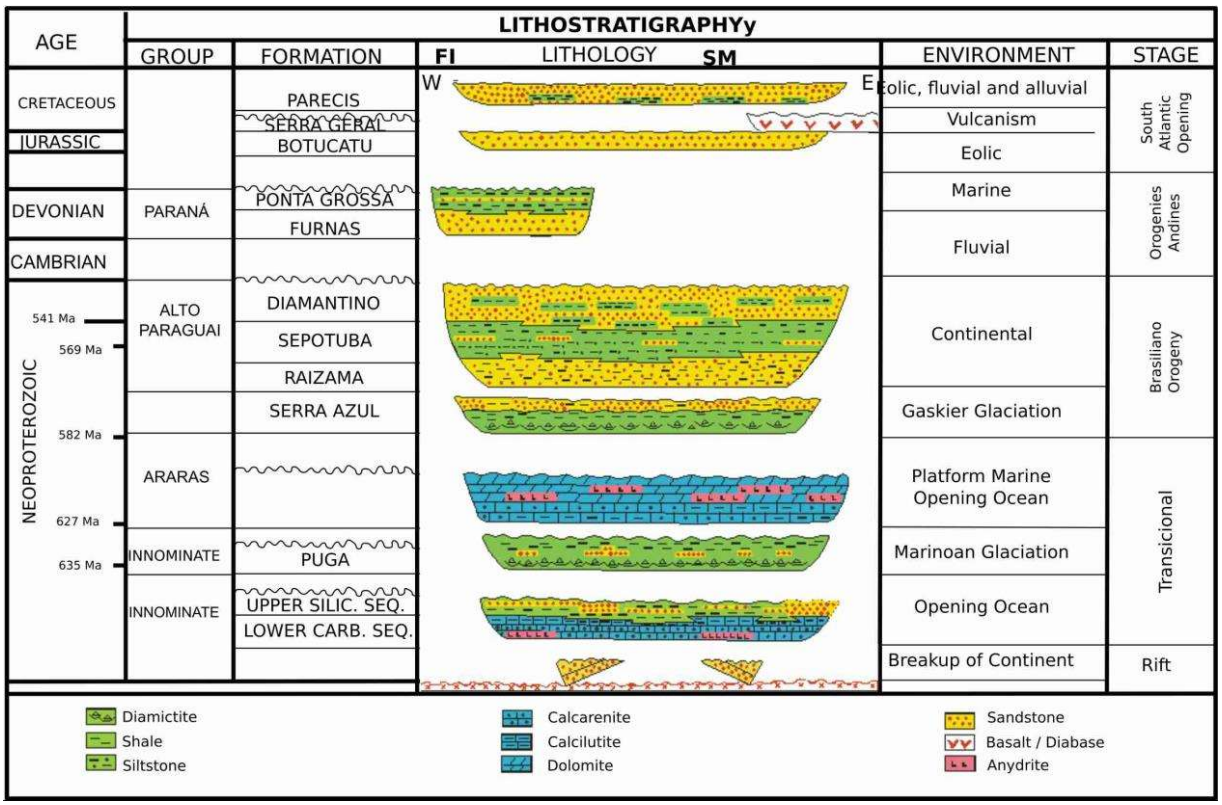


**Figure 2.5.** Stratigraphic chart of the Parecis Basin (from Loureiro et al., 2017, modified from Haeser et al., 2014).

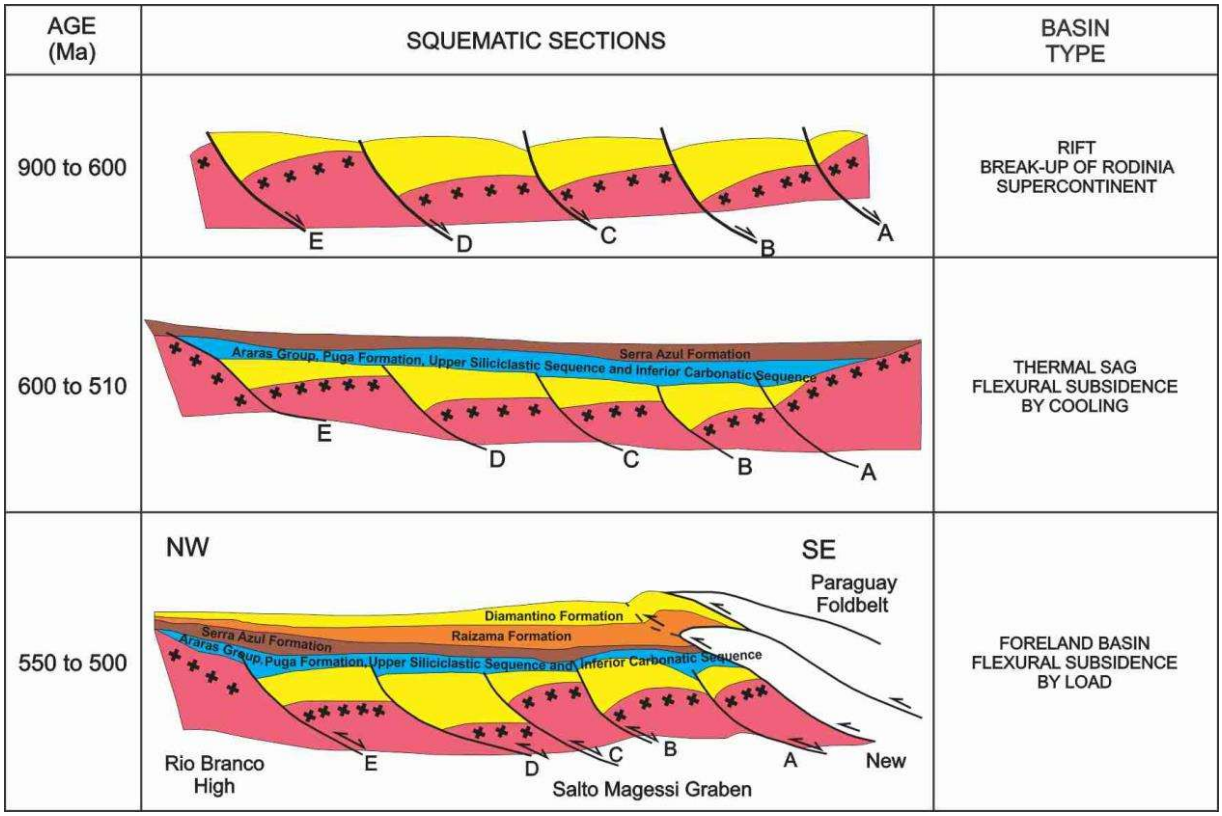


**Figure 2.6.** Tectonic evolution of the Parecis Basin proposed by Loureiro (2016).

# CHAPTER 3. STATE OF THE ART: ANALOGUE AND NUMERICAL MODELLING

Analogue and numerical modelling are techniques used to simulate the evolution of geological structures at laboratory and computational scales, respectively. The use of these techniques allows the better understanding of geological processes that may take millions of years, at smaller scales and in a relatively short amount of time.

Many studies have been developed through analogue and/or numerical modelling techniques, aiming to better understand the evolution of geological structures. Today these techniques are commonly applied to many geological contexts and sub-disciplines of Earth Sciences such as the development of extensional structures (Vendeville et al., 1987; Brune and Autin, 2013; Keppler et al., 2013; Zwaan et al., 2016; Beniest, 2017; Beniest et al., 2017; Duretz et al., 2020), salt tectonics (Rowan et al. 2012; Warsitzka et al., 2013), compressional structures (McClay and Whitehouse, 2004; Duarte et al., 2011; Rauch, 2013; Rosas et al., 2017), strike-slip structures (Schellart and Nieuwland, 2003; Schrank et al., 2008; Dooley and Schreurs, 2012; Gomes et al., 2019), mantle plumes and subduction (Schellart, 2004; Boutelier and Cruden, 2008; Davaille et al., 2011; Bajolet et al., 2013; Duarte et al., 2013; Mériaux et al., 2016), to get insight on seismic interpretation (Sherlock and Evans, 2001; Buddensiek, 2009; Krawczyk et al., 2013), and in the context of sedimentology and geomorphology studies (Bonnet et al., 2007; Del Ventisette et al., 2015).

In this chapter, a brief history of analogue and numerical modelling and the importance of these techniques for the better understanding of geological structures is presented.

## 3.1. Analogue modelling

Analogue modelling has been used since the 19$^{th}$ century (Koyi, 1997; Ranalli, 2001; Schellart, 2002; Schellart and Strak, 2016) to study the formation and development of geological structures. The first experiments in analogue modelling were developed by Sir James Hall to understand the development of ductile deformation (Koyi, 1997). Later, it was applied

in structural geology studies of compressional structures, such as folds and thrust belts (Cadell, 1888, Willis, 1893). Figure 3.1 shows an example of the simple apparatus used by Cadell, (1888).

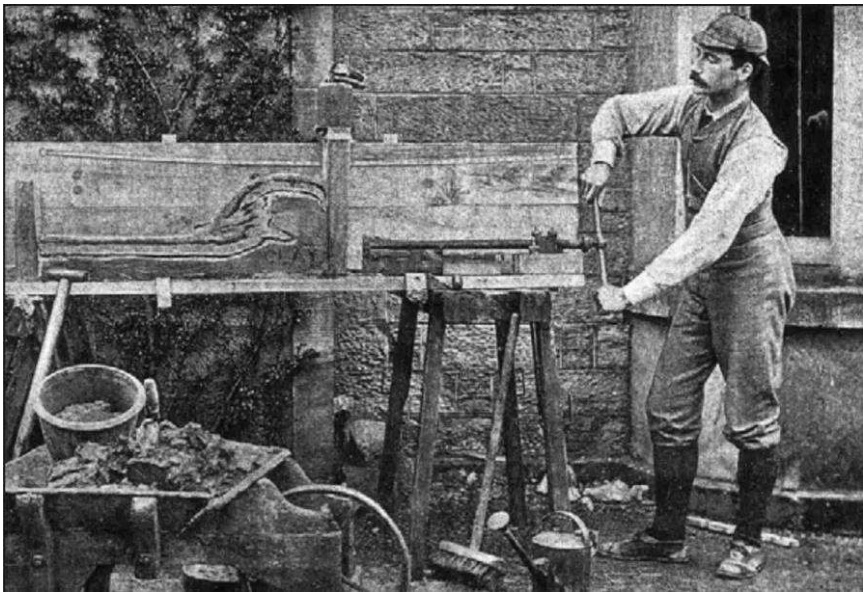

**Figure 3.1.** Cadell's experiment (1888, from Koyi, 1997).

With the understanding of the gravitational forces in the 1960's and 1970's, Hans Ramberg emphasized its importance and influence in the geological processes (Koyi, 1997). This allowed to create new experiments focusing on gravity dependent tectonics and structures.

Analogue modelling has been applied to industry and scientific research, showing its importance in the process of teaching/learning structural geology and tectonics. This is due to the possibility of simulating the entire development of geological structures, since nucleation to actual and future stages, at smaller scales than the natural analogues and within a relative short amount of time. The great advances in the techniques of analogue modelling, such as the use of auxiliary equipment for the interpretation of structures was possible thanks to its use by the oil industry. These techniques are used to understand different processes at various scales and the formation and development of structures of interest, such as hydrocarbon traps (Szatmari and Aires, 1987; Koyi, 1997). Seismic interpretation was another area that benefited from these advances of equipment and technology, allowing the development of models to obtain and interpret seismic data in sandbox apparatuses (Sherlock and Evans, 2001; Buddensiek, 2009; Krawczyk et al., 2013, Fig. 3.2.).

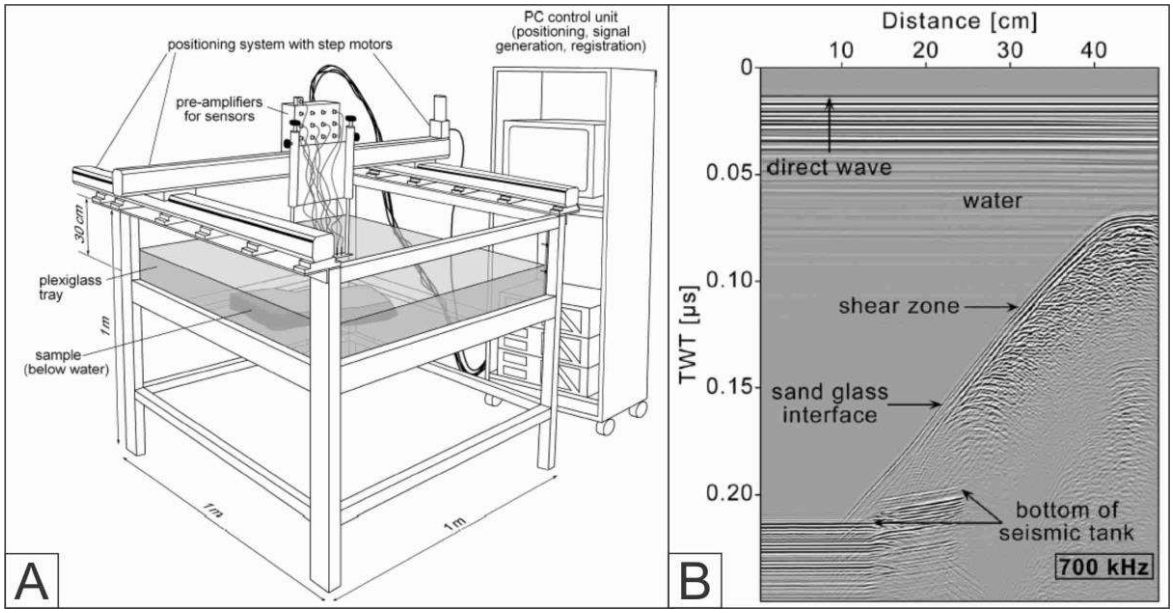


**Figure 3.2.** A. Example of an experimental apparatus and assemblage of a mini-seismic system in the laboratory. B. Example of a result from the models developed with the apparatus and system from A. Figures from Krawczyk et al. (2013).

One of the most evolved techniques is the Particle Image Velocimetry (PIV) software which allows the monitoring of experiments highlighting the movement of the particles in each instant of deformation (Adam et al., 2005; Schmatz et al., 2010; van Gent et al., 2010; Oliveira and Alves da Silva, 2016). This software assists the interpretation and analysis of analogue models by the digital record of images obtained during the experiments, using photographic cameras that allow the elaboration of 2D and 3D models. Figure 3.3 shows an example of results that can be obtained with PIV.

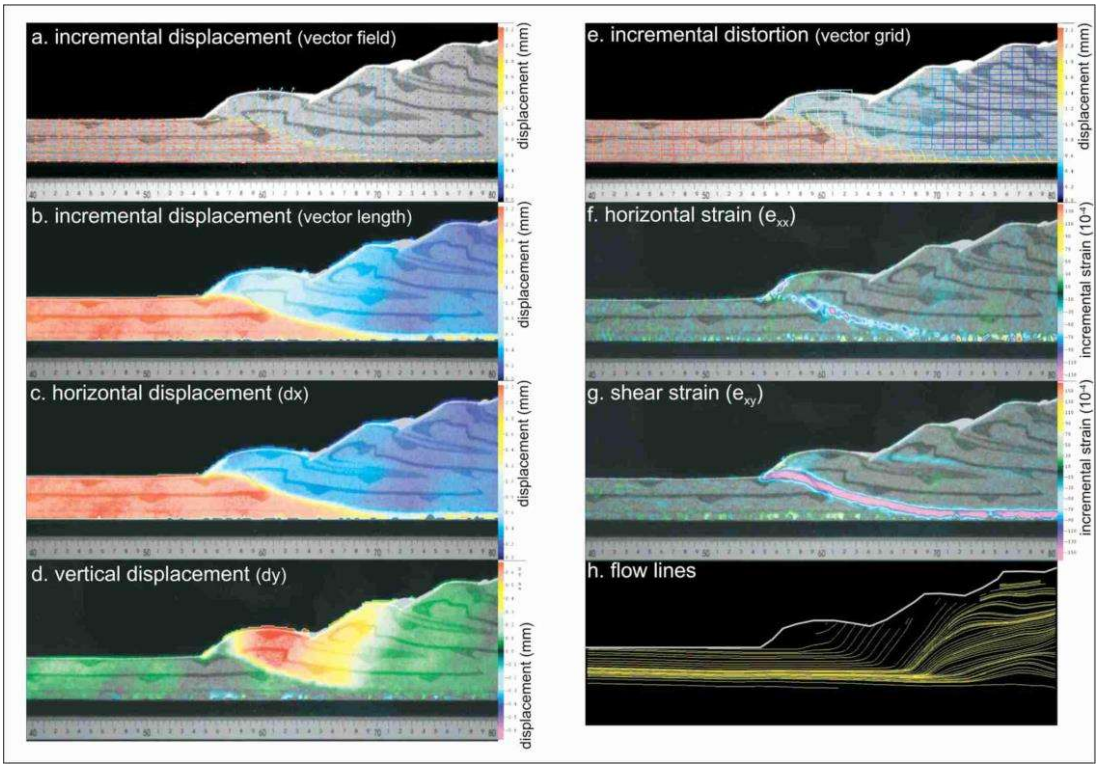


**Figure 3.3.** Results obtained from the digital image processing of the PIV software. a. Monitoring of the displacement vectors. b. Incremental displacement. c. Horizontal displacement component. d. Vertical displacement component. e. Visualized body distortion of the vector of the deformation mesh. f. Incremental horizontal strain. g. Shear strain. h. Visualization of the displacement of material particles by flow lines, showing the pattern of mass movement (from Adam et al., 2005).

## 3.2. Numerical modelling

The development of numerical modelling techniques is directly related to the geodynamics history. The establishment of plate tectonics during the 1960's brought new insights to the interpretation of data, from a more descriptive field (qualitative) to a more predictive physical science (quantitative field, Gerya, 2019).

As in analogue modelling, the rocks represented in numerical models must be similar to the existing rocks in nature. The behaviour of these materials is important to correctly simulate a geological structure. An important point to understand is that viscous (fluid-like) and elastic (solid-like) behaviours are characteristic of the Earth, depending on the time scale of deformation (Gerya, 2019). For example, the mantle is elastic in a "human" time scale but is viscous in geological time scales and it can be internally deformed due to solid-state creep (Gerya, 2019).

In 1970, the first 2D numerical models of subduction were performed by Minear and Toksöz (Gerya, 2019) and in the following years other 2D numerical models were developed from 2D mantle thermal convection models (Torrance and Turcotte, 1971) to numerical models of continental collision (Bird, 1978; Daignières et al., 1978) and subduction initiation (Matsumoto and Tomoda, 1983). The first 3D spherical mantle convection models were developed by Baumgardner (1985) and Machetel et al. (1986).

Since then, several codes have been used to portray 2D and 3D geological problems and although every code has its limitations, these techniques are powerful tools to understand tectonics and geodynamics (Gerya, 2019).

In this work, we used the Underworld code (Moresi et al., 2003, 2017, 2018; Moresi, 2013; Quenette et al., 2005, 2011, 2013, 2015; Stegman et al., 2006) to develop 2D numerical models. Underworld is an open-source geodynamical modular computational framework developed by researchers at Monash and Melbourne universities in Australia. This code uses variations of the particle-in-cell (PIC) and finite element methods and it allows for parallel computation of mechanical-thermal coupled tectonic problems (Moresi et al., 2007).

## 3.3. Scaling and materials

In analogue and numerical modelling, all models must be scaled according to the natural analogue – structure in nature that is intended to be simulated (Koyi, 1997). The evolution of the model should simulate the evolution that occurred in nature, even if at a smaller scale and with higher deformation velocities (Koyi, 1997). It is important to mention that although it is important to fully simulate a whole geological process, there are many complexities involved that cannot totally be simulated, and it is impossible to control all parameters involved. Therefore, simplified versions of complex geological processes are simpler to simulate and be applied not only to a determined structure, but also to similar developing structures.

To better portray the similarity between models and reality, Hubbert (1937) described the rules for performing scaled experiments of geological structures. Thus, Hubbert (1937) defined the concept of three similarities – geometric, kinematic and dynamic (Koyi, 1997):

"*1. – Two bodies are geometrically similar when all corresponding lengths are proportional, and all the corresponding angles within the two bodies are equal. The ratio*

*between model length and "prototype" length is constant. In order to achieve geometric similarity, this ratio needs to be applied to all the rock-body's length units simulated in the model."*

*"2. – Kinematic similarity is achieved if two geometrically-similar bodies undergo similar changes of shape or position (or both), provided the time required for any given change in one of the bodies is proportional to that required for the corresponding change in the other. The time-ratio must be constant for motion anywhere within the two bodies."*

*"3. – Two bodies which are geometrically and kinematically similar are also dynamically similar only if the ratio between the forces acting on corresponding particles in the two bodies, compared kind for kind, is constant:*

$$\frac{Fmg}{Fpg} = \frac{Fmv}{Fpv} = \frac{Fmf}{Fpf} = Fr \text{ (equation 1)}$$

*where: F is the force on the corresponding particles in the model (m) and the "prototype" (p); and subscripts g, v and f refer to gravitational, viscous, and frictional forces, respectively."*

A great number of analogue materials can be used in analogue modelling, to simulate the behaviour of natural rocks. These materials need to present similar physical characteristics to the natural rocks they are simulating (Szatmari and Aires, 1987). The most used material in analogue modelling experiments is dry quartz sand (natural or colour dyed), as was the case of the models here presented. Quartz sand is a good analogue for the upper crust rocks (Naylor et al., 1994), and has been used as an analogue for brittle materials (e.g. Vendeville et al., 1987; McClay, 1990; Schellart, 2000; Schreurs et al., 2006). Other materials, such as clay, plaster powder, glass microbeads, aluminium, silicone (used for the simulation of salt domes), honey (used for simulating the asthenosphere) are some of the examples that can also be used in analogue modelling.

Studies as Rossi and Storti (2003), Panien et al. (2006), Gomes and Caldeira (2011) and Gomes (2013) show the characterization of the granular materials by using the Ring Shear Tester (RST) equipment. RST reads the physical properties of granular materials such as cohesion, density, and internal friction angle. An example of this type of result is shown in

figure 3.4. The study of the physical properties of the materials has been more important and necessary to analogue modelling for making good comparisons with the natural analogues. The behaviour of the materials used in analogue modelling ultimately influences the way the structures are formed. The influence of the materials could depend on a series of other factors such as sphericity, rounding and size of the grains, which are beyond the techniques used on the preparation of the experiments (for example the sifting of the materials, Lohrmann et al., 2003). The actual behaviour of the deformation in laboratory experiments under low normal stress is more complex than used to be thought (Lohrmann et al., 2003).

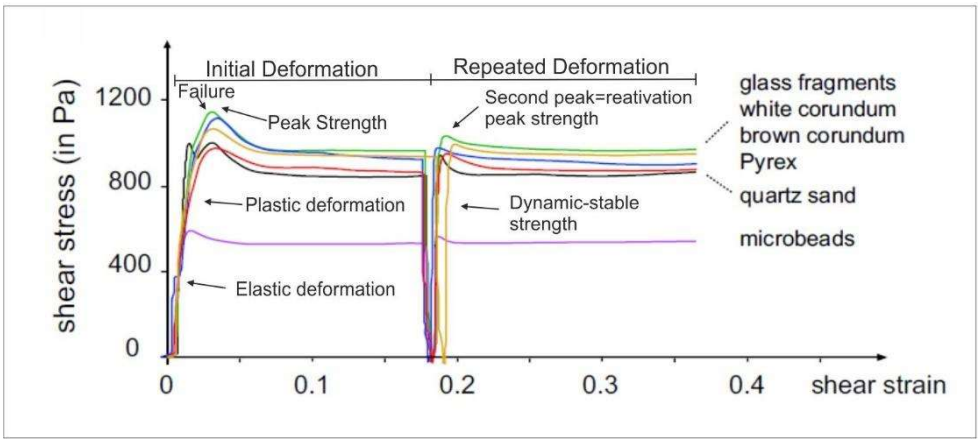


**Figure 3.4.** Example of the results obtained by Ring Shear Tester (RST), representing the variation of the shear stress with time and deformation by shear strain for some materials (from Panien et al., 2006).

# CHAPTER 4. EVOLUTION OF PARALLEL, OBLIQUE AND TRIPLE-JUNCTION RIFTS: INSIGHTS FROM ANALOGUE MODELLING

## Evolution of parallel, oblique and triple-junction rifts: insights from analogue modelling

Magda E. Oliveira[1] (corresponding author: magdaestrelaoliveira@gmail.com), Afonso S. Gomes[2,3], João C. Duarte[2,3], George S. França[1,4,5], Filipe M. Rosas[2,3], Reinhardt A. Fuck[1,4], Fernando A. Silva[6]

[1]Programa de Pós-Graduação em Geologia, Instituto de Geociências, Universidade de Brasília, Brasília, Brazil (magdaestrelaoliveira@gmail.com), [2]Instituto Dom Luiz (IDL), Faculdade de Ciências, Universidade de Lisboa, Lisbon, Portugal, [3]Departamento de Geologia, Faculdade de Ciências, Universidade de Lisboa, Lisbon, Portugal, [4]Instituto de Geociências, Universidade de Brasília, Brasília, Brazil, [5]Observatório Sismológico, Universidade de Brasília, Brasília, Brazil , [6]Departamento de Geologia, Universidade Federal do Rio Grande do Norte, Natal, Brazil

## Abstract

The study of extensional structures such as normal faults, grabens and rift systems using analogue model techniques has been widely used to understand the evolution of sedimentary basins. These have been particularly helpful to understand the generation of oil reservoirs and structural traps. The present work was inspired by the discussion on the origins of two sub-parallel grabens located in the intracratonic Parecis Basin in the centre-west of Brazil. Parallel, oblique or intersecting grabens may form by the reactivation of inherited basement weaknesses that can act as velocity discontinuities, with their geometry and proximity controlling the evolution of the resulting grabens. In this work, we use sandbox analogue experiments to investigate the geometric and kinematic evolution of two nearby, sometimes intersecting, grabens. We do this by varying the distance and the geometry of two basal velocity discontinuities (VDs). In all experiments, an extension of 3 cm (scaling to 12 km) was prescribed to affect a 3 cm thick sand pack. The materials were deformed using a plexiglas box

with two basal velocity discontinuities attached to two lateral movable walls. In a first set of experiments, we varied systematically the distance between the VDs. In the second set, we varied the angles between the VDs with different configurations, including situations in which the VDs intersect forming triple junctions. The results show that when the VDs are initially close (< 2 cm, corresponding to ~8 km in nature) there is the formation of a wide graben composed of two sub-grabens that interfere with each other, while if the spacing between the VDs is > 2 cm, the grabens develop independently and do not interfere. Furthermore, it is possible to conclude that whenever (not interfering) VDs are prescribed to the base of a sand pack it always leads to the formation of asymmetric grabens, except when the two VDs are initially close to each other. In the experiments with conjugate triple-junction VDs, the extension was shared between two independent asymmetric grabens where the VDs were at a certain distance from each other, and always led to the formation of a wide graben where the VDs were close or intersect each other.

**Keywords:** Analogue modelling; Rifting; Parecis Basin; Parallel grabens; Oblique grabens; Structural style of extensional graben interference.

## 1. Introduction

The formation of extensional structures that develop in the context of the evolution of sedimentary basins, has been widely studied through the use of analogue modelling techniques (Koyi, 1997). These studies include large-scale continental extension (Brune and Ellis, 1997; Corti et al., 2003; Beniest, 2017; Zwaan et al., 2019) the development of orthogonal and oblique rifts (Withjack and Jamison, 1986; McClay and White, 1995; Clifton et al., 2000; Corti et al., 2001; Zwaan et al., 2016) extensional deformation associated with inherited structures (Keep and McClay, 1997; Henza et al., 2011; Chattopadhyay and Chakra, 2013), and rift symmetry/asymmetry (McKenzie, 1978; Wernicke, 1985; Allemand et al., 1989; Brun and Beslier, 1996; Nagel and Buck, 2004).

The starting point to this work was the ongoing discussion on the origin of two nearby Neoproterozoic grabens located in the Parecis Basin, in Brazil (Fig. 1A), which developed during the early stages of intracratonic extensional deformation. The tectonic evolution of the

Parecis Basin is controversial, with two main conflicting hypotheses proposed for its evolution. One considers that the basin was formed in the Palaeozoic (Siqueira, 1989; Bahia et al., 2006, 2007), while the other argues that it started to form in the Neoproterozoic in association with the development of the Paraguay Fold Belt (Haeser et al., 2014; Vasconcelos et al., 2014; Loureiro, 2016). Despite this discrepancy, all the authors agree that the first stages of this basin evolution led to the formation of two sub-parallel grabens – Pimenta Bueno and Colorado (Fig. 1B). The specific geometry of these grabens suggests that they were formed by the reactivation of pre-existent structures of the Amazonian Craton. A simple sketch of the evolution of the grabens is represented in figure 1B. According to Loureiro (2016), the grabens resulted from an episode of E-W extensional deformation in the Neoproterozoic in the context of the break-up of the Rodinia supercontinent.

The objective of this work was to investigate the initial stages of continental rifting using analogue models inspired by the Parecis Basin. In particular, we aimed at understanding what are the conditions in which two grabens, forming nearby, mutually interfere? What is the minimum distance at which they no longer interfere? And what are the resulting deformational patterns? To achieve this objective, we have developed a series of experiments comprising the formation of parallel, oblique, and conjugate (triple-junction) grabens. We used basal velocity discontinuities (VDs) to localize the position of the different grabens, simulating basement weaknesses/heterogeneities (Deng et al., 2018; Zwaan et al., 2019). In the first set of experiments, we systematically varied the spacing between two parallel basal VDs. In a second set, we varied the angles between the VDs in different configurations. Finally, we discuss our results in the context of other experiments and natural examples.

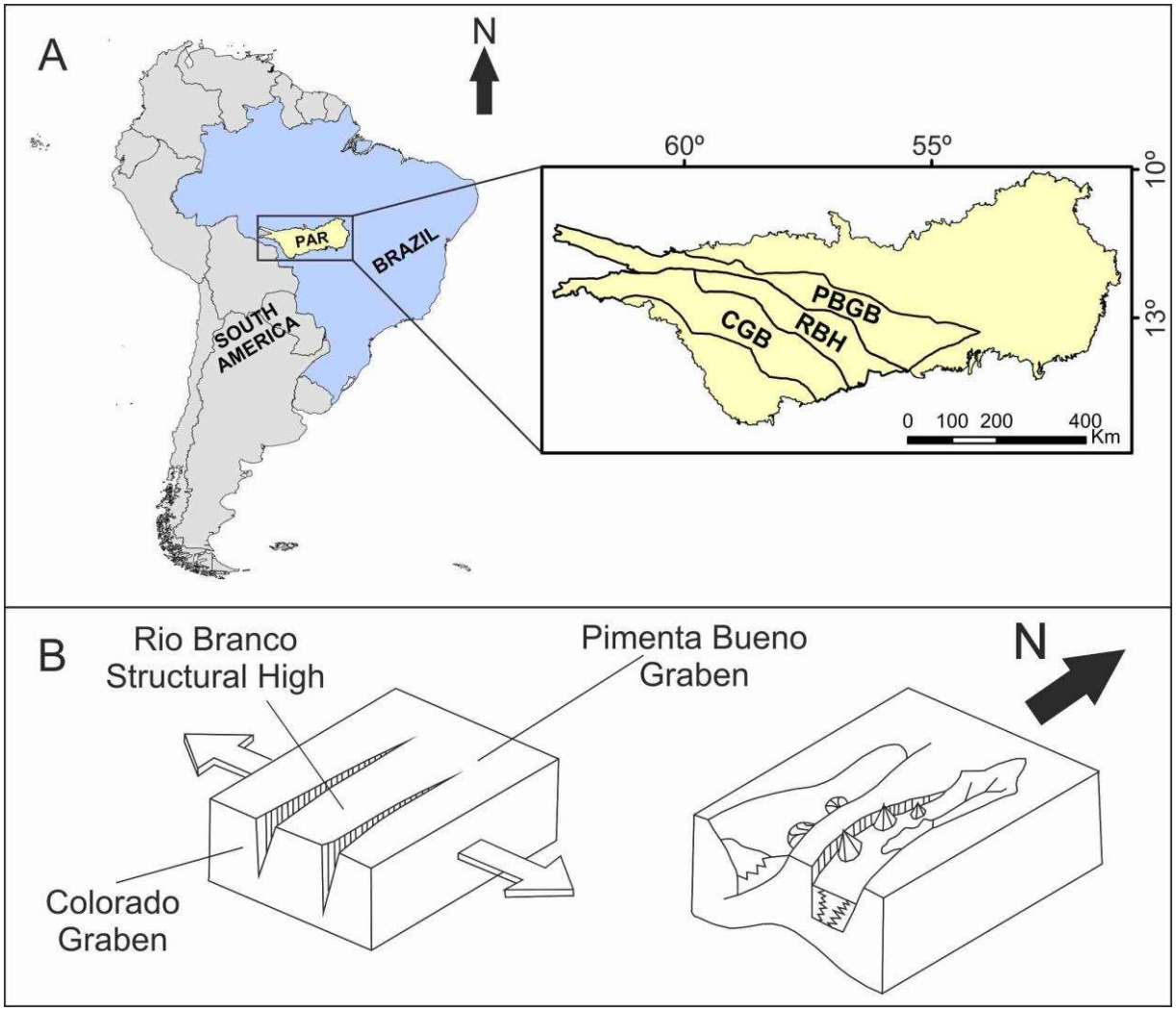


**Figure 1**. A. Location of Parecis Basin (PAR), Colorado (CGB) and Pimenta Bueno grabens (PBGB); RBH – Rio Branco High. B. Schematic representation of the initial stages of development of the Parecis Basin with the formation of the Pimenta Bueno and Colorado grabens (modified from Bahia et al., 2007 and Loureiro, 2016).

# 2. Methodology

## 2.1. Material properties and scaling

A large variety of analogue materials has been used in analogue modelling experiments, to mimic the behavior of a wide range of natural rocks and materials. In our experiments, we used natural and coloured quartz sand. Quartz sand is a good analogue for upper crustal rocks and it has been commonly used as an analogue for brittle natural materials (e.g. Vendeville et al., 1987; McClay, 1990; Schellart, 2000; Schreurs et al., 2006). Quartz sand deforms in a brittle

manner that follows the Coulomb criterion (Hubbert, 1937, 1951; Mandl, 1988; Schellart, 2000). The sand used is commercialized under the tradename SIFRACO NE34, which is a fine, well rounded, and well-sorted quartz sand (as in e.g., Klinkmüller et al., 2016; Rosas et al., 2017; Gomes et al., 2019).

According to Hubbert (1937), an adequate scaling of analogue materials is achieved when the ratios between model and natural prototype are independently established for the fundamental units of length ($\lambda$), time ($\tau$), and mass ($\mu$). The used sand has an internal friction coefficient of ~0.5-0.6, which is within the normal range for natural rocks of $0.5 \leq \mu_c \leq 0.8$ (Ranalli, 1995), and has a density of 1600 kg/m$^3$, corresponding to a density ratio to the natural prototype of $\delta \approx 0.62$. The 3 cm sand pack in the models simulates a ~12 km thick upper-crust, corresponding to a length ratio of $\lambda=2.5\text{x}10^{-6}$. The mass ratio was of $\mu=9.69\text{x}10^{-18}$. The material properties and scaling ratios are presented in table 1. Note that in sand-only experiments deformation is time independent. The inertial accelerations were considered negligible since their values (cm/yr/Ma) are at least 22 orders of magnitude lower than the acceleration of gravity, g=9.8 m/s$^2$.

**Table 1.** Analogue modelling material properties and scaling.

| Material properties and scaling parameters | Quartz sand (model) | Upper Crust (nature) | Ratio: model/nature |
|---|---|---|---|
| Grain shape | Well-rounded | - | - |
| Grain size (mm) | <0.30 | - | - |
| Density (kg/m$^3$) | 1600 | 2600 | $\delta = 0.62$ |
| Internal friction angle $\varphi$ (º) | ~30 | - | - |
| Coefficient of internal friction, $\mu_c$ | ~0.5-0.6 | ~0.5-0.8 | - |
| Cohesion, $C_0$ (Pa) | Negligible (~100) | 40 x 10$^6$ | - |
| Gravity acceleration (m/s$^2$) | 9.81 | 9.81 | $\Upsilon_g = 1$ |
| Length, L (m) | 0.3 (3.0 cm) | 12000 (12 km) | $\lambda = 2.5\text{x}10^{-6}$ |
| Mass, M (kg) | - | - | $\mu=9.69\text{x}10^{-18}$ |

## 2.2. Experiment configuration

We have performed two sets of analogue modelling experiments. In the first set, we systematically varied the distance between two basal velocity discontinuities (VDs). In the second, we tested different angles and modes of intersection between the two VDs. A complete

list of the experiments performed is presented in table 2. The sandbox was composed of two fixed walls and two parallel lateral moving walls made of acrylic plates (see Fig. 2). The two basal VDs were simulated by attaching two sandpaper sheets to the lateral moving walls (see Fig. 2 for the configurations of the VDs). These two VDs moved over the base of the box, which was also covered with a fixed sandpaper sheet in order to maintain a constant coefficient of friction all along the base of the experimental box. The box was then filled with a 3 cm thick sand cake composed of alternating layers of colored and natural (uncolored) sand. The sand was sieved over the box using a mobile elongated funnel running over lateral rails. The thickness of the model was scaled using data from Faria (2015). We did not use syntectonic sedimentation to avoid interfering with the experiment, and to be able to clearly map the structures forming on the surface of the experiment. The lateral walls were attached to two stepping motors and moved at a constant velocity of ~1.44 cm/h.

In the first set of experiments, we varied systematically the distance between two parallel VDs from 0 to 5 cm, in steps of 1 cm, corresponding to experiments P-00, P-01, P-02, P-03, P-04 and P-05 in Table 2 (see general configuration in Fig. 3A). In a second set, we tested further four initial VD's configurations: two oblique (O) and two triple-junction (TJ) geometries. In experiments O-01, O-02, and O-02a, we placed two VDs at an angle of ~6º (Fig. 3B, C). In experiment O-01, the VDs had an initial gap across the model width (i.e., in the direction parallel to the moving walls) varying from 0 to 4 cm (Fig. 3B). In experiments O-02 and O-02a this initial gap varied between 1 and 5 cm (Fig. 3C). The difference between these two experiments (O-02 and O-02a) is that in O-02a, one of the moving walls was stopped after 1.5 cm of finite extension, this is, after 0.75 cm of extension to each side, while the other wall continued to move for another 0.75 cm, totaling 2.25 cm of extension for the entire experiment, instead of the general 3 cm that all other experiments underwent (including experiment O-02). In the experiments TJ-01 and TJ-02, the VDs had three branches forming triple-junctions (see Results section). In experiment TJ-01, the VDs were placed in contact along the width of the box in its "southern" segment, progressively diverging away with an angle of 60º towards the "northern" lateral boundary of the box (see Fig. 3D). In the experiment TJ-02, the two VDs were placed obliquely at angles of 60º in relation to the moving walls and in relation to each other, with one sheet overlapping the other (see Fig. 3E).

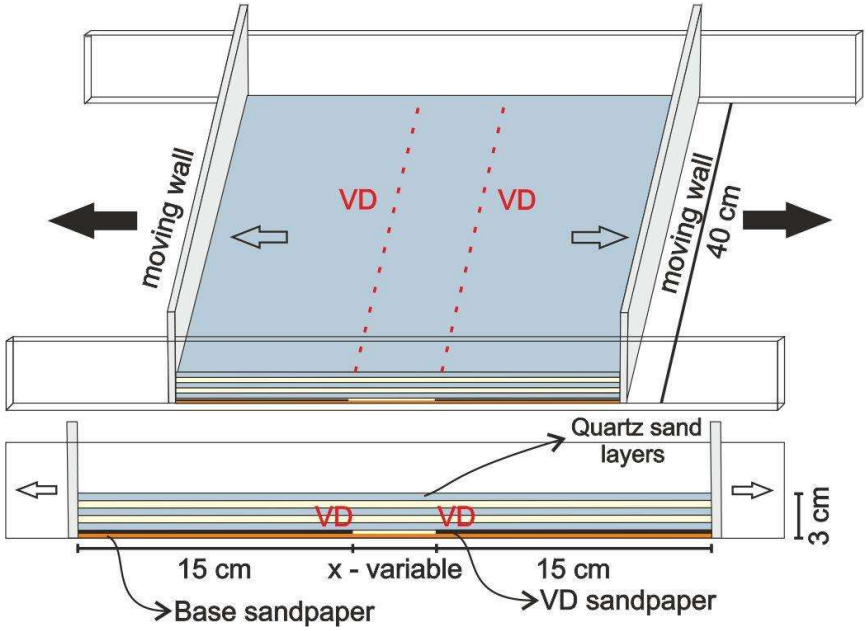


**Figure 2.** Initial configuration of the sandbox. The coloured layers represent quartz sand (natural and coloured). Each layer had a thickness of approximately 0.5 cm and the total thickness of the package was 3 cm. Note the variable position of the basal velocity discontinuities (VDs). Sandpaper sheet thickness is exaggerated for illustration purposes.

**Table 2.** Summary of the experiments performed in this study.

| | Experiment | Initial spacing between VDs | Angle between VDs | Scaled initial distance between VDs |
|---|---|---|---|---|
| 1st set | P-00 | 0 cm | 0º | 0 km |
| | P-01 | 1 cm | 0º | 4 km |
| | P-02 | 2 cm | 0º | 8 km |
| | P-03 | 3 cm | 0º | 12 km |
| | P-04 | 4 cm | 0º | 16 km |
| | P-05 | 5 cm | 0º | 20 km |
| 2nd set | O-01 | variable between 0 to 4 cm | ~6º | variable between 0 to 16 km |
| | O-02 | variable between 1 to 5 cm | ~6º | variable between 4 to 20 km |
| | O-02a | variable between 1 to 5 cm | ~6º | variable between 4 and 20 km |
| | TJ-01 | variable | 60º | variable |
| | TJ-02 | variable | 60º | variable |

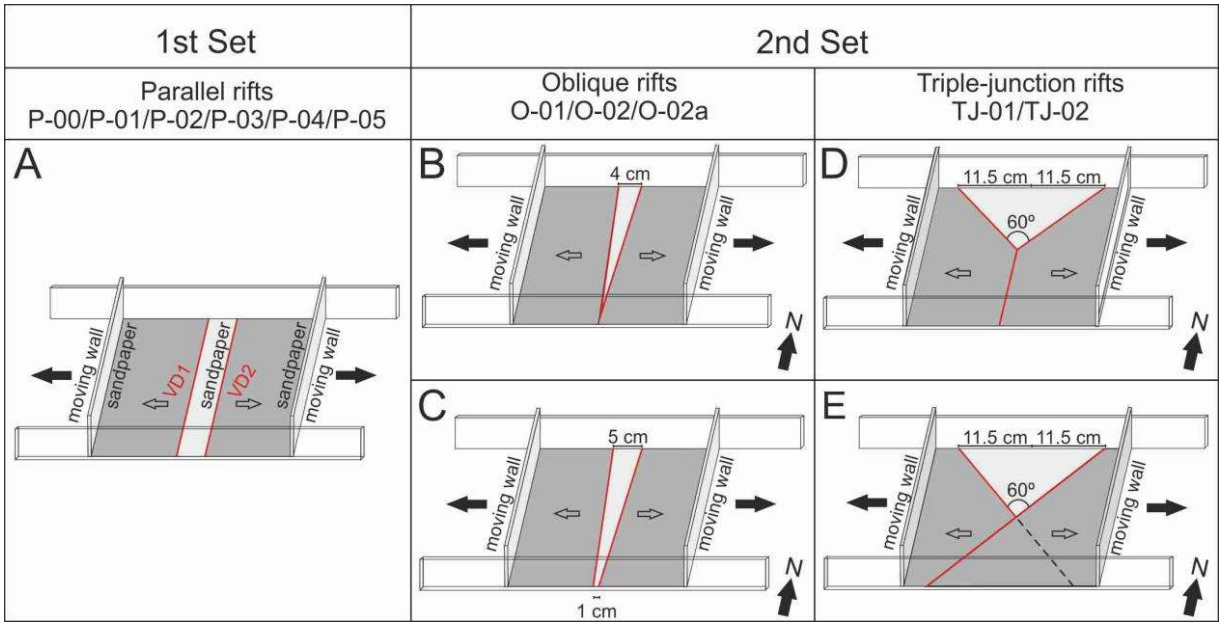


**Figure 3.** Configuration of all the experiments. A. Configuration of the 1st set of experiments (P-00, P-01, P-02, P-03, P-04, and P-05), with the spacing of the VDs varying between 0 and 5 cm in steps of 1 cm. B. O-01. The VDs were placed at an angle (~6º) with their distance varying continuously between 0 and 4 cm. C. O-02 and O-02a. The VDs were placed at an angle (~6º) with their distance varying continuously between 1 and 5 cm. D. TJ-01. The configuration between the VDs varies along-strike; they are placed parallel (orthogonal to the extension) in the southern part of the box and diverge with an angle of 60º towards the northern boundary. E. TJ-02. The VDs make an angle of 60º between them (and in relation to the moving walls), intersecting at the centre of the box. Note that in the southern part of the box one of the VDs is covered by the sandpaper attached to the other wall, and thus does not affect the sand cake. Note that this configuration causes the migration of the "triple-point" to the south as the experiment unfolds.

# 3. Experimental results

## 3.1. First set of experiments: parallel VDs

In the first set of experiments, we varied systematically the distance between two parallel basal VDs (between 0 and 5 cm, in steps of 1 cm). All experiments underwent a total extension of 3 cm (~10% of the total model width).

In experiment P-00, the two VDs were initially in contact. After 1 cm of extension (33.3% of the total prescribed extension) it was possible to observe a graben, 4.2 cm wide (scaling to 16.8 km) and parallel to the VDs (Fig. 4A). At 2 cm of extension, two new normal faults formed inside the graben parallel to the rift-borders (Fig. 4B). The final width of the graben was 6.5 cm (scaling to 26 km), and its lower parts had depths of ~1.8 cm (scaling to 7.2 km) (Fig. 4C). In

the final stage of the experiment, the rift system was composed of a nearly symmetric graben with a narrow low-elevation central ridge. In the cross-sections, it is possible to observe that most of the extension was accommodated by the two main rift-border faults. The two inner normal faults, which were no longer active at this stage, crosscut each other forming a central ridge (Fig 4D-F). The two main graben border faults dip 58º and have a strongly exposed planar scarp face, while the two (inferred) internal faults have higher angles varying between 60º and 70º.

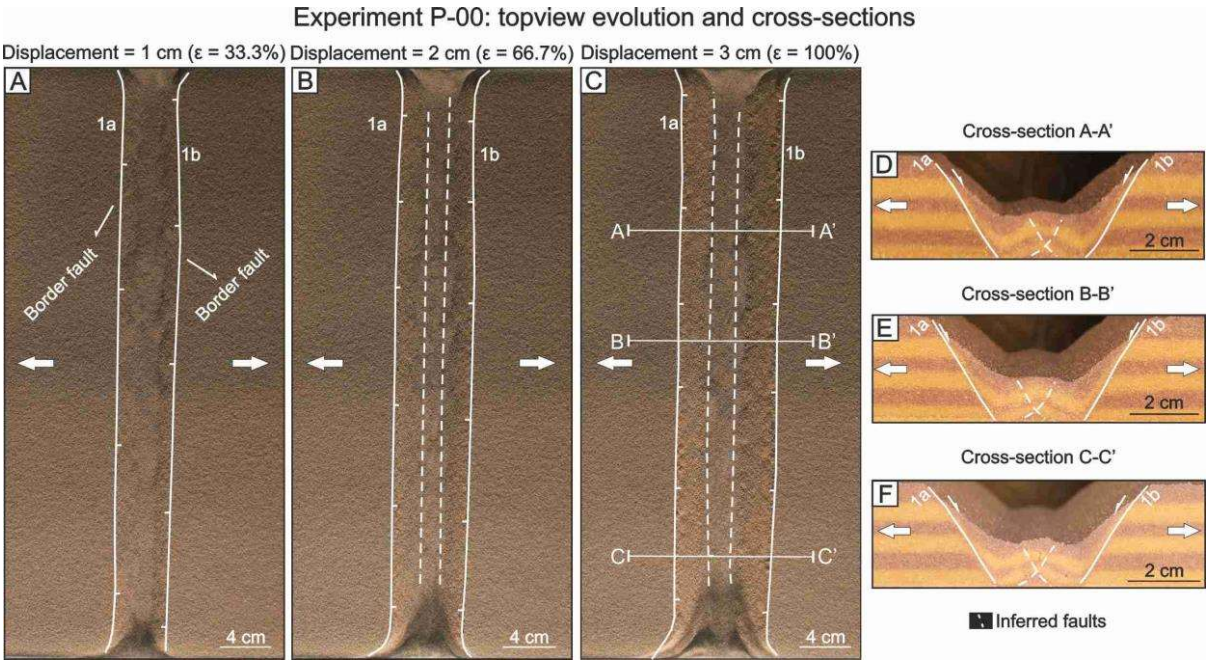


**Figure 4.** Results of the experiment P-00 with the two VDs initially in contact: topview evolution and cross-sections of the final stage. Note the formation of a symmetric graben. A. Stage corresponding to 1 cm displacement between the basal VDs – formation of two border faults with a linear geometry. B. Stage corresponding to 2 cm displacement – new inner faults develop inside the graben C. Final stage corresponding to a displacement of 3 cm – it is possible to observe two grabens with a smaller middle ridge. D, E and F. Cross-sections of the experiment at the final stage, showing the smaller middle ridge and the two border faults also observed in topview. 1a, 1b – first faults to develop (border faults).

In the experiment P-01 (Fig. 5), the initial distance between VDs was 1 cm. In the first stages of extension (33.3 %, Fig. 5A), it was possible to observe the formation of a large graben (4.3 cm wide, scaling to 17.2 km), limited by two main border normal faults, and with a middle ridge also limited by two normal faults but dipping towards (and crosscutting) each other. This ridge probably formed first as a sort of central graben limited by two antithetic listric faults but became relatively elevated as the extensional deformation migrated away towards the border faults and progressively concentrated in faults 2a, 2b, 3a, and 3b (Figs. 5B, 5C). The two

depocenters developed in a similar and symmetric way. With increasing displacement, new normal faults formed inside the sub-grabens, antithetically to the main bordering faults (Fig. 5C). If considered individually, the sub-grabens would have an asymmetric geometry, each with a main border fault and smaller antithetic faults on the inside elevation (see Fig. 5C-F). The border faults and the inner faults dip ~60º (see Figs. 5D-F). The final width of the entire rift structure comprising both grabens was 7.8 cm (scaling to 31.2 km in nature), with a maximum depth of ~1.6 cm (scaling to ~6.4 km, see Figs. 5D-F).

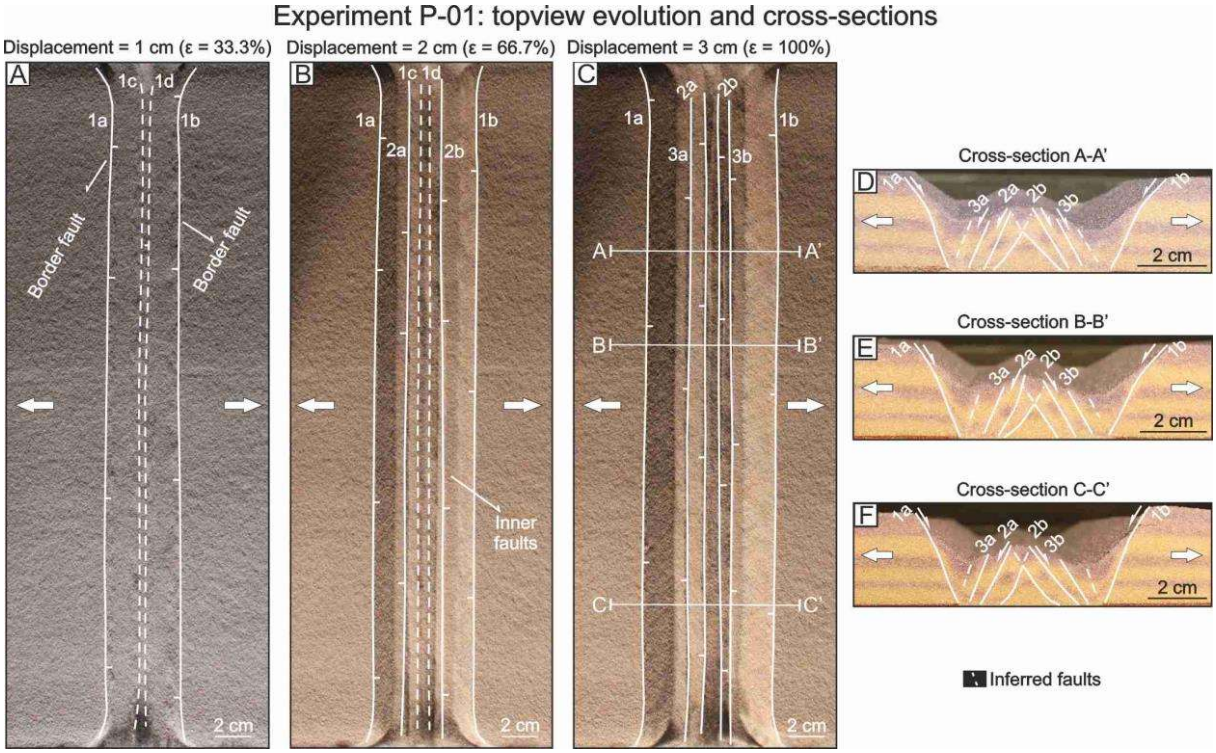


**Figure 5.** Results of the experiment P-01 with the two VDs initially distancing 1 cm: topview evolution and cross-sections of the final stage. A. Topview of the experiment after a displacement of 1 cm – it is possible to observe a wide graben limited by two normal sub-linear border faults. Two inner faults start to form (1c and 1d). B. Topview after a displacement of 2 cm – new inner normal faults formed, antithetic to the border faults. C. Topview photo of the final stage of the experiment after a displacement of 3 cm – at this stage it is possible to observe several faults which interfere and disassemble the internal ridge. D, E and F. Final cross-sections A-A', B-B' and C-C' showing the entire structure. It is possible to recognize a wide rift zone composed of two depocenters (sub-grabens). Here it is possible to observe that the two most inner faults crosscut each other. 1a, 1b – first developed border faults. 2a, 2b – new inner faults. 3a, 3b – last inner faults to form.

In the experiment P-02, the initial distance between the two VDs was 2 cm. From the topview images, we can observe that the initial stages of the experiment are similar to experiment P-01 (compare Figs. 5 and 6). After 1 cm of displacement two major normal border faults formed defining a 5.4 cm wide graben (scaling to 21.6 km; Fig. 6A). At this point, it was

also possible to observe two inner normal faults delimiting a central ridge, which (structurally) correspond to a narrow horst elevated between two parallel grabens. As extension increases, the grabens become deeper, and a new series of faults form progressively further away from the central horst, accommodating the increasing extensional strain (faults 2a, b, and 3a, b; Fig. 6). Both the border faults and the inner faults maintain an along-strike continuous linear geometry through the entire span of the experiment (Fig. 6C). Note also that even though the entire deformed region can be considered a symmetric wide graben separated by a median horst, each sub-graben is asymmetric, limited by a single border external fault, with several opposite dipping inner faults forming a listric system (see Figs. 6D-F). In this experiment, the median horst is clearly more elevated than in the two previous ones (~2.8 cm in experiment P-02, compared to 1.3 cm and 1.9 cm in experiments P-00 and P-01, respectively). The final total width of the rift system comprising the two sub-grabens was 8.8 cm (scaling to 32 km), with a maximum depth of ~1.4 cm (scaling to 5.64 km) in their lower parts. All the faults that formed in this experiment show dipping angles between 66º and 75º (Figs. 6D-F).

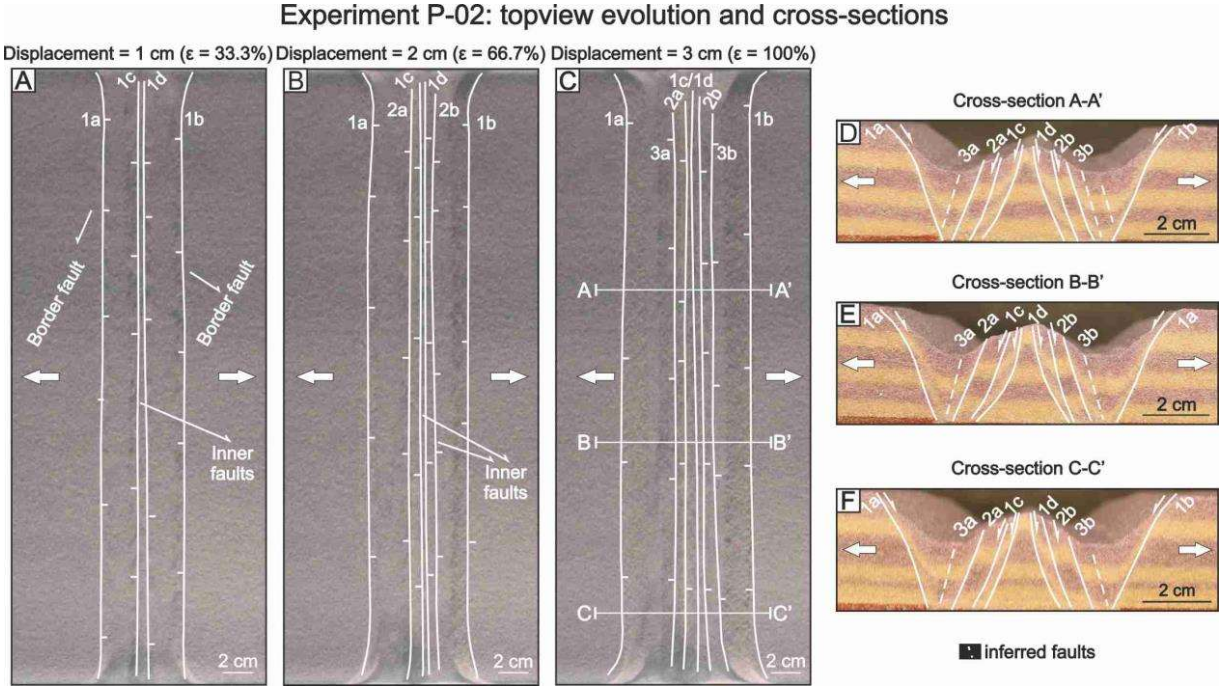


**Figure 6.** Results of the experiment P-02 with the two VDs initially distancing 2 cm: topview evolution and cross-sections of the final stage. A. Topview after a displacement of 1 cm – it is possible to identify two grabens each limited by linear normal border faults and normal inner faults. The normal inner faults define a narrow central horst. B. Topview after a displacement of 2 cm – it is possible to observe the formation of new inner faults propagating away from the central horst. C. Topview of the final stage (after a displacement of 3 cm) – new inner faults formed with the widening of the two grabens. D, E and F. Final cross-sections. It is possible to observe a narrow horst between the two grabens. The inner faults show a listric geometry in relation to the main border faults. 1a, 1b, 1c, 1d – first faults to develop. 2a, 2b – new inner faults. 3a, 3b – last faults to form.

In the experiment P-03, the initial spacing between the VDs was 3 cm (scaling to 12 km). In this experiment, it is also possible to observe that after 3.3% of extension two individual grabens were fully formed (Fig. 7A), separated by a horst that retained the full thickness of the sand pack (3 cm), and outwards limited by two prominent and linear border faults. Similarly, to the previous experiments, new inner faults progressively formed away from the middle horst, increasingly dismantling it, possibly due to the activation and rotation of faults 1c and 1d (Fig. 7B-C). The final width of the deformed area was of 9.8 cm (scaling to 39.2 km), with each graben extending for about ~4.3 cm (scaling to ~17.2 km), and with depths of ~1.4 cm (scaling to 5.6 km).

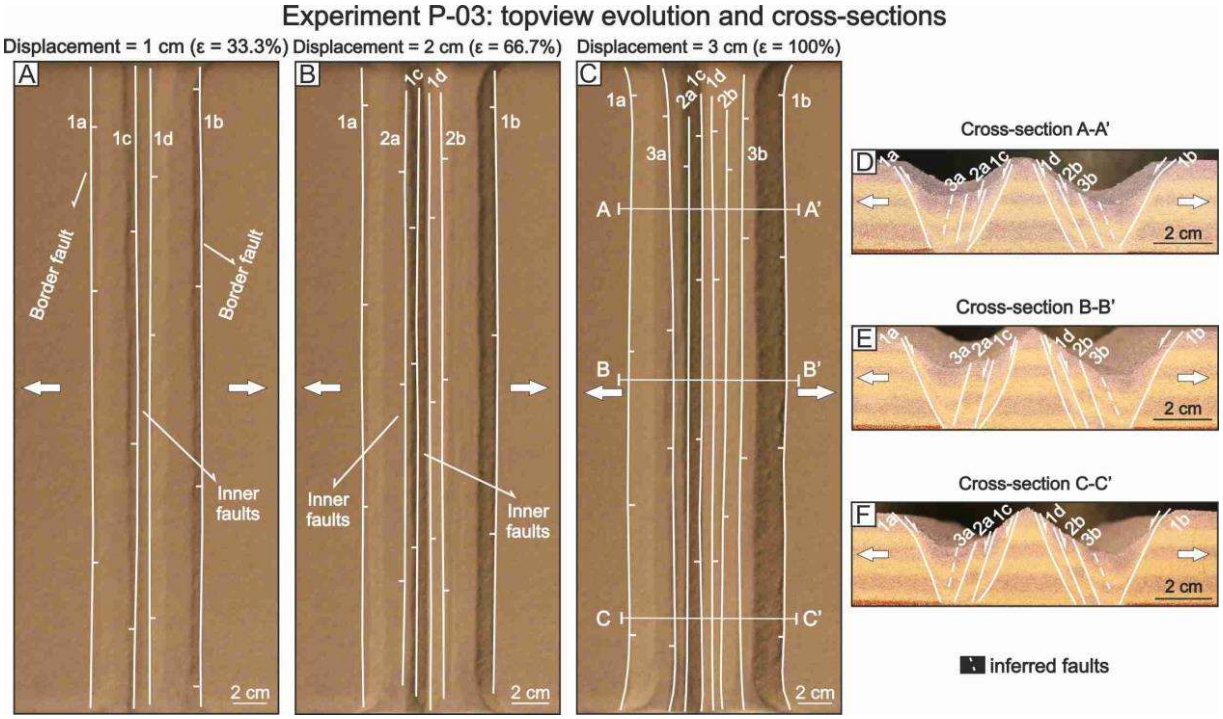


**Figure 7.** Results of the experiment P-03 with the two VDs initially distancing 3 cm: topview evolution and cross-sections of the final stage. A. Topview of the experiment after a displacement of 1 cm – it is possible to identify two grabens each limited by linear normal border faults and normal inner faults. The normal inner faults define a central horst, which is wider than the previous experiment. B. Topview after a displacement of 2 cm. C. Topview after a displacement of 3 cm. D, E and F. Final stage cross-sections A-A', B-B' and C-C' showing two distinct asymmetric grabens separated by a middle horst. 1a, 1b, 1c, 1d – first faults to form. 2a, 2b – new inner faults. 3a, 3b – last inner faults to form.

In the experiments P-04 and P-05 (Figs. 8 and 9, respectively), with spacing between the VDs of 4 and 5 cm, respectively (scaling to 16 and 20 km), the results were similar to experiment P-03, with each individual graben forming further away and limited by an increasingly wider horst. In the experiment P-05, the total deformed area reached a width of 10 cm (scaling to 40 km in nature). In figure 10 we compare the final stage cross sections for all the experiments. Here, we can observe that in experiments P-00, P-01 and P-02 the two VDs lead to the formation of a wide "symmetric" graben with two depocenters limited by a central structural elevation, while in experiments P-03, P-04 and P-05 they led to the formation of two distinct asymmetric grabens separated by a well-defined middle horst.

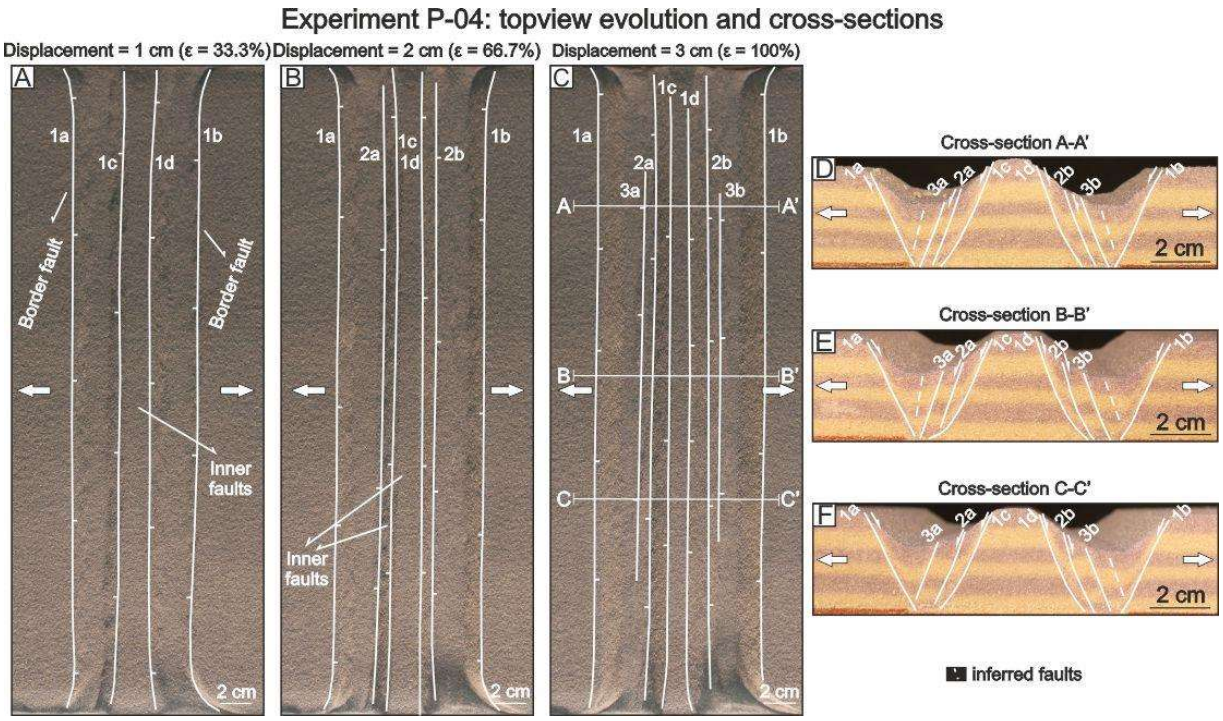


**Figure 8.** Results of the experiment P-03 with the two VDs initially distancing 3 cm: topview evolution and cross-sections of the final stage. A. Topview of the experiment after a displacement of 1 cm – it is possible to identify two grabens each limited by linear normal border faults and normal inner faults. The normal inner faults define a central horst, which is wider than the previous experiment. B. Topview after a displacement of 2 cm. C. Topview after a displacement of 3 cm. D, E and F. Final stage cross-sections A-A', B-B' and C-C' showing two distinct asymmetric grabens separated by a middle horst. 1a, 1b, 1c, 1d – first faults to form. 2a, 2b – new inner faults. 3a, 3b – last inner faults to form.

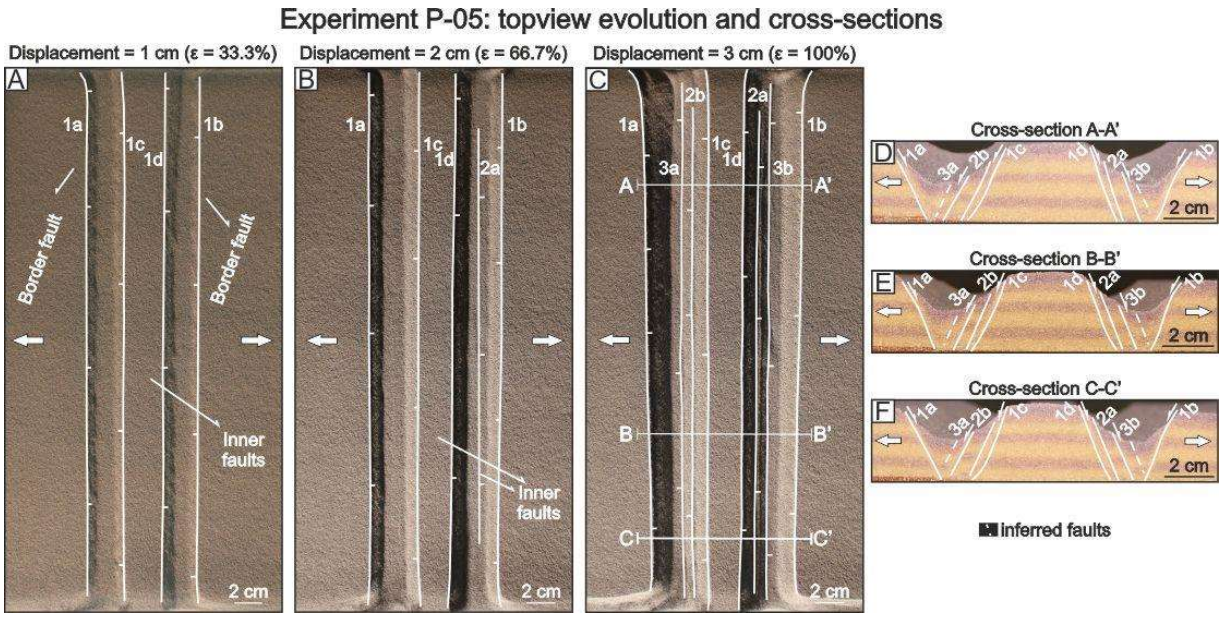


**Figure 9.** Results of the experiment P-05 with the two VDs initially distancing 5 cm: topview evolution and cross-sections of the final stage. A. Topview after a displacement of 1 cm. B. Topview after a displacement of 2 cm. C. Final stage. D, E and F. Cross-sections A-A', B-B', and C-C'. Note that the central horst is much wider than in the previous experiments. 1a, 1b, 1c, 1d – first faults to form. 2a, 2b – new inner faults. 3a, 3b – last inner faults to form.

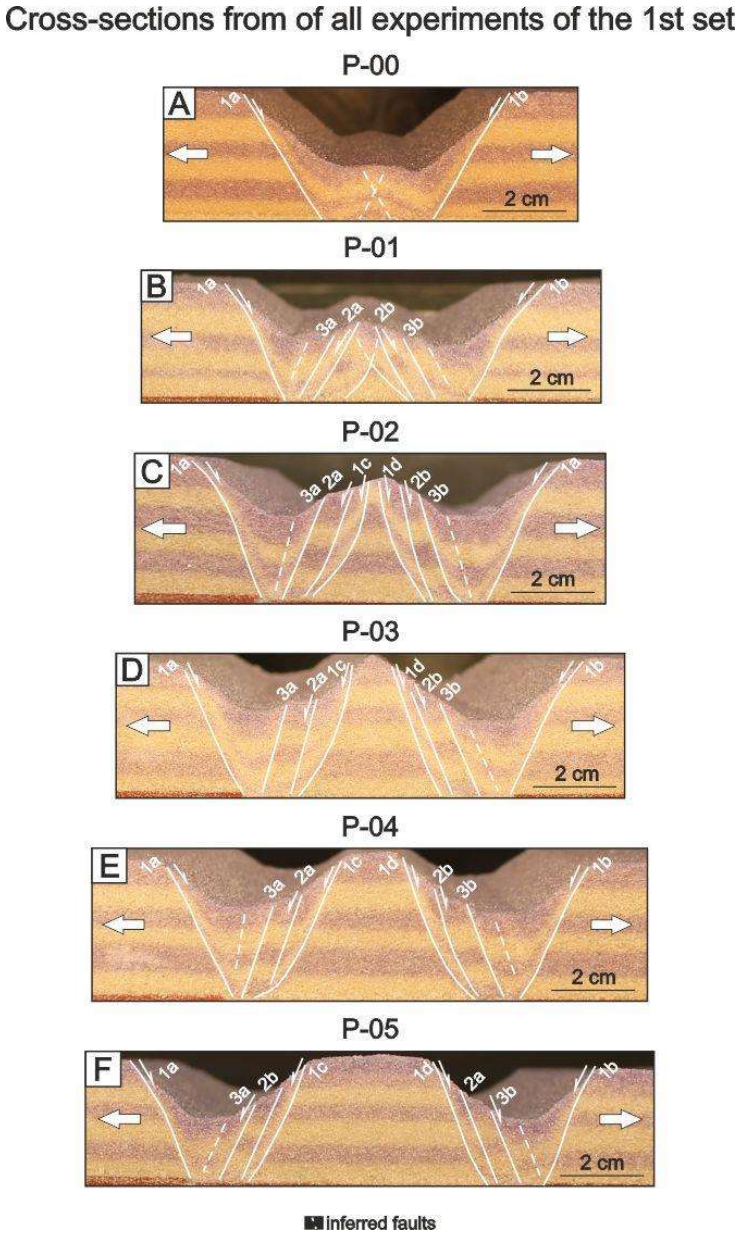


**Figure 10.** Comparison of the final stage of all experiments from set 1, with the spacing between the VDs varying between 0 and 5 cm, in steps of 1 cm. Note that in experiments P-00, P-01 and P-02 it is possible to observe a wide "symmetric" graben with a central ridge/horst, while in the experiments P-03, P-04 and P-05 two asymmetric sub-grabens are clearly individualized, separated by a fully formed middle horst.

## 3.2. Second set of experiments: oblique and triple-junction VDs

In the second set of experiments, we varied the angles between the VDs, carrying out a total of five experiments with different configurations (see Fig. 3B to E). The total amount of prescribed extension was kept at 3 cm (~10%), except for experiment O-02a, where total extension was just 2.25 cm. The experiments were divided into two sub-sets: Oblique VDs –

experiments O-01, O-02 and O-02a (see Figs. 3B, C) – and triple-junction VDs – experiments TJ-01 and TJ-02 (Figs. 3D, E).

In the experiments with oblique VDs we aimed at exploring the development of structures accommodating variable along strike extension and tectonic interference. This would comply with natural geological systems in which supracrustal extension is nucleated and propagated along two intersecting directions. To investigate the structural styles of such a configuration, and implied extensional tectonic interference, two VDs were set making an oblique angle with each other (Fig. 3B, C). In the triple-junction VD experiments, the goal was to understand the structural style imparted by different geometries of connected supracrustal extensional domains (or shallow rifts, Fig. 3D, E). In this set, an arbitrary spatial reference was used to simplify the description of the models - north (N), south (S), east (E) and west (W).

### 3.2.1. Oblique rifts

In experiment O-01, the initial distance between the VDs varied between 0 and 4 cm, forming an angle of 6º between the VDs (Fig. 3B). The experiments O-02 and O-02a had a similar angular configuration of experiment O-01, but the distance between the VDs varied between 1 and 5 cm instead (Fig. 3C). The difference between the two O-02 experiments was that in O-02a we stopped one of the moving walls after 1.5 cm of finite extension, continuing to move apart only the other one. We did this to understand if each rift system was affected by the two VDs or only by the respective underlying one ascribed to the corresponding moving wall.

In the experiment O-01, after 1 cm of extension (Fig. 11A), two ~3.2 cm-wide oblique grabens formed, each limited by two border normal faults and two normal inner faults. In the northern segment of the rift system, two initial individual grabens formed separated by a middle horst. The horst-bounding normal faults intersect towards the south, where the initial VD distance was between 0 and 3 cm, defining the southwards termination of the middle horst and the merging of the grabens. To the south of the intersection, initially there was a depression between the grabens, that progressively evolved to form a small ridge (see final step in Figs. 11C, F). With further increments of extension, new inner faults develop forming a complex interference pattern. In the northern segment of the rift, these new inner faults display an outwards dip polarity defining the flanks of the middle central horst. Conversely, in the southern

segment of the rift system the normal faults now dip inwards towards the centre of a simple main graben, being part of the border (outer) shoulders of a main structural depocenter (Fig. 11B). From the cross-sections obtained for the experimental end stage, it is possible to observe that in the northern part of the model there are two independent asymmetric grabens separated by a horst (cross-section A-A'; Fig 11D), with a total deformation region ~10 cm wide (scaling to ~40 km). In the southern part, one large graben formed displaying a central ridge system (cross-sections B-B' and C-C' in Figs. 11E and 11F, respectively), with a total deformation zone ~7 cm wide (scaling to ~28 km).

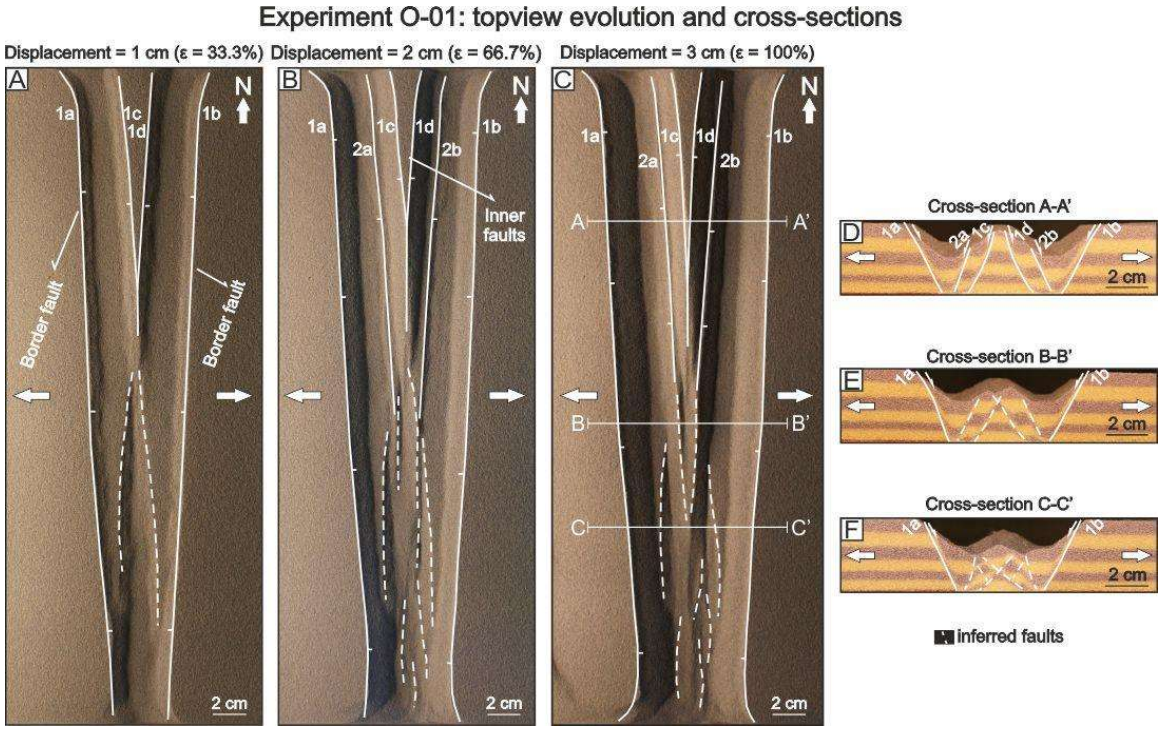


**Figure 11.** Results of the experiment O-01: topview evolution and cross-sections of the final stage. A. Topview after a displacement of 1 cm – it is possible to observe two oblique grabens, limited by two main border faults, that merge towards the southern part of the model. B. Topview after a displacement of 2 cm – new inner faults formed inside the grabens. C. Final stage – it is possible to observe a complex fault interference pattern, dominant in the southern part of the model. D, E and F. Final stage cross-sections A-A', B-B' and C-C'. In the north part, it is possible to recognize two individual asymmetric grabens, whereas to the south the grabens interfere forming a wide symmetric graben with a central ridge.

In the experiment O-02, the VDs configuration was the same as in the previous experiment, but the initial distance varied from 1 to 5 cm along-strike, also maintaining an angle of ~6º between the VDs. After 1 cm of extension (Fig. 12A), it is possible to observe that two oblique grabens were fully formed (~2.8 cm wide, scaling to 11.2 km), limited by two normal border faults and two inner faults that intersect in the southern half of the experiment. To the north of

the intersection, the grabens are limited by a central horst, while to the south one single main graben starts to form, although at this stage still encompassing two main depocenters separated by a fault-bounded middle ridge. The interference between the inner normal faults delineating the southwards narrowing of the central horst occurs where the initial distance between the VDs was less than 3 cm. At 2 cm of extension (6.7%, Fig. 12B) the two grabens widen, controlled by the border and inner faults. New inner faults are formed to the south of the intersection, where the grabens interfere. At the final stage of the experiment (3 cm of extension, Fig. 12C), the inner faults propagate to the north of the intersection (faults 2a and 2b in Fig.12C). To the south, a complex pattern of interfering normal faults is observed. The final width of the grabens was ~4.7 cm with depths of ~1.5 cm (scaling to 18.8 km and 6 km, respectively). In the final stage cross-sections (Figs. 12D-F), the rift system geometry varies as a function of the initial distance between the VDs. In the cross-section A-A' (Fig. 12D), two independent asymmetric grabens are observed over a ~10 cm wide deformation zone (scaling to 40 km), each limited by one border fault and several antithetic inner faults. The normal faults display angles varying between 62º and 70º. The horst shows a height of ~3 cm (original sand cake height, scaling to ~12 km) and the depth of the grabens is of ~1.5 cm. In cross-section B-B' (Fig. 12E), approximately at the centre of the model, it is still possible to observe two individual asymmetric grabens separated by a narrow middle horst ~3 cm high. In figure 12F, the cross-section C-C' shows two interfering grabens, with two inner faults cross-cutting each other. This means that this elevation is not technically a horst but was caused by the progressive relative deepening of the two grabens. In general, it can be observed that where the two VDs had an initial separation between 1 and 2 cm, two interfering grabens form a wide symmetric graben with two depocenters separated by an inner ridge. This is consistent with the experiments P-00 and P-01 of the first set (Figs. 5, 6). On the other hand, when the initial distance between the VDs was between 3 and 5 cm, two individual grabens clearly separating a central horst formed, which is consistent with experiments P-03, P-04 and P-05 from the first set (Figs. 7, 8 and 9, respectively).

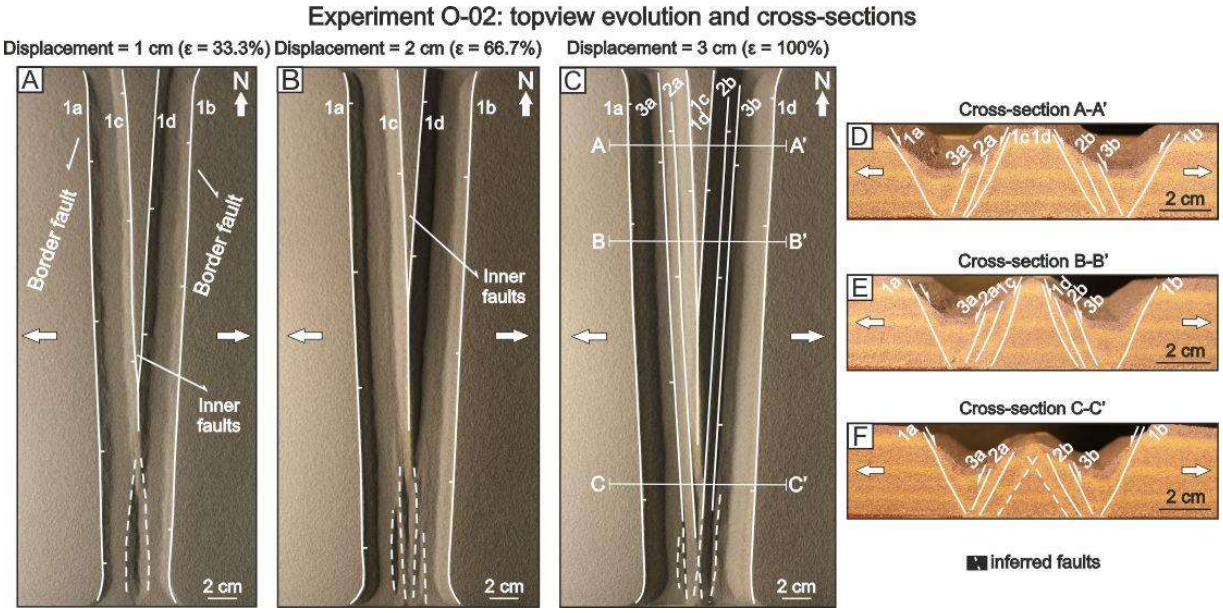


**Figure 12.** Results of the experiment O-02: topview evolution and final stage cross-sections A. Topview after a displacement of 1 cm. B. Topview after a displacement of 2 cm. C. Final stage. D, E and F. Final stage cross-sections A-A', B-B' and C-C'.

In the experiment O-02a, the configuration of the VDs was the same as in the previous experiment O-02, with an initial distance varying between 1 cm and 5 cm. However, in this case, one of the moving walls was stopped after 1.5 cm of symmetric absolute displacement (50% extension). Until this stage was reached (Fig. 13A) it was possible to observe similar structures to the ones formed for approximately equivalent amounts of extension in the two previous experiments (i.e., a pair of elongated, obliquely intersecting grabens – compare Figs. 11A, 12A, and 13A). To the north of the intersection, there are two independent grabens, approximately 3 cm wide (scaling to ~12 km), separated by a middle horst. To the south of the intersection, a depression formed where the two grabens interfere (similar to the previous experiment). From this stage onwards, the eastern wall was no longer moved, and the stretching of the model was exclusively achieved at the expense of the westward displacement of the west lateral wall. As extension increased (~1.75 cm of absolute displacement, Fig. 13B), the eastern graben did not undergo any new deformation. All the deformation was accommodated by the western graben, with the formation of a new inner fault. At this point, the eastern graben had a width of ~3.5 cm (scaling to ~14 km) whereas the western graben was ~4.1 cm wide (scaling to ~16.4 km). At the final stage of the experiment (Fig. 13C), yet another inner fault was formed on the western graben. The final width of the western graben was ~4.7 cm (scaling to ~18.8 km) and the final width of the eastern graben was ~3.7 cm (scaling to ~14.8 km). The final cross-sections (Fig. 13D-F) show two separate grabens to the north of the intersection and two

interfering grabens to the south of the intersection. In both cases, the western graben is more developed (deeper and wider) than the eastern graben.

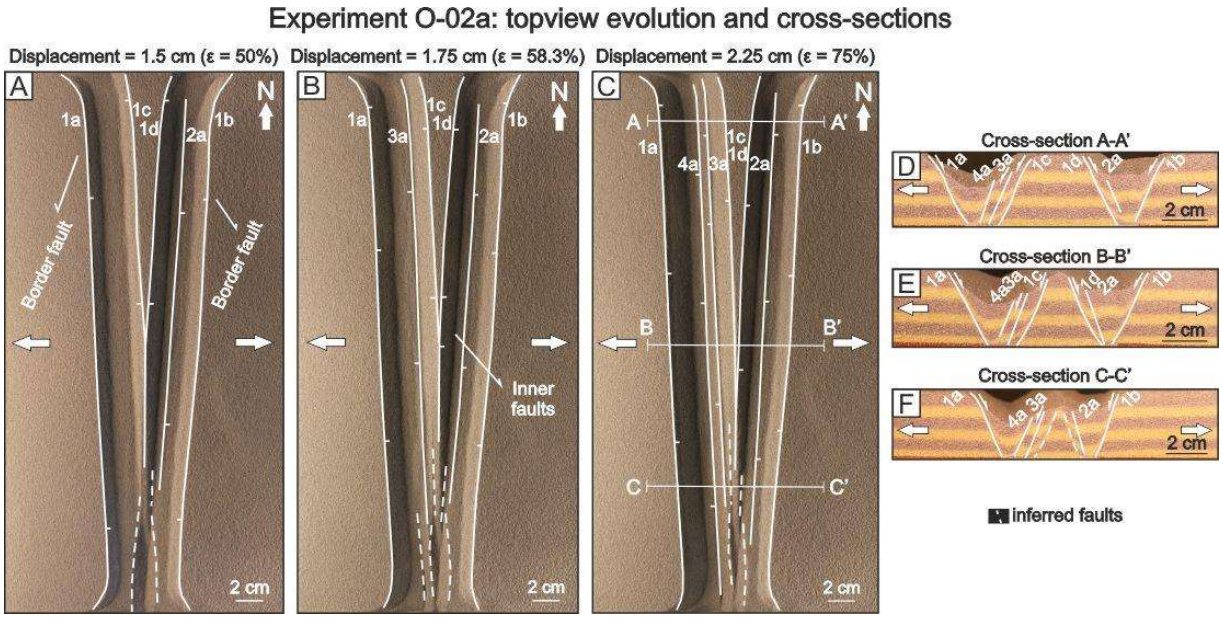


**Figure 13.** Results of the experiment O-02a: topview evolution and final stage cross-sections. A. Topview after a displacement of 1.5 cm. B. Topview after a displacement of 1.75 cm. C. Final stage. D, E and F. Final stage cross-sections A-A', B-B' and C-C'.

### 3.2.2. Triple-junction rifts

In the experiments TJ-01 and TJ-02, we varied the geometry of the basal VDs as shown in figures 3D and 3E to create two types of triple-junction configurations. In experiment TJ-01, the VDs formed an angle of 60º (oblique to the extension direction) in the north part of the model. In the south part of the model, the VDs were initially in contact with each other and aligned orthogonally to the extension direction. In the experiment TJ-02, the VDs also made an angle of 60º but with an overall different geometry that always simulated oblique extension (transtension). The total prescribed absolute stretching was in both cases of 3 cm (10% of extension).

In experiment TJ-01, in the initial stages of extension (1 cm, scaling to 4 km, Fig. 14A), three grabens formed. The graben 1 was 2.6 cm wide (scaling to 10.4 km) and the grabens 2 and 3 were ~2 cm wide (scaling to ~8 km); note the grabens intersect in the centre of the model and the border and the inner faults formed with linear geometries. As extension increased (2

cm of extension and scaling of 8 km, Fig. 14B), new inner faults developed inside graben 1 forming a middle ridge similar to the one formed in the experiments of set 1, P-00 and P-01 (Figs. 4, 5). At the final stage of extension (displacement of 3 cm, scaling to 12 km, Fig. 14C), it is possible to individualize two asymmetric grabens oblique to the extension direction, and one symmetric graben orthogonal to this direction. New inner faults formed in grabens 2 and 3. The final width of graben 1 was of approximately 6 cm (scaling to 24 km), while grabens 2 and 3 were ~4 cm wide (scaling to ~16 km). The intersecting faults observed at the centre of the model are represented in all topview figures by white dotted lines (Figs. 14A-C). In graben 1, new inner fault segments were observed (Fig. 14C). In the cross-sections shown in figures 14D to I, it is possible to observe the overall geometries across the different sections of the final stage of the model. Cross-sections A-A' (Fig. 14D) and B-B' (Fig. 14E) show two individual asymmetric grabens separated by a middle horst (~3 cm high, scaling to 12 km), with depocenters ~1.3 cm deep (scaling to ~5.2 km). The cross-sections from C to F (Figs. 14 F-I) show the intersection between the three grabens and the transition from two asymmetric grabens to one symmetric graben. In these cross-sections, the ridge/horst was between ~1.5 and 2 cm high (scaling to ~8 km).

In the experiment TJ-02, in the initial stages of extension (1 cm, scaling to 4 km, Fig. 15A), it is possible to recognize three distinct grabens, oblique to the extension direction, which intersect at the centre of the model. The eastern main border fault is the same for grabens 1 and 3, because they share the same initial VD. After 2 cm of extension (scaling to 8 km, Fig. 15B), two inner normal faults formed in graben 1 (faults 2a and 3a). At this stage, there is a clear difference in the width of the grabens. Graben 1 has a width of ~4,7 cm, while grabens 2 and 3 are ~3,6 cm wide. In the end stage of the experiment (equivalent to a total displacement of 3 cm = 12 km and an extension of 10%, Fig. 15C), it is possible to observe from topview that the main outer-bounding fault, common to grabens 1 and 3, presents a curved geometry near the intersection zone. At this stage, it is possible to observe newly formed inner faults in grabens 2 and 3. Both these grabens had final widths of ~4,2 cm, while graben 1 was ~5,8 cm wide. In the final stage cross-sections, it is possible to observe that all the three grabens developed an asymmetric geometry, except in the intersection zone where a wide symmetric graben with interfering faults formed (Fig. 15D-I).

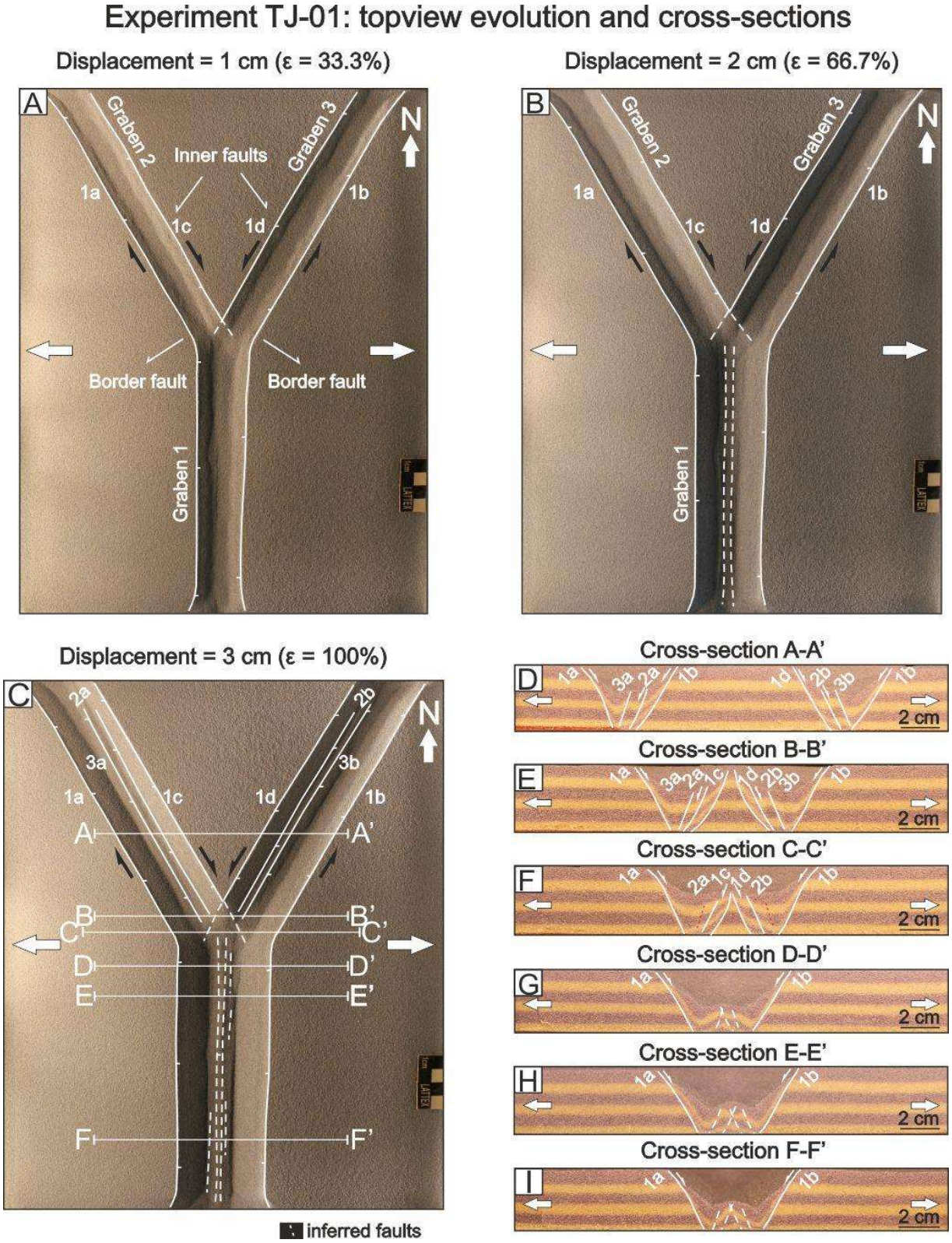


**Figure 14.** Results of the experiment TJ-01: topview evolution and final stage cross-sections. A. Topview after a displacement of 1 cm. B. Topview after a displacement of 2 cm. C. Final stage. D, E, F, G, H, and I. Final stage cross-sections A-A', B-B', C-C', D-D', E-E' and F-F'.

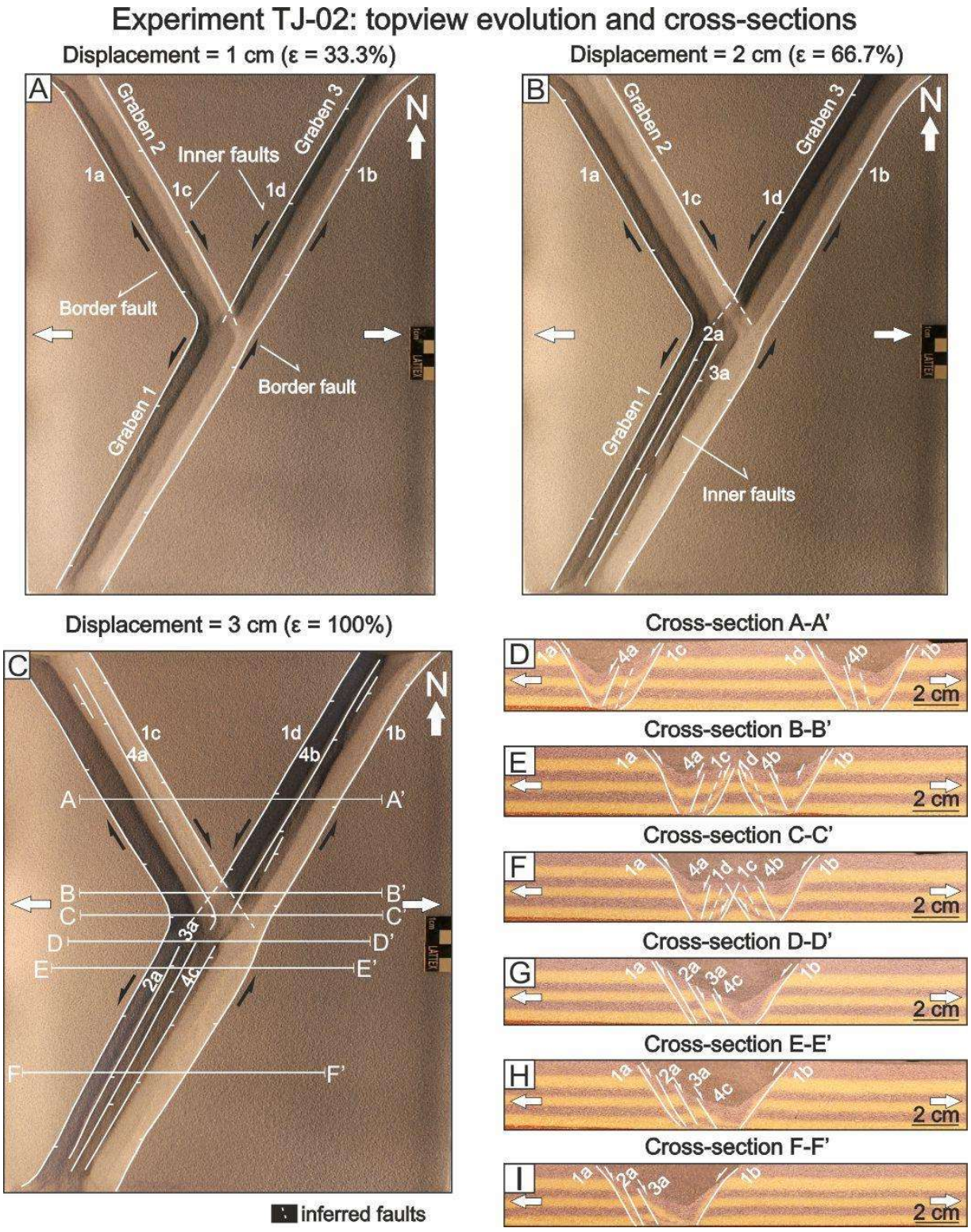


**Figure 15.** Results of the experiment TJ-02: topview evolution and final stage cross-sections. A. Topview after a displacement of 1 cm. B. Topview after a displacement of 2 cm. C. Final stage. D, E, F, G, H, and I. Final stage cross-sections A-A', B-B', C-C', D-D', E-E' and F-F'.

### 3.3. General considerations on the experimental results

In this work, we have systematically varied the geometric layout of two basal velocity discontinuities (VDs) in sandbox rifting models. These VDs simulate two pre-existing (inherited) basement heterogeneities in a developing crustal continental rift system (see Fig. 3). In all the performed experiments, the relative movement across each VD lead to the formation of a corresponding graben in the overlying sand pack, which either developed independently or interfered with other grabens, depending on the initial configuration of the VDs. All the grabens were limited outwards by a main border fault that remained active during the total span of the experiment (see Fig. 10). In general, when two parallel VDs were at an initial distance of ≥ 2 cm (scaling to 8 km, experiments P-02 to P-05), two independent asymmetric grabens developed. When they were closer, the two grabens interfered, forming a wide symmetric graben with a central ridge. However, when the VDs were 2 cm or 3 cm apart (scaling to 8 km and 12 km, respectively), the middle horst was always observed to be partially dismantled by several antithetic central normal faults (e.g., faults 1c-1d, 2a-2b, 3a-3b in Figs. 6C and 7C). Only when the VDs were at 4 or 5 cm (scaling to 16 and 20 km) did the middle horst maintain its initial height (see Fig. 10E-F).

In the case of the 1$^{st}$ set of experiments (with parallel VDs), the two grabens always increased their widths with increasing extension (Figs. 16A, B), as expected. The total deformed area increased ~1cm per each extensional increment of 0.5 cm (Figs. 16D). An interesting observation is that the distance between the first formed inner faults (in each graben) shows a slight decrease of ~0.1 cm per extensional increment of 0.5 cm, revealing that in all the experiments the central elevation was progressively disassembled, probably due to some rotation of the faults and erosion of the fault's scarps. Another interesting observation is that, despite the differences between the initial spacing of the VDs, the width and depth of the grabens remained relatively constant in all the experiments (see Figs 17A and 17B). This means that what is changing as a function of the spacing between the VDs is the width of the central horst (see Fig. 17C). Furthermore, it is also clear that when the initial distance between VDs is larger than 2 cm (scaling to 8 km), the formed horsts maintained their initial heights of ~3 cm until the end of the experiment (Fig. 17D). Below that value, the central horst/ridge is progressively disassembled with the evolution of the experiment, as mentioned above.

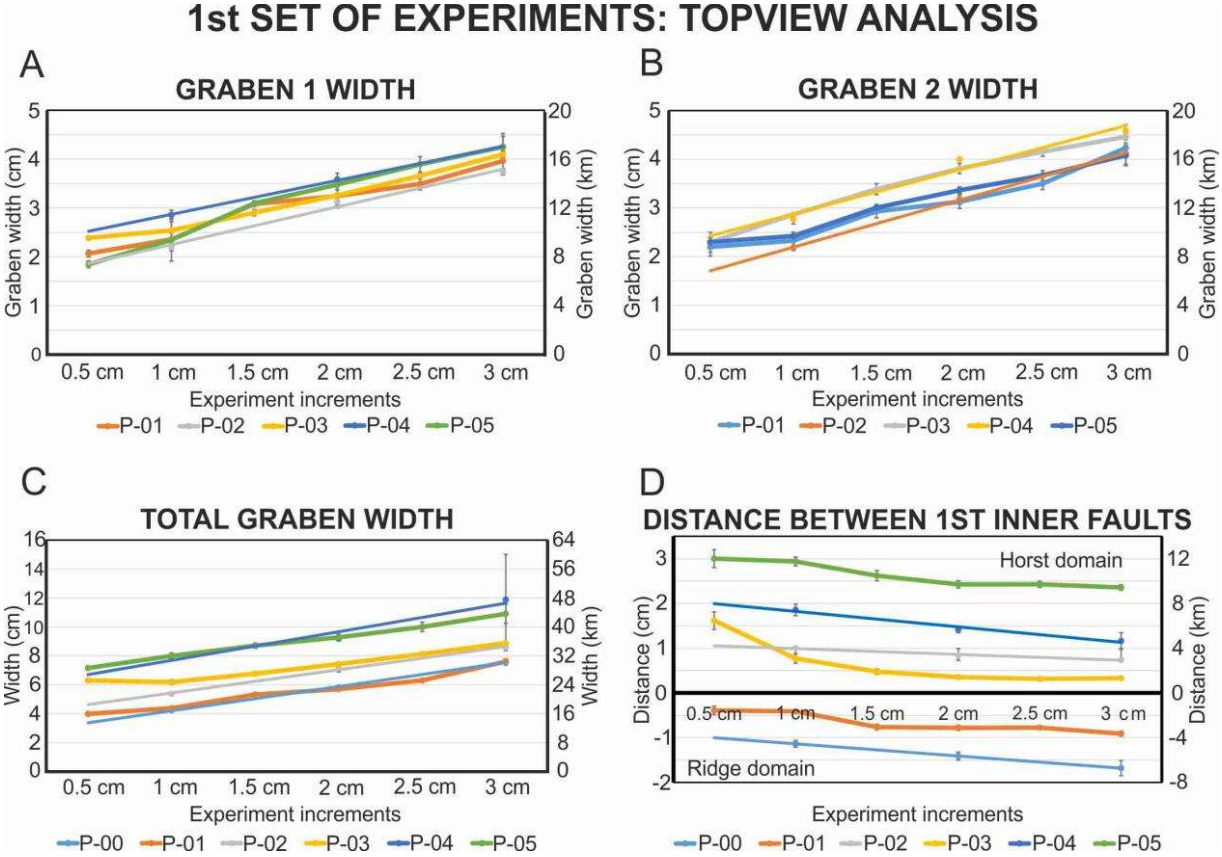


**Figure 16.** Analysis of the topview results of the 1st set of experiments with parallel VDs. A and B. Charts showing the evolution of the widths of grabens 1 and 2, respectively, for experiments P-01, P-02, P-03, P-04, and P-05. C. Chart showing the evolution of the total width of the grabens. D. Distance between the first formed inner faults (1c and 1d) in each graben; when these faults crosscut each other (as in experiments P-00 and P-01) their values are considered negative.

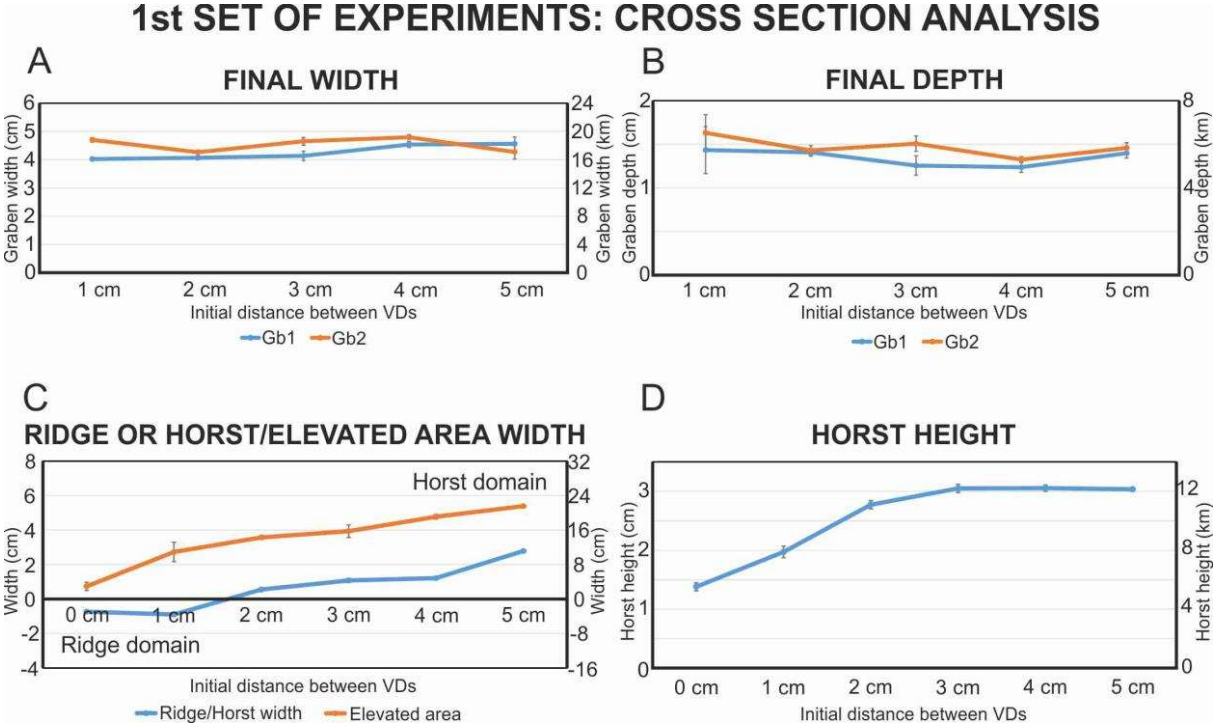


**Figure 17.** Analysis of the final cross-sections results of the 1st set of experiments with parallel VDs. A. Graben width for the different prescribed initial distances between VDs. B. Graben depths as a function of the different considered initial distances between VDs. C. Ridge/horst and elevated area widths as a function of the prescribed VDs initial distances. Ridge/horst width was the horizontal distance between faults 1c and 1d; The elevated area width is the horizontal distance between the last formed inner faults (faults 3a and 3b). D. Horst height as a function of different initial VDs distances.

In the 2nd set of experiments, the VDs were used to simulate pre-existing basement heterogeneities in other possible configurations. In the "O" and "TJ" experiments we varied the VDs initial distances in the along-strike direction, introducing a transtensional component in the deformation. In this set, all formed grabens were asymmetric, except for experiment TJ-01, in which a symmetric graben with a middle ridge formed (graben 1). In the experiments with oblique VDs, the formed grabens crosscut each other when the initial VDs distances were of 0 and 1 cm, resulting in the formation of a wide graben with a middle ridge, and sometimes a central depression (Figs. 11-13). When the VDs initial spacing was higher (between 2 and 5 cm), there was always the formation of two independent asymmetric grabens. We have also analysed the evolution of the graben's widths for experiments O-02 and O-02a (Figs 18A, B). It is possible to observe that the width of the grabens increases with increasing extension, as was expected from the analysis of the previous set. In the experiment O-02a, after we have stopped one of the moving walls, the extension in the respective graben stopped as well, although some minor deformation was still perceptible, meaning that it must have propagated

from the other, still active, graben (Fig. 18B). In any case, this was very minor, and means that each VD affects mostly only the corresponding graben.

In the experiments TJ-01 and TJ-02, with three branches of VDs (Figs. 18C, D), three grabens always formed. In the case of experiment TJ-01, two were oblique and one was orthogonal to the extension direction, while in TJ-02 three grabens formed oblique to the extension direction. In the experiment TJ-01, the graben that formed orthogonally to the extension direction (graben 1) was symmetric (as in experiment P-00 of the 1st set). Interestingly, in both experiments (TJ-01 and TJ-02), the width of graben 1 shows a faster growth than in the other two grabens (Figs. 18C, D). And contrary to what would be intuitively expected, the widths of grabens 2 and 3 are not half of the width of graben 1 (see Fig. 19A). This is because in the case of grabens 2 and 3, their width is summing up (because their corresponding VDs are well separated), while in the case of graben 1, the graben forms as a result of the interference of two closely placed VDs (Figs. 19B, C). And as consequence, it is like the grabens 2 and 3 are merged together, subtracting their individual widths.

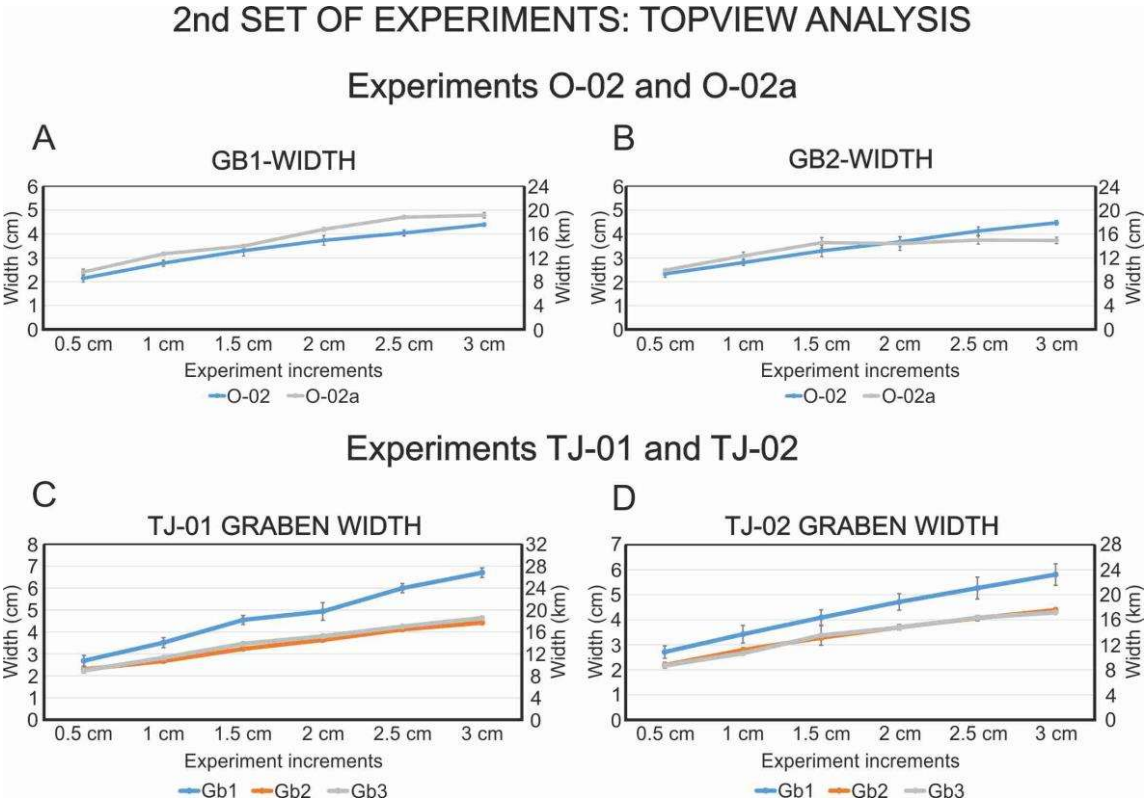


**Figure 18.** Analysis of the topview results of the 2nd set of experiments. A and B. Widths of the grabens 1 and 2 (GB1 and GB2) as a function of extension, for experiments O-02 and O-02a. C and D. Widths of the grabens 1, 2 and 3 (GB1, GB2 and GB3) as a function of extension, for experiments TJ-01 and TJ-02.

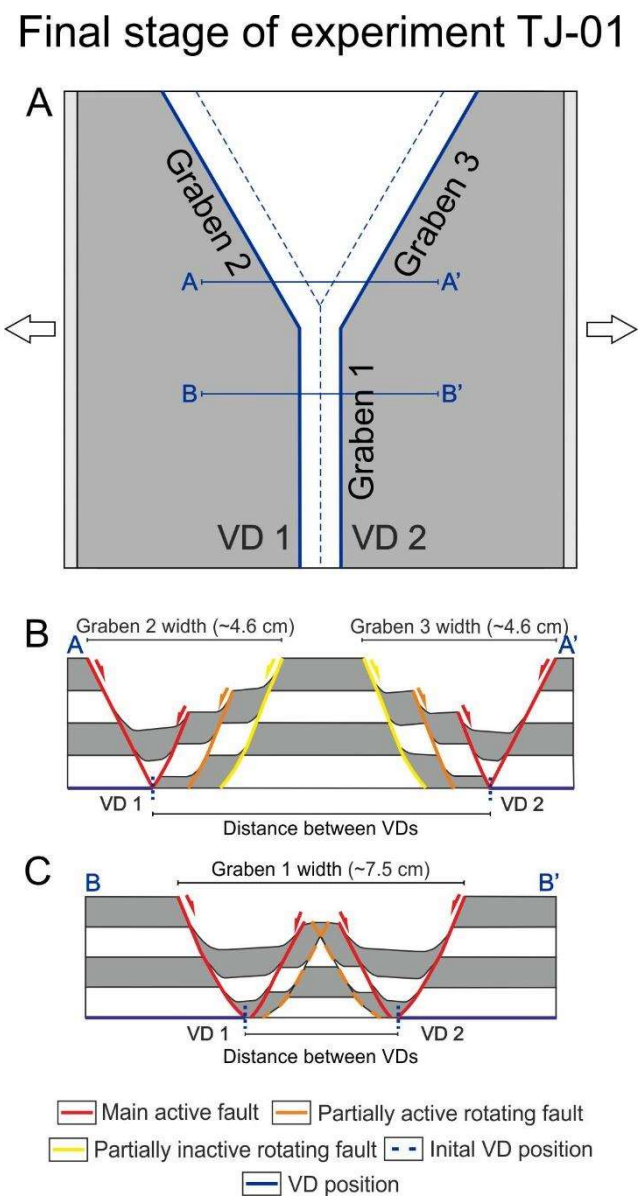


**Figure 19.** Scheme illustrating the final stage of experiment TJ-01. A. Blue dashed lines mark the initial positions of the VDs. B. Cross-section A-A' crosscutting grabens 2 and 3. C. Cross-section B-B' crosscutting graben 1.

# 4. Discussion

## 4.1. Rift asymmetry/symmetry

In our experiments, the VDs generally gave origin to two asymmetric grabens (each graben corresponding to one VD), with exception of the cases in which the VDs were initially in contact or less than 2 cm apart, in which wide symmetric grabens formed (Experiments P-00, P-01 and TJ-01). In fact, what happened in these cases was that the two potential grabens (above each

VD) merged together to form a wide graben. It is not trivial why each VD always leads to the formation of an asymmetric graben, and therefore it deserves a further analysis. In all experiments, each basal VD, simulating a basal heterogeneity with movement, gave origin to a main border fault that remained active for the entire span of the experiment and moved along with the VD (Fig. 20). In the first stages of the experiments in which the VDs were far apart (see Figs. 20E-H), an antithetic inner fault always formed, giving origin to a relatively symmetric graben (Fig. 20F). The main border fault then functioned as listric fault against which several antithetic faults formed sequentially, segmenting the initially formed graben. The deformation moves away from the central horst at the same time that new inner faults form (see Figs. 20F-H). The central horst was mostly preserved in these cases, depending on the initial distance between the VDs. With the evolution of the experiments, the first formed inner faults undergo some rotation and start to behave as a sort of a listric structure.

In the case where the VDs were close (see Figs. 20A-D), the two main faults also formed rooted in the respective VD. The first two respective inner antithetic faults also formed at a similar distance. However, because the VDs were initially in contact, or close, these inner faults intersected each other. As a consequence, the central structure was not a true horst, but simply a ridge that became more prominent as the experiment evolved and the grabens subsided. In the Experiment P-00 and in graben 1 of Experiment TJ-01, only two main faults and two intersecting faults formed, giving origin to a wide symmetric graben with a ridge in the middle. In the Experiment P-01, new inner faults formed progressively inside the graben away from the first formed inner faults. The final structure can still be interpreted as a wide graben with a middle ridge, as no central horst truly formed in the inside, between the two basal discontinuities.

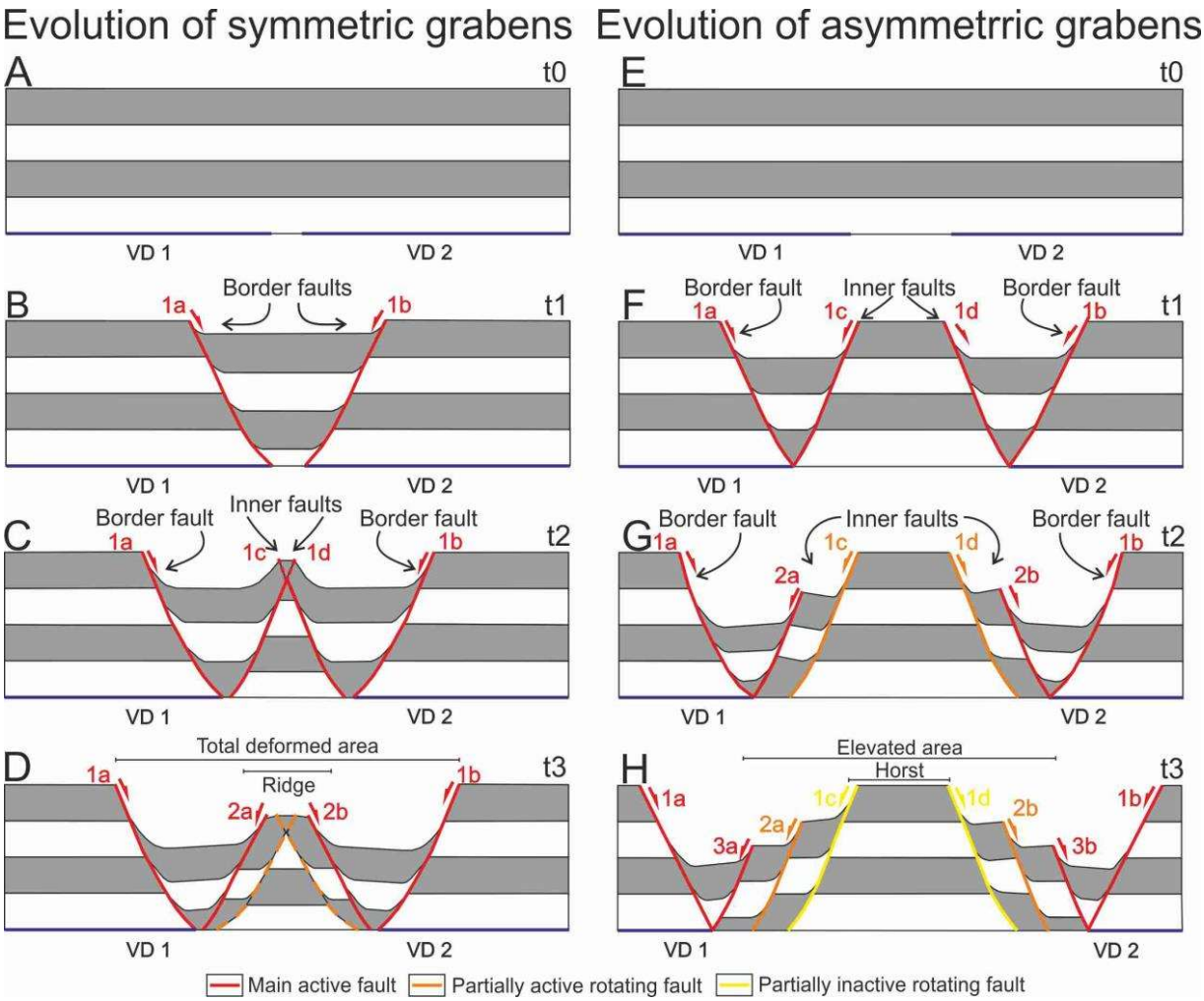


**Figure 20.** Scheme of the evolution of symmetric and asymmetric grabens in this work. A, B, C and D. Represent t0, t1, t2 and t3 stages of evolution similar to the graben evolution of experiments P-00, P-01 and graben 1 of experiment (TJ-01). E, F, G and H. Represent t0, t1, t2, and t3 stages of evolution similar to the graben evolution of experiments P-01, P-02, P-03, P-04, and P-05. Red lines – main active faults; Orange lines – partially active rotating faults; Yellow lines – partially inactive rotating faults.

## 4.2. Comparison with previous analogue models of rifting: rift symmetry

Many previous rift models were carried out at lithospheric level undergoing total finite extensional strain much larger than ours. These models are usually designed to understand how continental rifting evolves into break-up and oceanization (e.g. Brun and Beslier, 1996; Nagel and Buck, 2004). In our case, we focused on the upper crustal deformation of the early stages of intra-continental rifting resulting from the reactivation of basement heterogeneities. Therefore, it is not possible to discuss and directly compare our models in the light of the classic symmetric versus asymmetric models of rifting (McKenzie, 1978 and Wernicke, 1985,

respectively). However, in the initial stages of some of these models, prior to break-up, two rift zones separated by a central horst are formed (e.g., see Fig. 5 in Brun and Beslier, 1996), but with the evolution of the experiment, one of the systems is aborted (see section on the natural examples below). In any case, our asymmetrical rifts formed as the consequence of the movement along a basal VD much like, but at a smaller scale, as in the Wernicke (1985) asymmetric model, in which the extension is mostly accommodated along one main fault with the formation of several associated antithetic faults. The main fault remains active and connected with the VD during the entire span of the experiment, while antithetic faults form and are progressively deactivated. Moreover, some of the previous models rely on the existence of a pre-imposed weak zone (or zones) inducing a deformation that propagates into the upper crust, therefore playing a similar role to our basal VDs, which simulated an inherited structure (e.g., the contact between two cratons or faults existing in old intracratonic orogens).

Other previous models have tested apparatus, which despite some crucial differences, are comparable with ours. For example, Allemand et al. (1989) used basal VDs to impose extensional deformation to a sand-silicone cake (they additionally used syntectonic sedimentation). In their experiments, the VDs were always initially in contact. Some comparisons can be made with our models. When the VDs were in contact and both walls moved away symmetrically, a wide symmetric rift was generated with a middle elevated less deformed region, comparable with our own models with a middle ridge (Fig. 5 of Allemand et al., 1989). When only one of the walls was moved, the result was the formation of an asymmetric rift system. Their results show that for a simple sand-silicone system, simulating e.g., a middle-upper crust, the symmetric or asymmetric movement along a basal asymmetry leads to symmetric and asymmetric rift geometries, respectively, but only when the VDs were initially in contact. We anticipate that if they had two VDs set apart, they would probably obtain two asymmetric rift systems. Allemand et al. (1989) also carried out experiments with an asthenosphere (made of honey) and a complex lithospheric layering (made of sand and silicone). In these cases, the extension was imparted in the model by two vertical lateral VDs, moving both in only one direction. Surprisingly, they obtained symmetric and asymmetric rift systems, which strongly depend on the strength of the lithospheric layers. The presence of a strong brittle intra-lithospheric layer always leads to a symmetric rift system (Fig. 3 of (Allemand et al., 1989), while a simpler brittle-ductile lithosphere leads to the formation of an asymmetric rift (Fig. 4 of Allemand et al., 1989).

Allemand and Brun (1991) tested the effect of two basal VDs initially in contact, for experiments with only sand and with a sand-silicone layering, but with syntectonic sedimentation. In their results with only sand, when both the VDs move away simultaneously there is the formation of a symmetric rift, which is comparable to our experiments in which the distance between the VDs was 0 cm (P-00, and graben 1 of experiments TJ-01 and TJ-02). When only one VD moved, the result was the formation of an asymmetric rift system, as in most of our experiments in which one of the VDs is significantly separated from the other. In both cases, the two firstly formed bordering faults are generated from the VDs and dictate the lateral limits of the graben for the remainder of the experiment. Allemand and Brun (1991) also carried out experiments with a basal layer of silicone, underneath the sand layer. In this case, the movement of one or two VDs also lead to symmetric and asymmetric rifting, respectively. However, in these cases, the rift systems strongly delocalized and lead to a much more complex evolution, with the rifts offset from the VDs and no fault rooting at the VDs.

Contrary to Allemand et al. (1989) and Allemand and Brun (1991), which analogue modelling studies were carried out to evaluate the impact of basal velocity discontinuities and asymmetries on the evolution of the overlaying rift systems, Corti and Manetti (2006) directly investigated the role of an initial geometric asymmetry in the Moho surface. These authors concluded that a pre-rifting asymmetric Moho geometry always leads to asymmetric rifting.

### 4.3. Other previous rifting models and implied constraints

Different authors have opted to use different materials and rheological layering, depending on the problem they were investigating. There are examples of rifting models using only quartz-sand (McClay and White, 1995; Keep and McClay, 1997), clay (Withjack and Jamison, 1986; Clifton et al., 2000), sand and silicone (Corti et al., 2001; Zwaan et al., 2019), glucose-sand-silicone (Brun and Beslier, 1996) or more complex layering such as in Molnar et al. (2019). In this last work, sand mixed with ceramic microspheres was used to simulate the brittle crust, silicone putty was used to model the ductile crust, silicone putty mixed with plasticine and glass beads to simulate the lithospheric mantle, and a solution of Natrosol® 250 HH with sodium chloride in deionized water to simulate the asthenosphere.

The objective of our models was to test the impact of a pre-existent basal discontinuity in the initial stages of continental rifting, which would act as a velocity discontinuity. We opted

to use a very simple apparatus, with only one sand layer. We did not simulate syntectonic sedimentation nor the inclusion of a viscous layer, as these often involve interacting with the experiment or may induce significant initial pertubations, respectively, that we wanted to avoid. In particular, our objective was to model the initial stages of rifting in a thick and cooler lithosphere. In any case, models with a higher level of complexity are useful for investigating a number of other parameters and more complex cases of rift evolution. Of particular interest are the investigation of multiple rifting phases (sometimes oblique to each other), and to understand how the fabric that is formed in the initial phases of rifting influences the subsequent ones. Examples include the work of Keep and McClay (1997), Henza et al. (2010, 2011) and Chattopadhyay and Chakra (2013). These authors used different systems to induce rifting to the brittle sand layer. Keep and McClay (1997) used a central velocity discontinuity covered with silicone, Henza et al. (2010, 2011) used a rubber sheet, and Chattopadhyay and Chakra (2013) used a basal pitch layer that deformed by the divergent movement of wooden blocks. There are also several experiments that investigate rift obliquity using a number of different apparatus to induce extension. For example, Tron and Brun (1991) and Clifton et al. (2000) use basal VDs, Withjack and Jamison (1986) and McClay and White (1995) use a rubber sheet, and Zwaan et al. (2016) use a complex layering of foam, plexiglass, and silicone, including a silicone perturbation (seed).

An excellent systematic study of the possible different apparatus and their effects on the development of rift systems was carried out by (Zwaan et al., 2019). These authors showed that a single sand layer deformed by two basal rigid plates always leads to a strong coupling between the basement and the upper crust, and a strong localization of the deformation in the brittle layer. In contrast, a basal ductile layer would decouple the basement deformation from the upper brittle crust. According to the same authors, a strong basement-upper crust coupling would correspond to a natural analogue with a cold and thick upper crust, which would lead to the formation of a highly localized rift. This is precisely what occurred in our models, in which the first and main faults to form limited the evolution and geometry of the rift system for the remainder of their evolution.

## 4.4. Natural analogues

Analogue modelling has been widely used to study a number of natural rift systems. This particular work was inspired by two sub-parallel Neoproterozoic grabens located in the Parecis Basin, in Brazil, which developed during the early stages of intracratonic extensional deformation. A map of the present-day geometry of the basin, and the two grabens, is shown in figure in 21A. An interpreted seismic profile across the basin is presented in figure 21A (Haeser et al., 2014), showing the two grabens separated by a ~20 km-wide middle horst (the Rio Branco High), with the total width of the system being ~180 km (along the profile section, but up to 245 km in its widest point).

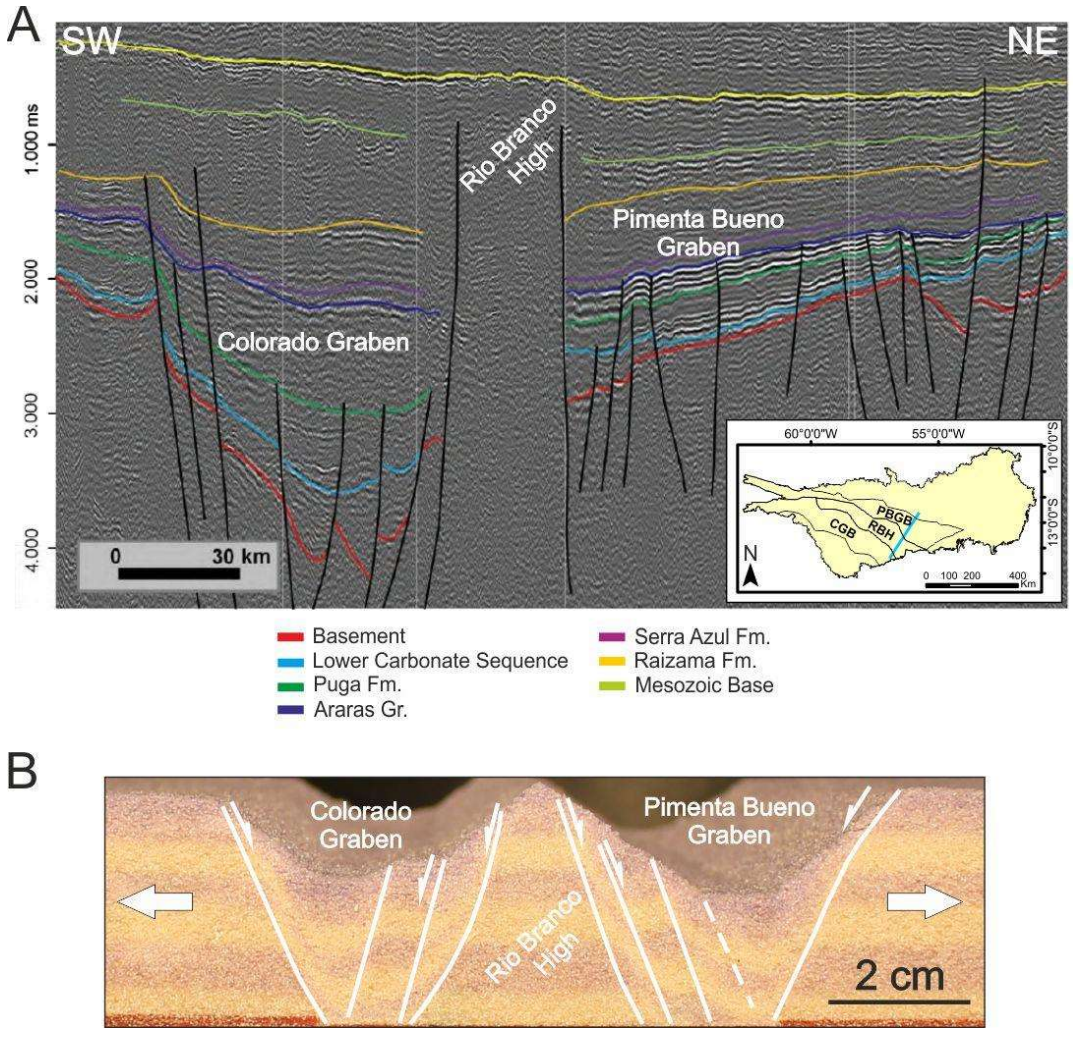


**Figure 21.** A. Interpreted seismic line 0295_0001 crossing both Pimenta Bueno and Colorado grabens (modified from Haeser et al., 2014). Basement – Paleoproterozoic; Lower Carbonate Sequence – Neoproterozoic (more than 635 My); Puga Formation – Neoproterozoic (between 635 and 627 Ma); Araras Group – Neoproterozoic (between 627 and 582 My); Serra Azul and Raizama Formations – upper Neoproterozoic. B. A comparable cross-section of one of our experiments (P-03).

Our first set of experiments (P experiments), as well as the oblique rifts experiments of the second set, were designed to gain insight on the minimum distance needed for parallel linear basement heterogeneities to be reactivated yielding two separated grabens. In particular, we wanted to test if the two grabens could have formed as the result of the reactivation of one basement structure, or instead, have formed as the result of two, eventually oblique pre-existent structures. Our experimental results suggest that the second option is more likely. This is because in the natural example, we can clearly distinguish two asymmetric grabens separated by a well-defined horst. Also, the Colorado Graben (and the Pimenta Bueno to some degree) seems to be controlled by an outer fault system against which a number of smaller antithetic faults seem to be rooted. This geometry resembles our experiments P-02 to P-05, in which the initial VDs were placed at a distance of > 2 cm, scaling to > 8 km (between 2 and 5 cm, scaling to 8-20 km, precisely) and the resulting horst had widths between ~1 and 3 cm (scaling to 4 and 12 km; see Fig. 17C). A significant difference is that the natural example is wider than our scaled experiments. The total deformed area along the profile is ~180 km wide, while in our experiment the widest deformed area is of ~12 cm wide (scaling to ~48 km), in Experiment P-05. This means that in nature the system may have undergone more fine extensional deformation than that simulated in our experiments (3 cm, scaling to 12 km). There may also be other scale effects that were not considered here, which could affect the deformation in the natural example (e.g., rheological layering of the sedimentary units).

There are other examples of formation of parallel basins separated by a mid-horst in the context of initial stages of rifting. However, in most cases, the deformation in one graben generally does not propagate to the other one nearby, as shown in our experiments (see experiment O-02a). Therefore, once break-up takes place it is expected that the deformation focuses along one of the rift structures, with the other one being aborted. This was likely the case of the Lusitanian Basin, located in the Atlantic margin of west Iberia (Europe). There, the extension resulted from the break-up of Pangea, which started in the Late Cretaceous (Kullberg et al., 2006; Pena dos Reis et al., 2010), and the first extensional event resulted in the formation of two parallel grabens with a central middle horst – the Berlengas Horst. This is an interesting example, as it is known that the continental rifting localized along pre-existing NNW-SSE and NE-SW late-Variscan faults. This shows that in the initial stages of continental rifting, the inherited pre-existing basement structures may play a fundamental role in localizing deformation. Only once the thermal swelling of the asthenosphere and necking of the lithosphere takes over, does the deformation localize in one rift system.

When two rift systems intersect, forming a triple-junction, the deformation styles may differ depending on the direction of the initial heterogeneities and their angle in relation to the extension direction. This may have been the case of the Afar triple-junction formed by the East African Rift, the Gulf of Aden, and the Red Sea. However, in two of the branches oceanization seems to have already started, and therefore we should be cautious when comparing to our experiments. In any case, in Zwaan et al. (2020), figure 14 seems to suggest that some branches may undergo pure shear deformation (resulting in symmetric rifting) while others undergo simple shear deformation (with the formation of an asymmetric rift). This is also observed in our TJ experiments and we would argue that such symmetry/asymmetry may be strongly dependent on the initial inherited fabrics that control the initial stages of continental rifting.

## 5. Conclusions

In this work, we have investigated the evolution of nearby rift systems using a very simple apparatus simulating a cold continental crust. We have tested different geometric configurations nucleated by basal velocity discontinuities (VDs): parallel, oblique, and triple-junction. This work was partially inspired by the initial stages of continental rifting in the Parecis Basin in Brazil, where two slightly oblique intracratonic grabens are observed. The main conclusions of this work are:

- The extensional movement along one rigid basal VD always leads to the formation of an asymmetric and localized rift system in the brittle sand cover. In the initial stages, two main conjugate faults are formed. Then, the evolution of the system is controlled by one of the faults that acts as main listric border fault and remains connected to the VD, while a number of antithetic faults form progressively and migrate towards the depocenter.
- When the two VDs are initially in contact, or very closely placed, there is the formation of one wide symmetric graben, often with a middle ridge (experiments P-00 and P-01).
- When two basal VDs are at an initial distance of ≥ 2 cm (scaling to 8 km), with a 3 cm thick sand cover (scaling to 12 km), two independent rift systems are formed (Experiments P-02 to P-05).
- When a brittle sand pack lies directly on top of a rigid basement and the VDs are placed at a distance, two separate rift systems are formed, and the deformation imparted to one

of the rifts is independent and does not propagate to the other nearby rift system (Experiment O-02a).

- At upper crustal levels in nature, separated rift systems may not form in the case of more complex lithospheric rheologies or when a ductile layer is present (e.g., salt, or a ductile middle crust). Instead, early delocalization may prevail.
- When the VDs are oblique to the moving walls the first faults form in a segmented way but rapidly connect in longer faults when deformation progresses. This is the case for the oblique and intersecting rift experiments (P-O and TJ).
- The Parecis Basin was likely formed as the result of the reactivation of two nearby linear basement structures, eventually inherited from a previous orogenic cycle.
- In the initial stages of continental rifting, the localization of deformation may be strongly dependent of the existence of basement heterogeneities and their geometry, which may lead to the formation of several independent graben systems with different deformation styles.

## Acknowledgments

This study was financed in part by the Fundação de Apoio à Pesquisa do Distrito Federal and Coordenação de Aperfeiçoamento de Pessoal de Nível Superior - Brasil (CAPES) - Finance Code 001. The study had the support of Instituto Nacional de Ciência e Tecnologia Estudos Tectônicos (INCT-ET) and Conselho Nacional de Desenvolvimento Científico e Tecnológico (CNPq). M. E. Oliveira acknowledges the Laboratório de Tectonofísica e Tectónica Experimental (LATTEX), the Faculdade de Ciências da Universidade de Lisboa, and the Instituto Dom Luiz (IDL) for the assistance in performing the experiments presented in this research and also the Laboratório de Modelagem Estrutural of Universidade Federal do Rio Grande do Norte, for the assistance in the development of the initial experiments. M.E. Oliveira also acknowledges Ilísio Boaventura and Nuno Carmo for helping in the laboratory and Eveline Sayão for helping with the development of area maps. A.S. Gomes acknowledges a Ph.D. grant by the Fundação para a Ciência e Tecnologia, ref: SFRH/BD/146726/2019. J.C. Duarte, F.M. Rosas and A.S. Gomes acknowledge funding from the FCT through the project UIDB/50019/2021-IDL. G. S. França and R.A. Fuck acknowledge CNPq for Research

Fellowship. We thank the editor Andres Folguera, Francisco Hilario Bezerra and another anonymous reviewer for the constructive revision of the original manuscript.

## References

Allemand, P., Brun, J.P., 1991. Width of continental rifts and rheological layering of the lithosphere. Tectonophysics 188, 63–69. https://doi.org/10.1017/cbo9780511975417.004

Allemand, P., Brun, J.P., Davy, P., Van Den Driessche, J., 1989. Symmetry and asymmetry of rifts and mechanism of lithosphere thinning. Bull. Soc. Geol. Fr. 5, 445–451.

Bahia, R.B.C., Martins-Neto, M.A., Barbosa, M.S.C., Pedreira, A.J., 2006. Revisão estratigráfica da Bacia dos Parecis – Amazônia. Rev. Bras. Geociências 36, 692–703.

Bahia, R.B.C., Martins-Neto, M.A., Barbosa, M.S.C., Pedreira, A.J., 2007. Análise da evolução tectonossedimentar da Bacia dos Parecis através de métodos potenciais. Rev. Bras. Geociências 37, 639–649. https://doi.org/10.25249/0375-7536.2007374639649

Beniest, A., 2017. From continental rifting to conjugate margins: Insights from analogue and numerical modelling. Université Pierre et Marie Curie/IFP Energies nouvelles.

Brun, J.P., Beslier, M.O., 1996. Mantle exhumation at passive margins. Earth Planet. Sci. Lett. 142, 161–173. https://doi.org/10.1016/0012-821x(96)00080-5

Brune, J.N., Ellis, M.A., 1997. Structural features in a brittle-ductile wax model of continental extension. Lett. to Nat. 387, 67–70.

Chattopadhyay, A., Chakra, M., 2013. Influence of pre-existing pervasive fabrics on fault patterns during orthogonal and oblique rifting: An experimental approach. Mar. Pet. Geol. 39, 74–91. https://doi.org/10.1016/j.marpetgeo.2012.09.009

Clifton, A.E., Schlische, R.W., Withjack, M.O., Ackermann, R. V., 2000. Influence of rift obliquity on fault-population systematics: Results of experimental clay models. J. Struct. Geol. 22, 1491–1509. https://doi.org/10.1016/S0191-8141(00)00043-2

Corti, G., Bonini, M., Conticelli, S., Innocenti, F., Manetti, P., Sokoutis, D., 2003. Analogue modelling of continental extension: A review focused on the relations between the patterns of deformation and the presence of magma. Earth-Science Rev. 63, 169–247. https://doi.org/10.1016/S0012-8252(03)00035-7

Corti, G., Bonini, M., Innocenti, F., Manetti, P., Mulugeta, G., 2001. Centrifuge models simulating magma emplacement during oblique rifting. J. Geodyn. 31, 557–576. https://doi.org/10.1016/S0264-3707(01)00032-1

Corti, G., Manetti, P., 2006. Asymmetric rifts due to asymmetric Mohos: An experimental approach. Earth Planet. Sci. Lett. 245, 315–329. https://doi.org/10.1016/j.epsl.2006.02.004

Deng, C., Gawthorpe, R.L., Fossen, H., Finch, E., 2018. How does the orientation of a preexisting basement weakness influence fault development during renewed rifting? Insights from three-dimensional discrete element modeling. Tectonics 37, 2221–2242. https://doi.org/10.1029/2017TC004776

Faria, H.P.A., 2015. Caracterização de domínios tectono-geofísicos na Bacia dos Parecis com base em dados de métodos potenciais. Universidade de Brasília.

Gomes, A.S., Rosas, F.M., Duarte, J.C., Schellart, W.P., Almeida, J., Tomás, R., Strak, V., 2019. Analogue modelling of brittle shear zone propagation across upper crustal morpho-rheological heterogeneities. J. Struct. Geol. 126, 175–197. https://doi.org/10.1016/j.jsg.2019.06.004

Haeser, B. S., Zalán, P.V., Ferreira, M.A., Petersohn, E., 2014. Revisão litoestratigráfica da Bacia dos Parecis e implicações para a exploração de petróleo, in: Rio Oil & Gas Expo and Conference. Rio de Janeiro, p. 10.

Henza, A.A., Withjack, M.O., Schlische, R.W., 2011. How do the properties of a pre-existing normal-fault population influence fault development during a subsequent phase of extension? J. Struct. Geol. 33, 1312–1324. https://doi.org/10.1016/j.jsg.2011.06.010

Henza, A.A., Withjack, M.O., Schlische, R.W., 2010. Normal-fault development during two phases of non-coaxial extension: An experimental study. J. Struct. Geol. 32, 1656–1667. https://doi.org/10.1016/j.jsg.2009.07.007

Hubbert, M.K., 1951. Mechanical basis for certain familiar geologic structures. Bull. Geol. Soc. Am. 62, 355–372. https://doi.org/10.1130/0016-7606(1951)62[355:MBFCFG]2.0.CO;2

Hubbert, M.K., 1937. Theory of scale models as applied to the study of geologic structures. Geol. Soc. Am. Bull. 48, 1459–1520. https://doi.org/10.1130/GSAB-48-1459

Keep, M., McClay, K.R., 1997. Analogue modelling of multiphase rift systems. Tectonophysics 273, 239–270. https://doi.org/10.1016/S0040-1951(96)00272-7

Klinkmüller, M., Schreurs, G., Rosenau, M., Kemnitz, H., 2016. Properties of granular analogue model materials: A community wide survey. Tectonophysics 684, 23–38. https://doi.org/10.1016/j.tecto.2016.01.017

Koyi, H., 1997. Analogue modelling: from a qualitative to a quantitative technique - a historical outline. J. Pet. Geol. 20 (2), 223–238.

Kullberg, J.C., Terrinha, P., Pais, J., Reis, R.P., Legoinha, P., 2006. Arrábida e Sintra: dois exemplos de tectónica pós-rifting da Bacia Lusitaniana, in: Dias, R., Araújo, A., Terrinha, P., Kullberg, J.C. (Eds.), Geologia de Portugal No Contexto Da Ibéria. Universidade de Évora, pp. 369–396.

Loureiro, E.M.L., 2016. Caracterização geológico-tectônica da Bacia dos Parecis. Uma interpretação integrada. Universidade do Estado do Rio de Janeiro.

Mandl, G., 1988. Mechanics of tectonic faulting. Elsevier.

McClay, K.R., 1990. Extensional fault systems in sedimentary basins: a review of analogue model studies. Mar. Pet. Geol. 7, 206–233. https://doi.org/10.1016/0264-8172(90)90001-W

McClay, K.R., White, M.J., 1995. Analogue modelling of orthogonal and oblique rifting. Mar. Pet. Geol. 12, 137–151. https://doi.org/10.1016/0264-8172(95)92835-K

McKenzie, D., 1978. Some remarks on the development of sedimentary basins. Earth Planet. Sci. Lett. 40, 25–32. https://doi.org/10.1016/0012-821X(78)90071-7

Molnar, N.E., Cruden, A.R., Betts, P.G., 2019. Interactions between propagating rifts and linear weaknesses in the lower crust. Geosphere 15, 1617–1640. https://doi.org/10.1130/GES02119.1

Nagel, T.J., Buck, W.R., 2004. Symmetric alternative to asymmetric rifting models. Geology 32, 937–940. https://doi.org/10.1130/G20785.1

Pena dos Reis, R., Pimentel, N., Garcia, A., 2010. A evolução da Bacia Lusitânica (Portugal) e dos sistemas petrolíferos associados. Rev. Electrónica Ciências da Terra 19, 1–4.

Ranalli, G., 1995. Rheology of the Earth, 2nd ed. Chapman & Hall, London.

Rosas, F.M., Duarte, J.C., Almeida, P., Schellart, W.P., Riel, N., Terrinha, P., 2017. Analogue modelling of thrust systems: Passive vs. active hanging wall strain accommodation and

sharp vs. smooth fault-ramp geometries. J. Struct. Geol. 99, 45–69. https://doi.org/10.1016/j.jsg.2017.05.002

Schellart, W.P., 2000. Shear test results for cohesion and friction coefficients for different granular materials: scaling implications for their usage in analogue modelling. Tectonophysics 324, 1–16. https://doi.org/10.1016/S0040-1951(00)00111-6

Schreurs, G., Buiter, S.J.H., Boutelier, D., Corti, G., Costa, E., Cruden, A.R., Daniel, J.M., Hoth, S., Koyi, H.A., Kukowski, N., Lohrmann, J., Ravaglia, A., Schlische, R.W., Withjack, M.O., Yamada, Y., Cavozzi, C., Del Ventisette, C., Elder Brady, J.A., Hoffmann-Rothe, A., Mengus, J.M., Montanari, D., Nilforoushan, F., 2006. Analogue benchmarks of shortening and extension experiments. Geol. Soc. Spec. Publ. 253, 1–27. https://doi.org/10.1144/GSL.SP.2006.253.01.01

Siqueira, L.P. de, 1989. Bacia dos Parecis. Bol. Geociências Petrobras 3, 3–16.

Tron, V., Brun, J.P., 1991. Experiments on oblique rifting in brittle-ductile systems. Tectonophysics 188, 71–84. https://doi.org/10.1016/0040-1951(91)90315-J

Vasconcelos, C.S., Morales, I.V.F., Figueiredo, M.F., 2014. Revisão da estratigrafia da Bacia dos Parecis-Alto Xingu, in: 47o Congresso Brasileiro de Geologia. Salvador, p. 1.

Vendeville, B., Cobbold, P.R., Davy, P., Brun, J.P., Choukroune, P., 1987. Physical models of extensional tectonics at various scales. Geol. Soc. Spec. Publ. 28, 95–107. https://doi.org/10.1144/GSL.SP.1987.028.01.08

Wernicke, B., 1985. Uniform-sense normal simple shear of the continental lithosphere. Can. J. Earth Sci. 22, 108–125. https://doi.org/10.1139/e85-009

Withjack, M.O., Jamison, W.R., 1986. Deformation produced by oblique rifting. Tectonophysics 126, 99–124. https://doi.org/10.1016/0040-1951(86)90222-2

Zwaan, F., Corti, G., Keir, D., Sani, F., 2020. A review of tectonic models for the rifted margin of Afar: Implications for continental break-up and passive margin formation. J. African Earth Sci. 164, 1–22. https://doi.org/10.1016/j.jafrearsci.2019.103649

Zwaan, F., Schreurs, G., Buiter, S.J.H., 2019. A systematic comparison of experimental set-ups for modelling extensional tectonics. Solid Earth 10, 1063–1097. https://doi.org/10.5194/se-10-1063-2019

Zwaan, F., Schreurs, G., Naliboff, J., Buiter, S.J.H., 2016. Insights into the effects of oblique extension on continental rift interaction from 3D analogue and numerical models. Tectonophysics 693, 239–260. https://doi.org/10.1016/j.tecto.2016.02.036

# CHAPTER 5. DOUBLE-RIFT NUCLEATION ABOVE INHERITED CRUSTAL WEAKNESSES: INSIGHTS FROM 2D NUMERICAL MODELS

## Double-rift nucleation above inherited crustal weaknesses: insights from 2D numerical models

Magda E. Oliveira[1], Afonso S. Gomes[2,3], Filipe M. Rosas[2,3], João C. Duarte[2,3], George S. França[1,4,5], Jaime C. Almeida[2,3], Reinhardt A. Fuck[1,4]

[1]Programa de Pós-Graduação em Geologia, Instituto de Geociências, Universidade de Brasília, Brasília, Brazil; [2]Instituto Dom Luiz (IDL), Faculdade de Ciências, Universidade de Lisboa, Portugal; [3]Departamento de Geologia, Faculdade de Ciências, Universidade de Lisboa, Portugal; [4]Instituto de Geociências, Universidade de Brasília, Brasília, Brazil; [5]Observatório Sismológico, Universidade de Brasília, Brasília, Brazil

### Abstract

Weak mechanical heterogeneities inherited from previous tectonic cycles are known to work as nucleating rifting-seeds during subsequent continental rift evolution. However, during rift-to-drift evolution the common occurrence of double-rifting, in which two main rift branches evolve before only one of them renders continental break-up, is still not fully understood. We thus carried out a numerical study to investigate the influence of pre-existent rifting-seeds in the nucleation, and potential tectonic interference, of early formed grabens during rifting of a continental crustal segment. We considered not only the influence of the number and distance at which the seeds are located, but also the potential mechanical control exerted by different archetypal ("Crème Brûlée" vs. "Jelly Sandwich") crustal rheological configurations. Our results show that none of these factors can by themselves alone explain the mechanics underlying the formation of early rifting geometries and ensuing crustal break-up configurations. It is thus only when their combined influence is considered that a coherent explanation for these diversified geometries and modes of evolution arises. Moreover, in view

of this new insight, it becomes apparent that double rifting is what to expect when only a single rifting-seed is present in the crust, or even in the absence of any inherited weaknesses, providing a possible explanation for the ubiquity of this type of rifting pattern in nature.

**Keywords:** Rift nucleation; Inherited crustal weaknesses; Numerical modelling

## 1. Introduction

Continental rifting is one of the fundamental evolutionary steps of the Wilson Cycle (Wilson, 1966; Dewey, 1969; Dewey and Burke, 1974) and an important process in Plate Tectonics, consisting in the formation of intracratonic extensional basins that potentially evolve into intervening oceans, ultimately leading to the formation of new continents. It is known that new rift systems commonly result from the extensional reactivation of pre-existing crustal/lithospheric weaknesses (e.g., previous main tectonic faults, ancient paleogeographic boundaries, fossilized suture zones) inherited from previous tectonic cycles (Henza et al., 2011; Chattopadhyay and Chakra, 2013; Zwaan and Schreurs, 2017). These weaknesses often lead to the early-rift development of two main grabens nucleating at variable distances from one another, and which subsequent evolution commonly leads to the abandonment of one of these structures, and to the simultaneous extensional-strain localization in the other (through which crustal/lithospheric break-up eventually occurs). Although this double rift evolution is well documented in different periods of Earth's evolution (Siqueira, 1989; Bahia et al., 2006, 2007; Kullberg et al., 2006; Pena dos Reis et al., 2010; Haeser et al., 2014; Loureiro, 2016; Zwaan et al., 2020), a clear geodynamic explanation for its causes is still lacking. In the present work, we use numerical models to understand the combined control on double-rift early-stage evolution, exerted by both: a) inherited rift-nucleating crustal weaknesses, and b) different (typical) continental crust strength profiles.

Studies on continental rifting have been carried out for different geological settings and through a variety of techniques, including numerical and analogue modelling (e.g., Brune and Ellis, 1997; Corti et al., 2003; Allken et al., 2011; Brune and Autin, 2013; Beniest et al., 2017, 2018; Koptev et al., 2017; Zwaan et al., 2019; Molnar et al., 2020; Yoshida et al., 2020). Several numerical modelling contributions have recently focused on the role of inherited structures in

rift nucleation and early continental rift evolution (Manatschal et al., 2015; Balázs et al., 2017; Brune et al., 2017; Duretz et al., 2020), on the interaction between orthogonal and oblique rifts (Allken et al., 2012; Zwaan et al., 2016) and on the geodynamic controls on symmetric/asymmetric rift geometry (Huismans and Beaumont, 2002; Li et al., 2020). In the present work, we use 2D numerical modelling to investigate the geodynamics of early double-rift nucleation triggered by inherited (i.e., pre-existent) continental crust weaknesses (rheological seeds). We specifically aim at understanding the effects of varying the distance between these weaknesses while assuming different (archetypical) continental-crust rheologic profiles. We further discuss the mechanical insight arising from our numerical experiments in view of some generical, well documented, natural occurrences of early double-rift evolution at different geological times.

# 2. Methodology

## 2.1. Numerical method

All models were developed using the Underworld code (Moresi et al., 2003, 2007), an open-source geodynamic modular computational framework that uses particle-in-cell (PIC) and finite element methods, allowing for the parallel computation of thermo-mechanical tectonic problems. Underworld solves the equations of conservation of mass (assuming fluid incompressibility, eq. 1), conservation of momentum (Stokes's equation, eq. 2), and temperature (eq. 3):

$$\nabla \cdot \boldsymbol{u} = 0 \qquad (1)$$

$$\nabla \cdot \boldsymbol{\sigma} = f \qquad (2)$$

$$\frac{\partial T}{\partial t} + u \cdot \nabla T = \kappa \nabla^2 T + Q(t) + \frac{H_S + H_A}{\rho C_P} \qquad (3)$$

with $\boldsymbol{u}$ (eq. 1) corresponding to the velocity vector and $\boldsymbol{\sigma}$ (eq. 2) to the stress tensor. The latter is defined as:

$$\boldsymbol{\sigma} = \boldsymbol{\sigma}' - PI \quad (4)$$

with $P$ being the pressure and $I$ the identity tensor. $\boldsymbol{\sigma}'$ is the deviatoric stress tensor:

$$\boldsymbol{\sigma}' = 2\eta\dot{\boldsymbol{\varepsilon}} \quad (5)$$

in which $\eta$ represents the dynamic viscosity and $\dot{\boldsymbol{\varepsilon}}$ is the strain rate tensor:

$$\dot{\boldsymbol{\varepsilon}} = \frac{1}{2}[\nabla\boldsymbol{u} + (\nabla\boldsymbol{u})^T] \quad (6)$$

In equation 3, $T$ is the temperature, $\kappa$ the thermal diffusivity and $Q$ the radiogenic heat production (representing how much is the heat production in each layer). $H_S$ is the shear heating term defined as:

$$H_s = \boldsymbol{\sigma}' \cdot \dot{\boldsymbol{\epsilon}}' \quad (8)$$

with $\dot{\boldsymbol{\epsilon}}'$ representing the deviatoric strain rate tensor. $H_A$ is the adiabatic heating term:

$$H_A = -T\alpha\frac{\partial P}{\partial t} \quad (9)$$

with $\alpha$ corresponding to the thermal expansion coefficient. In table 1 are represented the values of each equation parameter.

**Table 1.** Parameters for the Temperature Equation (eq. 3).

| Temperature Equation | | | | | |
|---|---|---|---|---|---|
| **Model** | **Layer** | **Thermal expansivity (α)** $K^{-1}$ | **Diffusivity (κ)** $m^2/s$ | **Capaciy (Cp)** $J/kgK$ | **Radiogenic Heat Production (Q)** $W/m^3$ |
| **RI** | UC | $3.00^{-5}$ | $1.00^{-6}$ | $1.00^{3}$ | $1.15^{-6}$ |
| | LC | $3.00^{-5}$ | $1.00^{-6}$ | $1.00^{3}$ | $2.50^{-7}$ |
| **RII** | UC | $3.00^{-5}$ | $1.00^{-6}$ | $1.00^{3}$ | $1.15^{-6}$ |
| | LC | $3.00^{-5}$ | $1.00^{-6}$ | $1.00^{3}$ | $2.50^{-7}$ |
| **RIII** | UC | $3.00^{-5}$ | $1.00^{-6}$ | $1.00^{3}$ | $1.15^{-6}$ |
| | LC | $3.00^{-5}$ | $1.00^{-6}$ | $1.00^{3}$ | $2.50^{-7}$ |

Our models used non-Newtonian thermal-dependent creep laws, in which the (empirically established) relationship between imposed deviatoric stresses and resulting strain rates is expressed by the so-called Patrice-Arrhenius equation:

$$\eta = \frac{1}{2} A^{\left(\frac{-1}{n}\right)} \dot{\varepsilon}_{II}^{\left(\frac{1}{n}-1\right)} e^{\left(\frac{E_a+V_aP}{nRT}\right)} (10)$$

with $\eta$ being the viscosity, $A$ the pre-exponential factor, $n$ the stress exponent, $E_a$ the activation energy, $V_a$ the activation volume, and $R$ the universal gas constant. In table 2 are presented the parameters for this equation.

**Table 2.** Parameters of the Patrice-Arrhenius equation (eq.10) for the models here presented. Note that in all the models, the effective viscosity of the UC and LC layers was constrained by upper and lower limits of $10^{18}$ Pa.s and $10^{24}$ Pa.s.

| Patrice-Arrhenius | | | | | | |
|---|---|---|---|---|---|---|
| **Model** | **Layer** | **A** $MPa^{3.5\times s^{-1}}$ | **Default** $\dot{\varepsilon}\ s^{-1}$ | **n** | **E** J/mol | **V** $m^3/mol$ |
| **RI** | UC | $3.20^{-3}$ | $1.00^{-17}$ | 3.5 | $1.54^{5}$ | $8.00^{-6}$ |
| | LC | $3.20^{-3}$ | $1.00^{-17}$ | 3.5 | $1.54^{5}$ | $8.00^{-6}$ |
| **RII** | UC | $3.20^{-3}$ | $1.00^{-17}$ | 3.5 | $1.54^{5}$ | $8.00^{-6}$ |
| | LC | $3.30^{-3}$ | $1.00^{-17}$ | 3.5 | $2.38^{5}$ | $1.20^{-5}$ |
| **RIII** | UC | $3.20^{-3}$ | $1.00^{-17}$ | 3.5 | $1.54^{5}$ | $8.00^{-6}$ |
| | LC | $3.30^{-3}$ | $1.00^{-17}$ | 3.5 | $2.38^{5}$ | $1.20^{-5}$ |

Rock plasticity behaviour was modelled assuming a Drucker-Prager plastic yielding criterion:

$$\sqrt{\tau_{II}} = sin\emptyset p + Ccos\emptyset \qquad (11)$$

where $\tau_{II}$ is the second invariant of the deviatoric stress tensor, $\emptyset$ is the internal frictional angle, and $C$ is the cohesion. For conditions where the strain = 0, the $\emptyset$ and $C$ are associated with an equation of strain softening. These parameters are specified in table 3.

**Table 2.** Drucker-Prager plastic yielding criterion parameters. The Internal Friction Coefficient ($\mu_c$) and Cohesion ($C$) vary exponentially between the maximum and minimum values, depending on applied strain rate (strain rate weakening). A strain weakening condition is also applied, $\emptyset = \mathbf{tan^{-1}}(\boldsymbol{\mu_c})$.

| | | Drucker-Prager | | | |
|---|---|---|---|---|---|
| **Model** | **Layer** | **Internal Friction Coefficient ($\mu_c$) (max)** | **Internal Friction Coefficient ($\mu_c$) (min)** | **Cohesion (max) ($C$) *MPa*** | **Cohesion (min) ($C$) *MPa*** |
| **RI** | UC | 0.7 | 0.007 | 44 | 0.0004 |
| | LC | --- | --- | --- | --- |
| **RII** | UC | 0.7 | 0.007 | 44 | 0.0004 |
| | LC | 0.7 | 0.007 | 44 | 0.0004 |
| **RIII** | UC | 0.7 | 0.007 | 44 | 0.0004 |
| | LC | 0.7 | 0.007 | 44 | 0.0004 |

## 2.2. Model setup and boundary conditions

All performed models consisted of a 300.6 x 50.4 km 2D domain (Fig.1), discretized with a resolution of 668 x 112 (corresponding to 450 x 450 m square cells with 60 particles per cell). Free surface boundary conditions (BCs) were ascribed to the model top boundary, comprising a 10.4 km thick air layer (Fig.1) to accommodate the development of model topography. Bottom BCs were set by an isostatic compensation condition along the model basal limit. The two (vertical) lateral boundaries were each defined by symmetrical diverging velocities of 1.5cm/yr (simulating an extension rate of 3 cm/yr).

A total of 21 numerical modelling experiments were carried out (Table 4), in which the distance between two rifting-seeds weak zones was varied in combination with three different modes of crustal rheological configuration (RI, RII and RIII; see Table 1). The distance between

the two seeds was serially varied between 10 and 50 km (with increments of 10 km, corresponding to 5 numerical runs). Two additional trials per experimental set were also performed: one in which only one seed was prescribed, and another without any seeds. The three different considered crustal rheological profiles were set to vary according to the following specifications:

a) The first rheological profile (RI, Fig. 1A and Table 4) comprises a strong 10 km thick upper-crust (UC) atop a 30 km thick weak lower-crust (LC). Non-Newtonian (and thermal dependent) viscous rheologies were ascribed to both the UC and the LC, following a Patrice-Arrhenius empirical law (see eq. 10 above, section 2.1). However, while the UC was set to accommodate plastic yielding (following a Drucker-Prager criterion, see eq. 11 above), the LC was set to deform only viscously, i.e., in the absence of any prescribed type of yielding criteria. The resulting rheological configuration was thus set to simulate a brittle thin UC and a weak thick LC, in compliance with a so called “Crème Brûlée” rheological profile (Chen and Molnar, 1983);

b) In the second rheological profile (RII, Fig. 1B and Table 4), the upper and lower crust were set with the same thicknesses as in RI. However, the LC was also ascribed a Drucker-Prager plastic yielding. The resulting (non-linear, thermal dependent) strength-depth configuration comprised an interbedded thin weak layer (~1.5 km thick) between the strong upper and lower crusts, conforming with a “Thin-Jelly Sandwich” rheological configuration;

c) The third rheological profile (RIII, Fig. 1C and Table 4) was also set by ascribing the same (Patrice-Arrhenius) viscous rheology and (Drucker-Prager) plastic yielding to both upper and lower crust. However, in this case, both crustal units were additionally set with equal (20 km) thicknesses. This rendered an overall rheological configuration comprising a weak 10 km thick layer interbedded between strong upper and lower crust domains, in compliance with an overall rheology structure corresponding to a "Thick-Jelly Sandwich” configuration (Burov and Watts, 2006).

The assumed default densities for the UC and LC were 2700 and 2900 kg/m$^3$, respectively, although these vary slightly depending on temperature (see the thermal expansivity parameter in Table 1). The prescribed rift-seeding crustal weaknesses were simulated by small vertically elongated bodies located at the base of the UC. These were set as iso-viscous, weak mechanical heterogeneities, with a fixed low viscosity of $10^{18}$ Pa.s, and were neutrally buoyant with respect to the UC. We understand that the rheological profiles of “Crème Brûlée” and “Jelly Sandwich”

are normally used to define the rheological structure of the lithosphere, however, in this case we applied these concepts only to the crust.

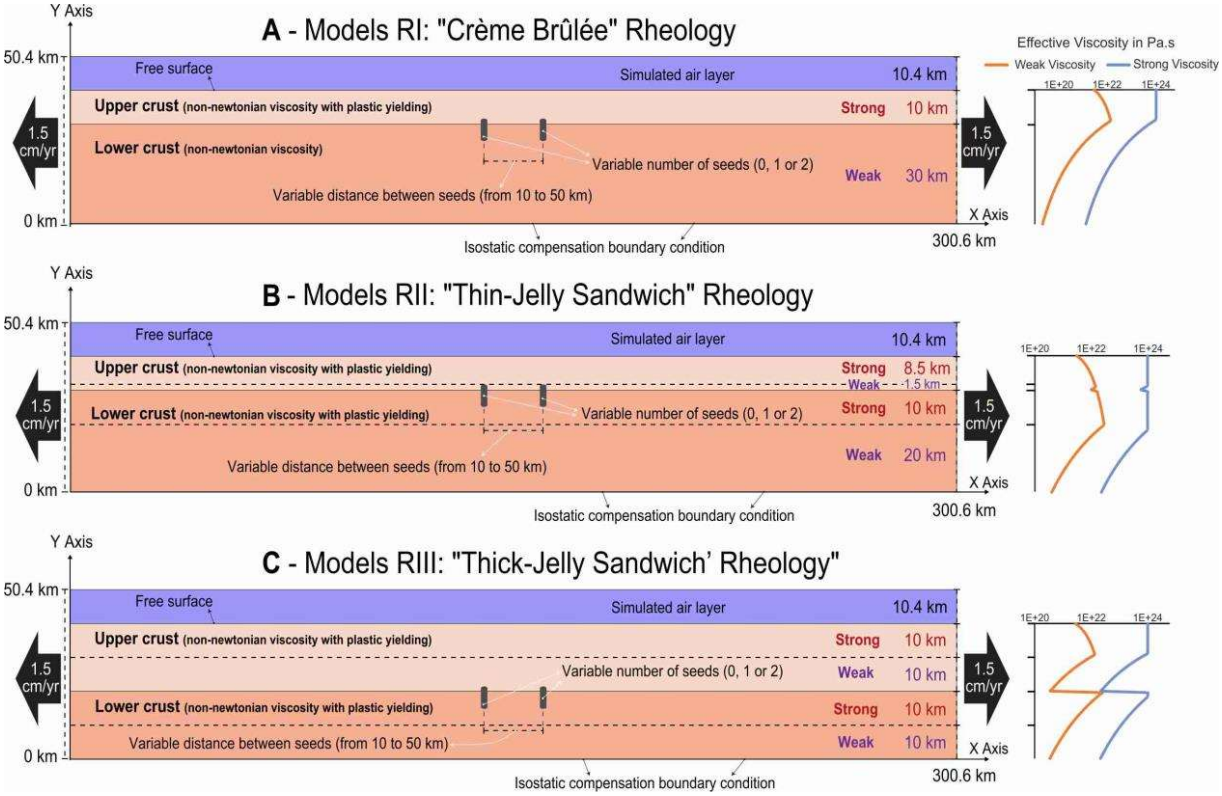


**Figure 1.** Conceived model setup for the three (RI, RII and RIII) groups of carried-out numerical experiments. All models have the same (300.6 x 50.4 km) domain dimensions, the same boundary conditions, and the same number of (0, 1 or 2) rift-seeding weaknesses, set at the same range of tested distances (10 to 50 km). A – "Crème Brûlée" RI model setup: both a 10 km thick upper crust (UC) and a 30 km thick lower crust (LC) were ascribed non-Newtonian, thermal-dependent, viscous rheologies (Patrice-Arrhenius viscosity). However, the upper crust was additionally set to be able to yield plastically (Drucker-Prager criterion). B – "Thin-Jelly Sandwich" RII model setup: the upper and lower crust have the same thicknesses as in RI, but a plastic yielding criterion was additionally ascribed to the LC in this case. C – "Thick-Jelly Sandwich" RIII model setup: as in RII, non-Newtonian viscosity and plastic yielding were ascribed to both the upper and lower crust, although in this case both these units were set to have a thickness of 20 km. In the Effective Viscosity charts, the strong viscosity (in the colour blue) assumes the default strain rate of $10^{-17}s^{-1}$, and corresponds to the crustal profile in a region away from the seeds in the final stages of the model, after the localization of the deformation along discrete shear zones; the weak viscosity (in the colour orange) assumes a strain rate of $10^{-15}s^{-1}$, corresponding to the early stages of deformation, when deformation is more homogeneous.

**Table 4.** Summary of the performed experiments: modes of rheological crustal configuration (rheological strength profiles RI, RII and RIII) and prescribed distances between rift-seeding weaknesses.

| SET | EXPERIMENTAL MODEL | CRUSTAL STRENGTH PROFILE | | Number of weaknesses | Distance between weaknesses |
|---|---|---|---|---|---|
| | | UPPER CRUST | LOWER CRUST | | |
| RI | 1 | "*Crème Brûlée*" | | 0 | - |
| | 2 | | | 1 | - |
| | 3 | | | 2 | 10 km |
| | 4 | | | 2 | 20 km |
| | 5 | Strong (10 km thick) | Very weak (no yielding criteria, 30 km thick) | 2 | 30 km |
| | 6 | | | 2 | 40 km |
| | 7 | | | 2 | 50 km |
| RII | 8 | *"Thin-Jelly Sandwich"* | | 0 | - |
| | 9 | | | 1 | - |
| | 10 | | | 2 | 10 km |
| | 11 | Strong top (8.5 km thick) + Weak thin bottom (1.5 km thick) | Strong top (10 km thick) + Weak bottom (20 km thick) | 2 | 20 km |
| | 12 | | | 2 | 30 km |
| | 13 | | | 2 | 40 km |
| | 14 | | | 2 | 50 km |
| RIII | 15 | *"Thick-Jelly Sandwich"* | | 0 | - |
| | 16 | | | 1 | - |
| | 17 | | | 2 | 10 km |
| | 18 | Strong top (10 km thick) + Weak bottom (10 km thick) | Strong top (10 km thick) + Weak bottom (10 km thick) | 2 | 20 km |
| | 19 | | | 2 | 30 km |
| | 20 | | | 2 | 40 km |
| | 21 | | | 2 | 50 km |

# 3. Results

## 3.1. Set RI "Crème Brûlée" rheology

In all of the carried-out sets, the models without any rifting-seeds were taken as a benchmark reference, i.e., as a term of comparison against which the other models of the same set were analysed. In set RI ("Crème Brulée"), the benchmark model RI-01 (Fig. 2A) revealed the development of a markedly delocalized fault-pattern in the thin (brittle) upper crust, characterized by a great number of pervasive, equally spaced, sets of conjugate normal faults (Fig. 2-A1 to A2). In the underlying thicker and weaker lower crust, the same amount of extensional strain was instead accommodated by ductile viscous flow. This lasted for

approximately 1.6 Ma, when extensional strain became strongly localized, leading to crustal rifting and eventually to symmetric upper crustal break-up (Fig. 2-A3).

In experiment RI-02 (Fig. 2B), the prescribed (single) seed triggered extensional strain localization at a much earlier time, promptly leading to quick asymmetric rifting marked by a well-defined hemi-graben configuration (Fig. 2-B1). This asymmetry was further amplified as extensional strain localization was intensified above and around the seed (Fig. 2-B2), leading to the formation of a detachment fault (possibly precluding crustal break-up through the formation of a *metamorphic core complex* type of structure, Coney, 1980; Lister and Davis, 1989, Fig. 2-B3).

In experiment RI-03 (Fig. 2C), the two close seeds at the base of the UC initially defined a wider weak zone, above which a more pervasive number of interfering conjugate normal faults was early localized (Fig. 2-C1). As whole-model extension continued, strain got preferentially accommodated above only one of the seeds (Fig. 2-C2), before consummation of crustal break-up occurred through the development of a symmetric rift configuration (Fig. 2-C3).

In experiment RI-07 (Fig. 2D), early extensional strain was also initially localized above the prescribed distant seeds, forming two independent asymmetric rift centres (Fig. 2-D1). As in the previous case, one of them was abandoned, while extension continued to concentrate on the other (Fig. 2-D2). However, crustal break-up was in this case assisted by markedly asymmetric rifting (see structural hemi-graben configuration in Fig. 2-D3).

In the experiments with two seeds, rifting was always observed to preferentially localize in only one of these initially prescribed crustal weaknesses (while the other waned and became inactive). Additionally, whenever some degree of tectonic interference was observed between the two initial rifts, a symmetric break-up rift-geometry was also always attained. Conversely, the absence of early inter-rift tectonic interference always led to the formation of an independent, asymmetric, rift configuration during crustal break-up.

# Set RI: *"Crème Brûlée"* rheology

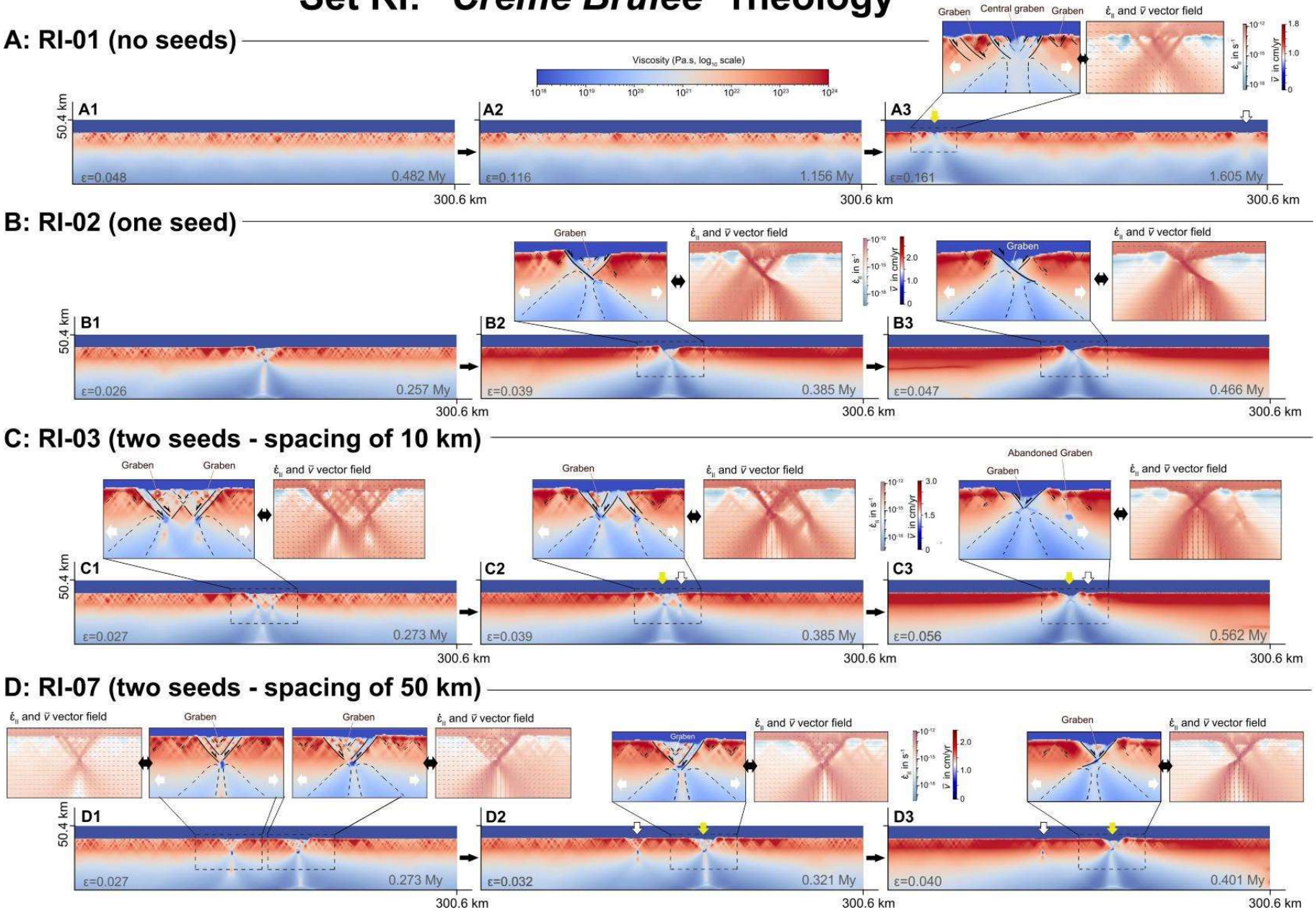

**Figure 2. (previous page)** "Crème Brulée" RI model results. A – RI-01 benchmark model (absence of rifting-seeds). A1 to A2: initial markedly delocalized fault pattern in the upper crust, and simultaneous (homogeneous) viscous strain accommodation in the lower crust; A3: relatively late rift nucleation and crustal break-up. B – RI-02 model (single rifting-seed). B1: relatively early rift nucleation above the seed, amid still some fault-delocalization in the upper crust; B2: accentuated (extensional) strain localization above the seed and markedly asymmetric rift development; B3: asymmetric break-up. C – RI-03 model (two rifting-seeds, 10 km apart). C1: early (extensional) strain nucleation above both nearby seeds (note the upper crust tectonic interference between both corresponding main grabens); C2: preferential (extensional) strain accommodation above one of the seeds, while rifting around the other starts to wane; C3: symmetric single-rift crustal break-up. D – RI-07 model (two rifting-seeds, 50 km apart). D1: early incipient development of two individual rifts, with two main asymmetric grabens forming above each of the distant seeds; D2: waning and eventual abandonment of one of the early formed upper crustal grabens, and simultaneous development of the other as an asymmetric rift; D3: asymmetric single-rift crustal break-up. All insets depict the (line drawing) interpretation of the main structures above the viscosity output, and the corresponding strain-rate output overlain by the velocity field. Yellow arrows: sites of strong (extensional) strain localization, rifting and eventual crustal break-up. White arrows: sites of rift waning and shutdown.

## 3.2. Set RII "Thin-Jelly Sandwich" rheology

In the benchmark experiments without any prescribed seeds (Fig. 3A), a diffuse fault delocalization pattern was observed to form throughout the two strong upper-crustal layers (Fig. 3-A1), whereas viscous extensional strain was homogeneously accommodated in the weak layers. After ~1.6 My, rifting was eventually nucleated in a narrow domain in the upper crust, because of intense extensional strain localization along two conjugated sets of upper crust faults, defining two interfering extensional grabens (Fig. 3-A2). Their main bounding faults cut across the interbedded thin weak layer, and through the underlying strong LC layer. Crustal break-up was finally attained after some degree of extensional waning in one of the grabens and concomitant strain localization in the other, although an overall symmetric structural configuration was preserved in this case (Fig. 3-A3).

In experiment RII-09 (Fig. 3B), extensional strain localization was promptly triggered at a much earlier stage (~0.4 My) by the prescribed single crustal seed, resulting in the formation of a main graben (Fig. 3-B1). Conversely to what was observed in the corresponding "Crème Brûlée" case (Fig. 2B), rifting configuration was in this situation markedly symmetric. Intense strain localization in the initial graben was gradually accentuated resulting in two main rift-bounding faults (Fig. 3-B2). These subsequently propagated across the underlying intermediate thin weak layer, and across the strong LC, to produce symmetrical crustal break-up (with well-defined rift shoulders limiting a central downwards collapsed domain, Fig. 3-B3).

The main observed difference between these "Thin-Jelly Sandwich" double-seed experiments (Fig. 3C and 3D) relatively to their "Crème Brulée" counterparts (Figs. 2C and 2D), was the tendency for the first to render symmetric, rather than asymmetric, grabens and ensuing break-up rift structures. Apart from this, the different distances at which the seeds were set bore the same influence in both cases: proximal seeds promoted more intense interference between early-forming (strain-localizing) grabens, resulting in relatively wider final rift and break-up structures (experiment RII-10, Fig. 3C), whereas more distant seeds favoured an independent evolution of the same early formed grabens, which yielded narrower rift break-up structures (experiment RII-14, Fig. 3D). As in all other previous cases with two rifting-seeds, extensional strain localization was always preferentially nucleated in only one of the evolving early rifts, while the other was systematically seen to wane and shut down (Figs. 3-C3 and D3).

In these "Thin-Jelly Sandwich" experiments, only a minor degree of strain-accommodation decoupling was observed, between the strong crustal layers above and below the sandwiched (thin) weak one. This was expressed essentially by a somewhat faster localization rate in the strong UC than in the strong LC, in which a pervasive, equally spaced, fault distribution pattern tended to last longer (see inset of Fig. 3-B2 and C2).

# Set RII: "*Thin-Jelly Sandwich*" rheology

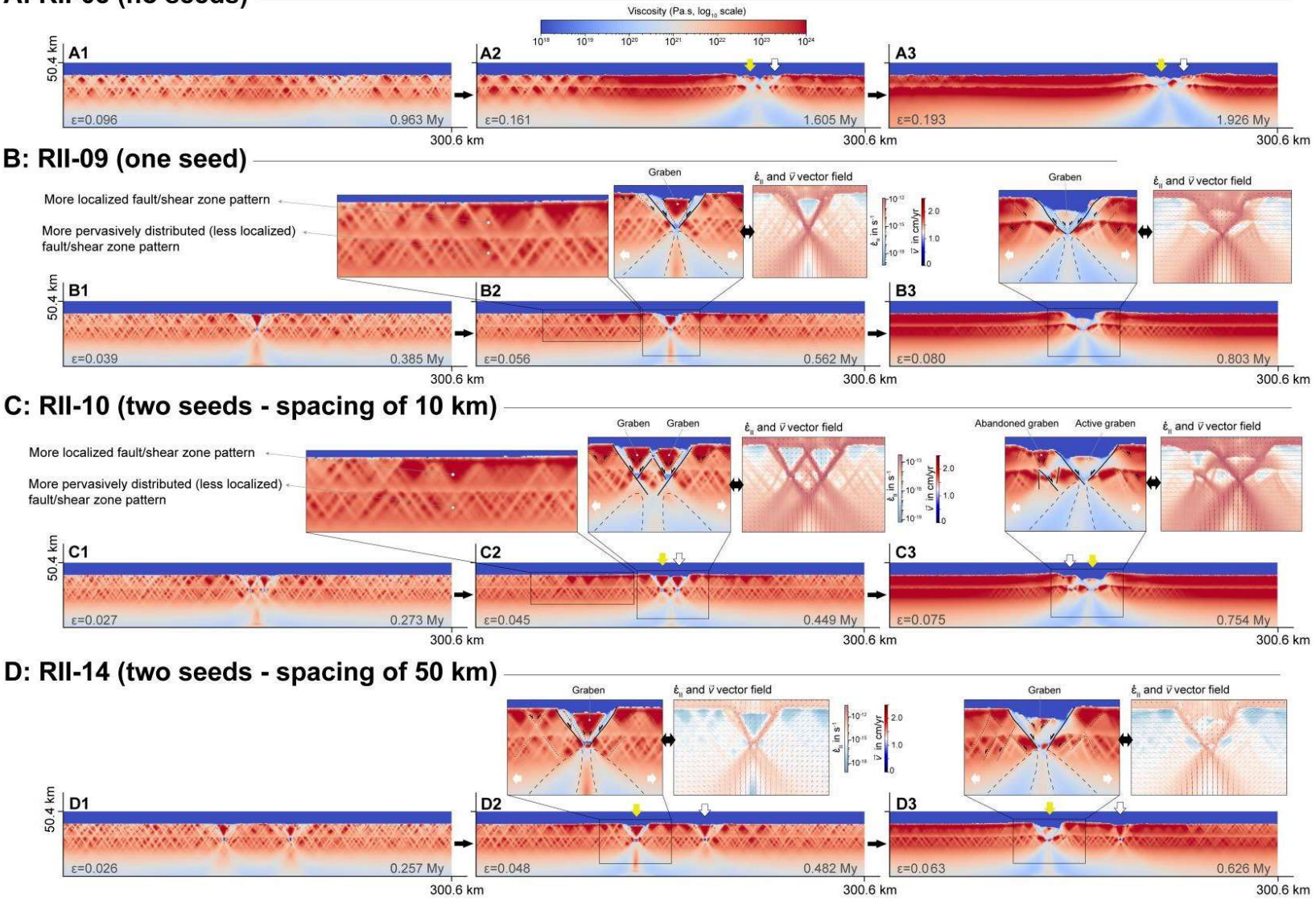

**Figure 3. (previous page)** "Thin-Jelly Sandwich" RII model results. A – RII-08 (absence of rifting-seeds). A1: initial markedly delocalized fault pattern affecting both strong crustal layers above and below the weak thin (sandwiched) layer; A2: rift nucleation in two interfering upper-crustal grabens; A3: crustal break-up achieved throughout one of the grabens and simultaneous waning of extensional rifting in the other. B – RII-09 model (single rifting-seed). B1: relatively early rift nucleation above the seed; B2: continued strong strain localization in the rift-seeded graben with a markedly symmetric configuration; B3: symmetric crustal break-up. C – RII-10 model (two rifting-seeds, 10 km apart). C1-C2: early (extensional) strain nucleation above both nearby seeds and formation of two (tectonically interfering) main grabens; C3: crustal (relatively wider) break-up is achieved through only one of the grabens, while the other is abandoned. An overall symmetric geometry is nevertheless preserved. D – RII-14 model (two rifting-seeds, 50 km apart). D1: early development of two individual, symmetric, main grabens, nucleated above each of the distant seeds; D2: one of the grabens begins to shut down while the other evolves to become a symmetric rift; D3: symmetric, single-rift, crustal break-up. All insets depict the (line drawing) interpretation of the main structures above the viscosity output, and the corresponding strain-rate output overlain by the velocity field. Yellow arrows: sites of strong (extensional) strain localization, rifting and eventual crustal break-up. White arrows: sites of rift waning and shutdown.

## 3.3. Set RIII "Thick - Jelly Sandwich" rheology

In the experiments without any rifting seeds (RIII-15, Fig. 4A), the prescribed bulk extension was accommodated by homogeneous viscous strain in the thick (middle-crust) weak layer, while an initially pervasive fault/shear zone-distribution pattern formed in the overlying strong portion of the UC (Fig. 4-A1). This pattern evolved to define a larger inter-fault spacing, separating the domains in which strain was preferentially localized (Fig. 4–A2). Conversely, no fault/shear zone pattern of similar sort was ever formed in the top section of the LC, which was only slightly perturbed when relative very late rifting (~2.7 My) affected the brittle overlying portion of the UC.

In the experiments with one prescribed rifting-seed (RIII-16, Fig. 4B), this weakness was observed to rupture the strong top section of the LC from the on-set of all experiments. As such, relative early (~0.8 My) extensional-strain localization was readily nucleated in the UC above this seed-related rift, consisting in the formation of two main graben-like structures (Fig. 4-B1). These grabens were consistently observed to align atop each of the flanks of the underlying seed-related rift. Both grabens initially evolved into well-defined rifts in the brittle UC, while the underlying seed-related LC rift bulged and widened (Fig. 4-B2). As extension continued, one of the UC rifts was eventually abandoned with strain being fully localized in the other, while the bulging and widening in the seed related LC rift was further accentuated (Fig. 4-B3). This evolution yielded a final break-up wide structural configuration expressing a significant

degree of decoupling in the way extension was accommodated above and below the thick middle-crust weak layer.

In the experiments with two closely spaced seeds (RIII-17, Fig. 4C) the results were very similar to the ones just described above for a single seed. The only difference was that the initial rupture of the strong LC occurred in two closely spaced locations, corresponding to the prescribed nearby rifting-seeds (Fig. 4-C1). However, this proximity had a rheological-controlling effect on the overall rifting evolution similar to the one exerted by a single (wider) seed as previously observed (cf. Fig. 4B and 4C). In fact, the two nearby seeds evolved and interfered during the overall accommodation of extension to form a single, wider, LC weak heterogeneity and a very similar decoupled crustal break-up configuration in the experimental end-stage (Fig. 4-C3).

In the experiments with two distant rifting seeds (RIII-17, Fig. 4D), for each of the prescribed LC weaknesses a pair of graben structures was early nucleated in the strong portion of the overlying UC (Fig. 4-D1). As in previous cases, these grabens initially evolved to form UC rifts before (in each one of the considered pairs) one waned and eventually shut down in favour of localizing the whole of the extensional-strain in the other (Fig. 4-D2). The overall resulting crustal break-up configuration (Fig. 4-D3) was similar to the one observed in the previous cases (see Fig. 4-B3 and C3), corresponding mostly to the lateral duplication of the same decoupled structural-rifting pattern, thus rendering a considerably wider rifting arrangement.

# Set RIII: "*Thick-Jelly Sandwich*" rheology

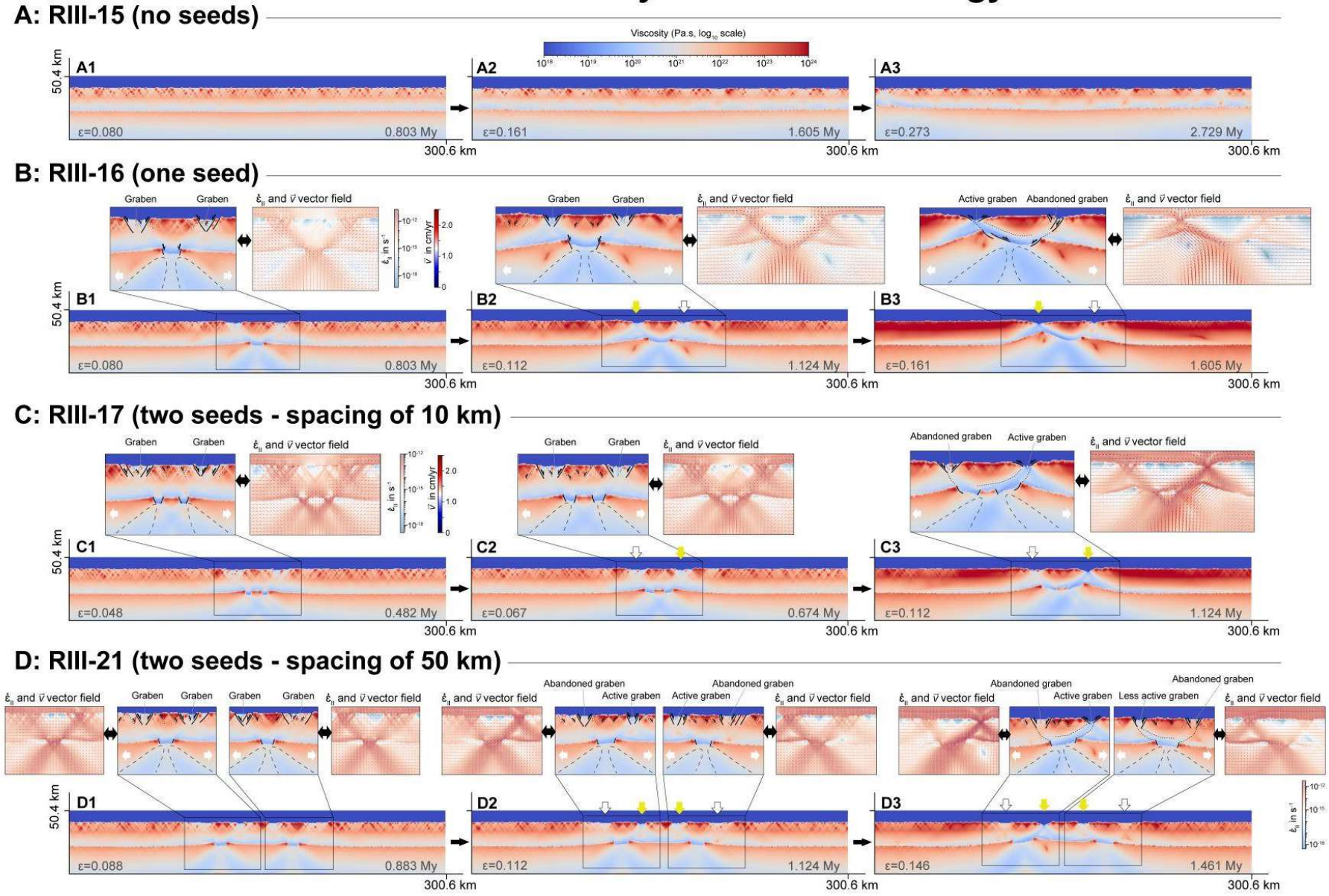

**Figure 4. (previous page)** "Thick-Jelly Sandwich" RIII model results. A – RIII-15 (absence of rifting-seeds). A1: bulk extensional strain is accommodated by a pervasive delocalized fault pattern in the strong portion of the upper crust (UC), and by viscous homogenous stretching in the weak middle-crust layer. No faults/shear zones are localized in the strong top segment of the lower crust (LC); A2: continued fault localization in the strong UC renders a relatively larger distance between faults/shear zones (less pervasive distribution); A3: rifting is localized in the UC only at a relatively late stage. The underlying strong top portion of the LC is only mildly perturbed. B – RIII-16 model (single rifting-seed). B1: early extensional-strain nucleation above the LC rifting-seed marked by the formation of two UC main grabens. Note that the grabens are aligned atop each of the flanks of the seed-related LC rift; B2: strain localization in the previously formed UC grabens results in the formation of two main UC rifts. Simultaneously, the seed-related LC rift undergoes significant bulging and widening; B3: relative narrow crustal break-up configuration, expressing a significant amount of decoupling in the way through which extensional-strain is accommodated above and below the middle-crust weak layer. C – RIII-17 model (two rifting-seeds, 10 km apart). C1 to C3: evolution similar to the one depicted in B (RIII-16 model). The two closed seeds interfere and coalesce, exerting a rheological control on the evolving rift configuration similar to the one observed for the single rifting-seed case above. D – RIII-21 model (two rifting-seeds, 50 km apart). D1: early development of two UC graben-like structures above each of the two LC seed-related rifts; D2: the previously formed pairs of UC grabens evolve into well-defined rift structures, although only one in each pair eventually evolves to render UC break-up (while the other wanes and shuts down); D3: final, wide, laterally duplicated, crustal break-up configuration, denoting the same decoupled nature of extensional-strain accommodation as in B3 and C3. All insets depict the (line drawing) interpretation of the main structures above the viscosity output, and the corresponding strain-rate output overlain by the velocity field. Yellow arrows: sites of strong (extensional) strain localization, rifting and eventual crustal break-up. White arrows: sites of rift waning and shutdown.

# 4. Discussion

Our results show that the influence of pre-existent crustal mechanical heterogeneities on continental rift evolution (including rift nucleation, inter-rift interference and crustal break-up completion), is highly dependent on the assumed general rheological configuration of the extending crustal segment. The rationale for the fundamental mechanical/rheological control on the geometry/kinematics of continental rifting has been previously put forward by several authors (Ord and Hobbs, 1989; Buck, 1991; Brun et al., 1994; Ranalli, 1995; Brun, 1999; Buck et al., 1999; Nagel and Buck, 2004, 2006, 2007; Keppler et al., 2013), and is here discussed in view of our results for the two main considered scenarios of "Crème Brûlée" and "Jelly Sandwich" rheological configurations.

## 4.1. "Crème Brûlée" double-rift evolution

When assuming a "Crème Brûlée" rheology, the tensile stress applied to the continental crust is essentially accommodated by the viscous homogenous response of the much thicker

underlying (weak) lower crust (Brun et al., 1994; Brun, 1999; Tirel et al., 2006, Fig. 5-A1). This ductile homogenous stretching determines an also distributed extensional accommodation response on the overlying thin brittle layer, expressed by the development of a pervasive delocalized fault/shear zone -pattern. This is exactly what is observed in our RI-01 benchmark experiment (see Fig. 2A), in which the absence of any rifting-seed weaknesses explains the absence of early-stage main hemi-grabens in the thin brittle UC (with few symmetric grabens occurring only at relative much later stages and at relative much greater inter-graben distances (Fig. 2-A3). Note that in this case, the late nucleation of UC grabens was preceded by the imprint of a long lasting pervasively distributed fault-pattern in this shallow brittle domain. This consisted in sets of conjugated normal faults/shear zones with a symmetric whole-graben geometry, which formed the mechanical grain driving the subsequent late graben nucleation. As such, these late formed grabens tend to display an also symmetric configuration (see inset of Fig. 2-A3), although in contradiction with what would be expected from the mechanical control exerted by an overall "Crème Brûlée" rheological stratification (Fig. 5-A2).

Conversely, in the models with a single seed a strong strain localization was observed from the onset of the extension (see Fig. 2 B). The bulk tensile stress was in this case essentially accommodated by a single main normal-fault, which was active throughout the whole of the experiment (insets of Fig. 2-B2 and B3). As previously shown by several authors (e.g., Nagel and Buck, 2004, 2007), this is only made possible by the "Crème Brûlée" rheological configuration, since it allows the LC viscous material beneath the downwards collapsing hanging-wall to easily flow laterally, continuously assisting the normal-fault kinematics along the same structure for a long time (see inset of Fig. 5-A2). This intense strain localization also explains the hemi-graben asymmetry of the main evolving rift structure. Note that in the absence of a "Crème Brûlée" configuration, either by assuming a stronger (i.e., more viscous) LC, or by considering a much thinner sandwiched one, it would inevitably become energetically more advantageous to develop other normal faults in the brittle UC to accommodate the same amount of extension (Figs. 5B and C).

When two seeds were considered within the same "Crème Brûlée" rheological scenario, the registered rifting evolution essentially expressed different degrees of interference between early nucleated extensional grabens, before one was abandoned, and deformation localized in the other (see Fig. 2C and 2D). For closely spaced seeds, the early inter-graben interference favoured a somewhat more symmetric rift geometry, built on the grain of the conjugate sets of normal faults inherited from that tectonic interference stage (see insets of Fig. 2-C1 and C2).

When the prescribed inter-seed distance was too large to allow any significant inter-graben and inter-rift interference, this tendency for graben/rift symmetry was no longer observed, since asymmetric hemi-graben formation is strongly favoured by the governing "Crème Brûlée" rheology (see Figs. 2B and D and Fig. 5A). In such a situation, relative narrower, markedly asymmetric, independent rift structures were formed instead (see insets of Fig. 2-D1 to D3).

### 4.2. "Thin-Jelly Sandwich" double-rift evolution

Two main differences arise from the consideration of a "Thin-Jelly Sandwich" rheology (see Fig. 3): 1) A clear prevalence of symmetric rift geometries (contrasting with the asymmetric hemi-graben rift patterns that predominate in the "Crème Brûlée" case, c.f. insets of Fig. 2-B2 and Fig. 3-B2); and 2) a difference between the degree of localization/distribution of the fault/shear zone patterns in the brittle crustal domains above and below the weak thin middle-crust layer (see insets of Fig. 3-B2 and C2). Both these differences are determined by the "thin Jelly-Sandwich" rheological configuration.

Concerning symmetric vs. asymmetric extensional structures, the kinematics of a single active normal fault nucleated in the brittle UC implies the progressive downthrow of the hanging wall block into the underlying thin viscous layer (see inset of Fig. 5-A2). However, conversely to what generally happens for a "Crème Brûlée" rheology, in this case this fault movement cannot be much accommodated by an efficient enough escape of the underlying viscous material (Fig. 5B). The fault kinematics is thus progressively hampered, favouring the development of a new (conjugate) normal fault to be able to continue to accommodate the same amount of bulk tensile stress (inset of Fig. 5-B2). This process eventually renders a predominance of multiple symmetric grabens, rather than isolated asymmetric hemi-grabens, to the brittle UC fault distribution pattern.

Similarly, while the pervasively distributed fault pattern in the brittle LC is driven by the homogeneous viscous stretching that affects its underlying (weak) bottom portion, the slightly more localized (i.e., wider distributed) fault pattern in the UC is also due to the mechanical effects implied by the same "Thin-Jelly Sandwich" rheological assumptions, and specifically by the (small) thickness of the sandwiched ("jelly"/weak) layer in this case (Nagel and Buck, 2004, 2006, 2007; Keppler et al., 2013).

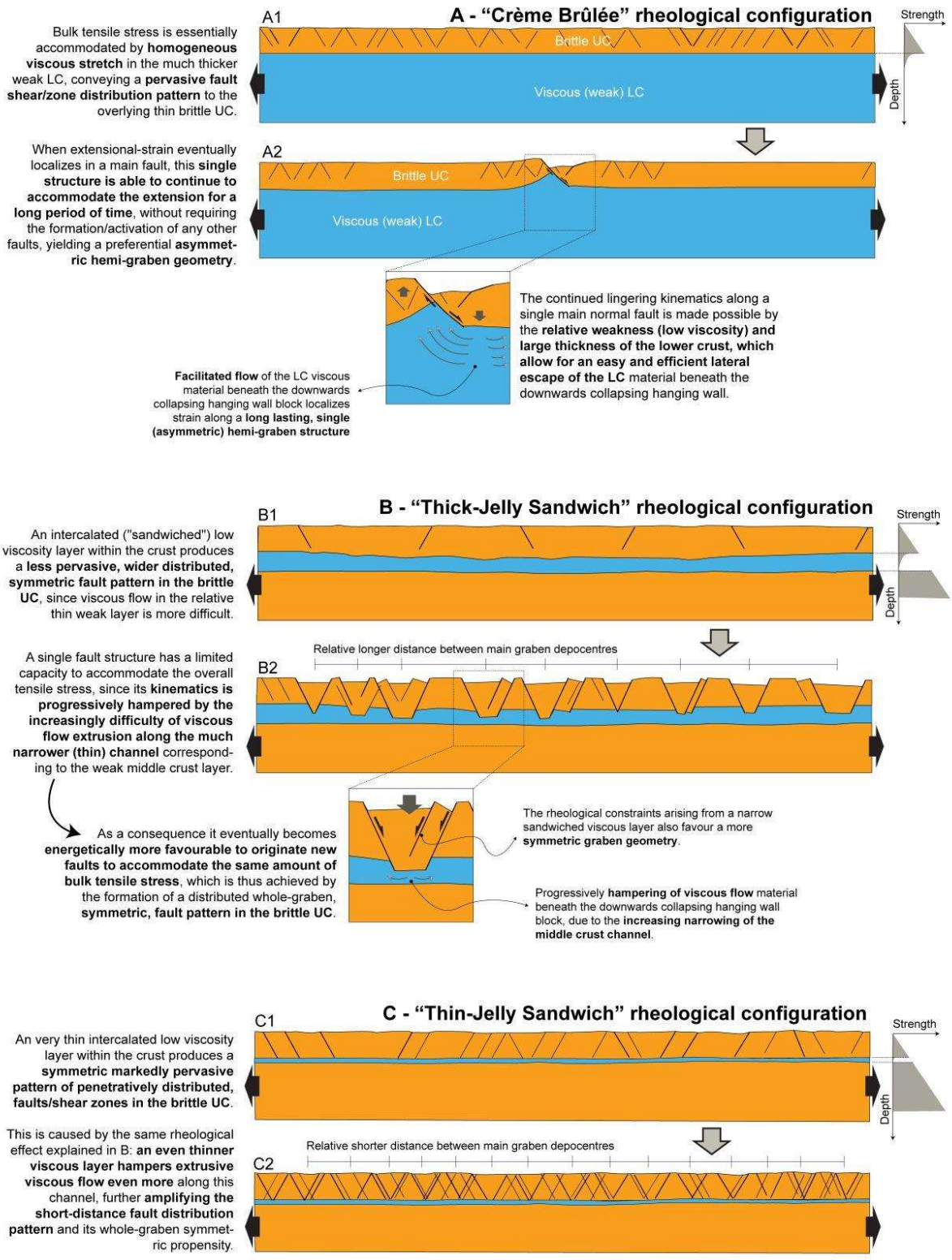
A - "Crème Brûlée" rheological configuration
A1
Strength
Brittle UC
Viscous (weak) LC
Depth
Bulk tensile stress is essentially accommodated by homogeneous viscous stretch in the much thicker weak LC, conveying a pervasive fault shear/zone distribution pattern to the overlying thin brittle UC.
A2
Brittle UC
Viscous (weak) LC
When extensional-strain eventually localizes in a main fault, this single structure is able to continue to accommodate the extension for a long period of time, without requiring the formation/activation of any other faults, yielding a preferential asymmetric hemi-graben geometry.
The continued lingering kinematics along a single main normal fault is made possible by the relative weakness (low viscosity) and large thickness of the lower crust, which allow for an easy and efficient lateral escape of the LC material beneath the downwards collapsing hanging wall.
Facilitated flow of the LC viscous material beneath the downwards collapsing hanging wall block localizes strain along a long lasting, single (asymmetric) hemi-graben structure
B - "Thick-Jelly Sandwich" rheological configuration
B1
Strength
Depth
An intercalated ("sandwiched") low viscosity layer within the crust produces a less pervasive, wider distributed, symmetric fault pattern in the brittle UC, since viscous flow in the relative thin weak layer is more difficult.
Relative longer distance between main graben depocentres
B2
A single fault structure has a limited capacity to accommodate the overall tensile stress, since its kinematics is progressively hampered by the increasingly difficulty of viscous flow extrusion along the much narrower (thin) channel corresponding to the weak middle crust layer.
As a consequence it eventually becomes energetically more favourable to originate new faults to accommodate the same amount of bulk tensile stress, which is thus achieved by the formation of a distributed whole-graben, symmetric, fault pattern in the brittle UC.
The rheological constraints arising from a narrow sandwiched viscous layer also favour a more symmetric graben geometry.
Progressively hampering of viscous flow material beneath the downwards collapsing hanging wall block, due to the increasing narrowing of the middle crust channel.
C - "Thin-Jelly Sandwich" rheological configuration
C1
Strength
Depth
An very thin intercalated low viscosity layer within the crust produces a symmetric markedly pervasive pattern of penetratively distributed, faults/shear zones in the brittle UC.
Relative shorter distance between main graben depocentres
C2
This is caused by the same rheological effect explained in B: an even thinner viscous layer hampers extrusive viscous flow even more along this channel, further amplifying the short-distance fault distribution pattern and its whole-graben symmetric propensity.

**Figure 5. (previous page)** Schematic illustration of the control exerted by different fundamental crustal rheological configurations on the formation of upper-crustal fault/shear-zone distribution patterns during continental rifting (e.g., Nagel and Buck, 2004, 2006, 2007; Keppler et al., 2013): A - "Crème Brûlée" rheological stratification; B - "Thick-Jelly Sandwich" rheological stratification and; C - "Thin-Jelly Sandwich" rheological stratification. UC: Upper crust; LC: Lower crust.

The slightly wider fault distribution pattern in the brittle UC (comparatively to the more pervasive one affecting the same domain in the "Crème Brûlée" experiments, c.f. Figs. 2A and 3A) also provides an explanation for the resemblance between the results obtained in the benchmark experiments without any seeds (RII-08, Fig. 3A), and the ones obtained for the experiments with two close seeds (RII -10, Fig. 3C). The reason why two main grabens end up by nucleating in the UC in the first case, is the fact that when the strain finally localizes it follows the inherited relative wider fault-distribution grain produced by the sandwiched thin weak layer. Thus, two adjacent but still independent and separated main grabens are formed in the upper crust of the benchmark experiment, which evolve in the same way as the pair of grabens observed to have nucleated above each of the rifting-seeds in the two seeds experiments (compare Fig. 3-A2 to A3 and Fig. 3-C2 to C3).

### 4.3. "Thick-Jelly Sandwich" double-rift evolution

The same fundamental mechanics of fault/shear zone distribution arises from the "Thick-Jelly Sandwich" rheological configuration in RIII experiments. However, in this case the viscous weak ("jelly") layer is thicker, rendering the development of a wider fault distribution pattern in the overlying brittle UC (Nagel and Buck, 2004, 2006, 2007; Keppler et al., 2013, Fig. 5B). Also, the underlying strong top domain of the LC does not accommodate any significant extension through fault/shear zone distribution/localization, resisting to the applied bulk tensile stress by high viscosity flowing (see Fig. 4A). When a rifting-seed is prescribed (see Fig. 4B), this strong LC top layer is rifted from the onset of the experiment, allowing for early intense extensional strain-rate localization in the closest pair of nearby grabens developing in the above UC (inset of Fig. 4-B1). This creates a conspicuous rifting pattern that comprises two shallower UC grabens nucleated above a single (relatively deeper) one (inset of Fig. 4-B2). Such rifting arrangement is the result of the combined mechanical effect exerted by both, a pre-existent (inherited) crustal weakness and, critically, by the assumed "Thick-Jelly Sandwich" rheological configuration. Note that the spacing between the pair of shallow UC grabens is "just

right" to render activation of both these structures at the expense of a single underlying weak seed (Fig. 6A). A shorter distance (Fig. 6B) would probably result in shallow graben tectonic interference leading to a single rift structure, while a wider one (Fig. 6C) would be highly dependent on the exact position of the seed relative to the overlying grabens. This suitable inter-fault/shear zone distance is determined by the ~10 km thickness of the weak (viscous) layer in our "thick-Jelly Sandwich" models. This is characteristic of many continental crust strength-depth profiles, in which a weak (viscously yielding) middle crust is intercalated between a brittle upper crust layer, and a strong lower crust or upper mantle (Ord and Hobbs, 1989; Brun et al., 1994; Brun and Beslier, 1996; Gueydan et al., 2003; Nagel and Buck, 2004, 2007; Wijns et al., 2005; Lavier and Manatschal, 2006).

Two nearby LC rifting-seeds produce the same double rift shallow pattern in the overlying UC (see Fig. 4C), since the implied overlapping of the two weakened crustal areas has the same strain localizing effect of considering just one seed. The robustness of this pattern was also confirmed in the experiments with two distant rifting-seeds, in which two shallower grabens also develop above each one of the two separated seeds (see Fig. 4D). This explains the lateral duplication of the number of UC rifts, rendering a much wider crustal break-up configuration to the experimental final stage (Fig. 4-D3).

### 4.4. A possible explanation for double upper-crustal rifting in nature

During rift-to-drift evolution, the early development of two main rifts, prior to the onset of continental break-up through only one of these structures, is well documented by several examples occurring at different times during the history of the Earth (Siqueira, 1989; Bahia et al., 2006, 2007; Kullberg et al., 2006; Pena dos Reis et al., 2010; Haeser et al., 2014; Loureiro, 2016; Zwaan et al., 2020). Among many others, the Neoproterozoic to lower Palaeozoic tectono-sedimentary record of the Parecis Basin (in central-West Brazil) records the early rifting evolution, and sin-tectonic siliciclastic infill of two main parallel grabens, prior to the occurrence of preferential strain localization through any of them (Siqueira, 1989; Bahia et al., 2006, 2007; Haeser et al., 2014; Loureiro, 2016). Jurassic to lower Cretaceous rifting in the Lusitanian Basin (West Iberia) also records the overall unfolding of a double-rift tectono-sedimentary evolution (e.g., Kullberg et al., 2006; Pena dos Reis et al., 2010; Soares et al., 2012). In this case, the abandonment of the rift basin that corresponds to the Lusitanian Basin

itself (giving rise to a so-called aulacogen, Burke, 1977), was matched by continental break-up and the opening of the Atlantic through the other major graben further to the West. It is also possible to recognize two main active rift systems in present day examples of continental rift, as in the East African Rift case that comprises two main Eastern and Western branches to each side of the Tanzania craton (e.g., Mougenot et al., 1986; Ebinger, 2005; Corti, 2009; Koptev et al., 2016).

Our results show that double rifting early evolution is generally possible, in any of the considered rheological scenarios, when the nucleation of two shallow UC grabens is caused by two (pre-existing/inherited) weaknesses: in RI experiments for a "Crème Brûlée" rheology (Fig. 2-D1 to D3) and in RII experiments for a "Thin-Jelly Sandwich" rheology (Fig. 3-C1 to C2 and D1 to D2). However, double rifting early evolution is also shown to be possible because of the way through which the general rheological structure controls the fault/shear zone distribution pattern in the brittle UC. Our results show that this is not only possible, but in fact probable to happen when only a single rifting-seed is prescribed for a "Thick-Jelly Sandwich" scenario (see Fig. 4B), and even in the absence of any seeds, when late extensional strain localization occurs for a "Thin-Jelly Sandwich" general rheological configuration (see Fig. 3A).

By showing that double rifting is quite what to expect when an overall "Jelly-Sandwich" rheological stratification is considered, our results provide an explanation for the relative ubiquity of double rifting in nature. They also show that single or double rifting configurations cannot be explained solely by the number (and spatial arrangement) of inherited weaknesses in an ancient crustal basement, but also by necessarily considering the specific rheological scenario under which rifting unfolds.

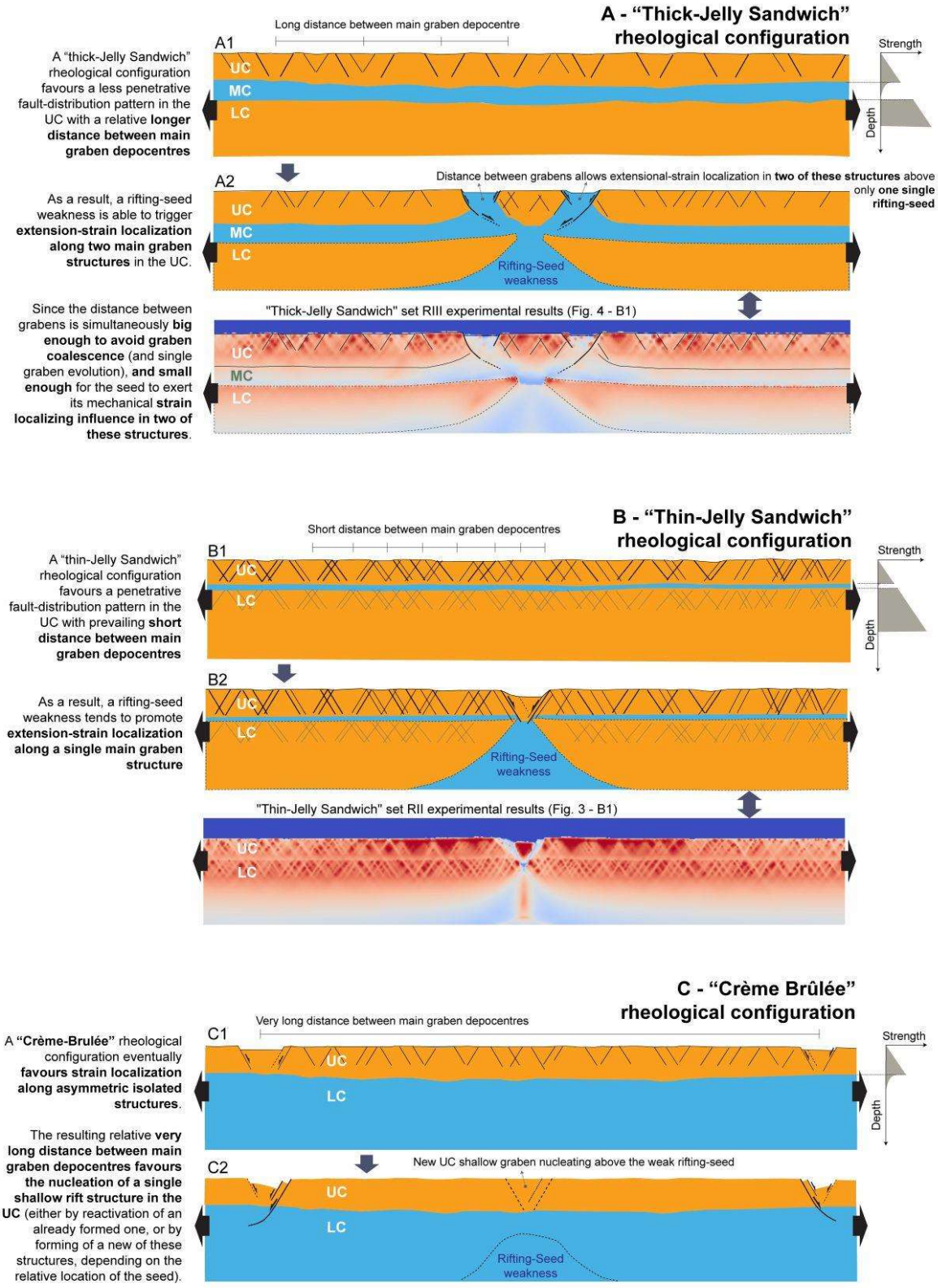
A - "Thick-Jelly Sandwich" rheological configuration
A "thick-Jelly Sandwich" rheological configuration favours a less penetrative fault-distribution pattern in the UC with a relative longer distance between main graben depocentres
Long distance between main graben depocentre
A1
UC
MC
LC
Strength
Depth
As a result, a rifting-seed weakness is able to trigger extension-strain localization along two main graben structures in the UC.
A2
Distance between grabens allows extensional-strain localization in two of these structures above only one single rifting-seed
Rifting-Seed weakness
Since the distance between grabens is simultaneously big enough to avoid graben coalescence (and single graben evolution), and small enough for the seed to exert its mechanical strain localizing influence in two of these structures.
"Thick-Jelly Sandwich" set RIII experimental results (Fig. 4 - B1)
B - "Thin-Jelly Sandwich" rheological configuration
A "thin-Jelly Sandwich" rheological configuration favours a penetrative fault-distribution pattern in the UC with prevailing short distance between main graben depocentres
Short distance between main graben depocentres
B1
As a result, a rifting-seed weakness tends to promote extension-strain localization along a single main graben structure
B2
"Thin-Jelly Sandwich" set RII experimental results (Fig. 3 - B1)
C - "Crème Brûlée" rheological configuration
A "Crème-Brulée" rheological configuration eventually favours strain localization along asymmetric isolated structures.
The resulting relative very long distance between main graben depocentres favours the nucleation of a single shallow rift structure in the UC (either by reactivation of an already formed one, or by forming of a new of these structures, depending on the relative location of the seed).
Very long distance between main graben depocentres
C1
C2
New UC shallow graben nucleating above the weak rifting-seed

**Figure 6. (previous page)** Schematic illustration of different possibilities of UC graben nucleation above a single rifting-seed weakness, depending on different assumed archetypal rheological configurations and implied modes of fault/shear zone – distribution/localization patterns. A: "Thick-Jelly Sandwich" rheological stratification renders a relatively less pervasive fault distribution pattern (relatively longer distance between main graben depocentres), which favours early double-graben nucleation and double-rift evolution above the rifting-seed; B - "Thin-Jelly Sandwich" rheological stratification renders a much more pervasive fault distribution pattern (relatively shorter distance between main graben depocentres), favouring early single-graben nucleation and single-rift evolution above the rifting-seed; C - "Crème Brûlée" rheological stratification renders a much wider fault distribution pattern (very long distance between main asymmetric hemi-graben depocentres), favouring again single-graben nucleation above the rifting seed.

# 5. Conclusions

The following main conclusions are drawn from the obtained numerical results:

1) Inherited (basal UC) mechanical weaknesses in a rifting basement always anticipate the nucleation of shallow graben structures directly above these weak heterogeneities, in which extensional strain is further localized. Such rifting-seed heterogeneities thus exert a strong mechanical control on the subsequent rift geometry and eventual crustal break-up.
2) Conversely, the absence of any rifting-seeds significantly prolongs the rifting evolution prior to major UC graben nucleation. As such, the main mechanical control on crustal tensile stress accommodation in this case is exerted by the assumed overall (strength-depth) rheological configuration of the rifting basement, which ultimately determines the way through which deformation is distributed/localized in the brittle UC.
3) When inherited rifting-seeds are considered, the resulting rift geometry and evolution cannot be solely explained by the potential tectonic interference between early formed main grabens (e.g., depending on their distance and relative position), but critically, by the conjugated effect resulting from the weakening pre-existent heterogeneities and the specific rheological stratification ("Crème Brûlée" vs. "Jelly-Sandwich") of the rifting basement in which they are embedded.
4) The following detailed consequences result from the previous point:
   - Asymmetric hemi-graben rifting mostly results from considering single or separated rift-seeding weaknesses under a "Crème Brûlée" crustal rheological stratification (e.g., Fig. 2B and D);

- Conversely, UC symmetric grabens and symmetric rifting are clearly favoured by a “Jelly Sandwich” rheological stratification (regardless of inter-seed distance, Fig. 3B, C and D). However, they can also arise under a “Crème Brûlée” general configuration, either as a consequence of graben late nucleation (in the absence of any seeds – Fig. 2A); or resulting from an early-rifting tectonic interference between two nearby hemi-grabens (e.g., Fig. 2C);
- Single rift evolution is always favoured by early nucleation of a main graben above a single rifting-seed (Figs. 2B and 3B). Less frequently, it can also result either from close inter-graben early tectonic interference (leading to graben coalescence and final single-rift break up – Fig. 2C); or in the absence of any rifting seeds, from late graben amplification/nucleation in durable over-extended domains under a “Crème Brûlée” rheological arrangement (Fig. 2-A3);
- Double rifting is a more common result than anticipated by the sole consideration of the number of prescribed rifting-seeds. Regardless of the assumed rheological stratification, it always results from early double graben nucleation and evolution above two separated seeds. However, it is also strongly favoured by the UC brittle distribution pattern of deformation that arises from a “Jelly-Sandwich” rheological stratification, which can cause double rifting above only one seed (e.g., Fig. 4B), or even in the absence of any seeds (Fig. 3A).

## Acknowledgements

M. E. Oliveira acknowledges a Ph.D. grant by Fundação de Apoio à Pesquisa do Distrito Federal and Coordenação de Aperfeiçoamento de Pessoal de Nível Superior – Brasil (CAPES) – Finance Code 001. The study had the support of Instituto Nacional de Ciência e Tecnologia - Estudos Tectônicos (INCT-ET, suported by CNPq, CAPES and FAPDF) and Conselho Nacional de Desenvolvimento Científico e Tecnológico (CNPq). A.S. Gomes acknowledges a Ph.D. grant by the Fundação para a Ciência e Tecnologia, ref: SFRH/BD/146726/2019 - Earthsystems-IDL. Jaime Almeida acknowledges a Ph.D. grant by the Fundação para a Ciência e Tecnologia, ref: PD/BD/135067/2017 - Earthsystems-IDL. A.S. Gomes, F.M. Rosas, J.C. Duarte, and J. Almeida acknowledge funding from the FCT through the project UIDB/50019/2021-IDL. G. S. França and R.A. Fuck acknowledge CNPq for Research

Fellowship. We also acknowledge Nicolas Riel for continued support with Underworld and discussions on geodynamic modelling.

## References

Allken, V., Huismans, R.S., Thieulot, C., 2012. Factors controlling the mode of rift interaction in brittle-ductile coupled systems: A 3D numerical study. Geochemistry Geophys. Geosystems 13, 1–18. https://doi.org/10.1029/2012GC004077

Allken, V., Huismans, R.S., Thieulot, C., 2011. Three-dimensional numerical modeling of upper crustal extensional systems. J. Geophys. Res. 116, 1–15. https://doi.org/10.1029/2011JB008319

Bahia, R.B.C., Martins-Neto, M.A., Barbosa, M.S.C., Pedreira, A.J., 2007. Análise da evolução tectonossedimentar da Bacia dos Parecis através de métodos potenciais. Rev. Bras. Geociências 37, 639–649. https://doi.org/10.25249/0375-7536.2007374639649

Bahia, R.B.C., Martins-Neto, M.A., Barbosa, M.S.C., Pedreira, A.J., 2006. Revisão Estratigráfica Da Bacia Dos Parecis – Amazônia. Rev. Bras. Geociências 36, 692–703. https://doi.org/10.25249/0375-7536.2006364692703

Balázs, A., Burov, E., Matenco, L., Vogt, K., Francois, T., Cloetingh, S., 2017. Symmetry during the syn-and post-rift evolution of extensional back-arc basins: The role of inherited orogenic structures. Earth Planet. Sci. Lett. 462, 86–98. https://doi.org/10.1016/j.epsl.2017.01.015

Beniest, A., Koptev, A., Burov, E., 2017. Numerical models for continental break-up: Implications for the South Atlantic. Earth Planet. Sci. Lett. 461, 176–189. https://doi.org/10.1016/j.epsl.2016.12.034

Beniest, A., Willingshofer, E., Sokoutis, D., Sassi, W., 2018. Extending continental lithosphere with lateral strength variations: effects on deformation localization and margin geometries. Front. Earth Sci. 1–11. https://doi.org/10.3389/feart.2018.00148

Brun, J.P., 1999. Narrow rifts versus wide rifts: inferences for the mechanics of rifting from laboratory experiments. Philos. Trans. Math. Phys. Eng. Sci. 357, 695–712.

Brun, J.P., Beslier, M.O., 1996. Mantle exhumation at passive margins. Earth Planet. Sci. Lett. 142, 161–173. https://doi.org/10.1016/0012-821x(96)00080-5

Brun, J.P., Sokoutis, D., Van Den Driessche, J., 1994. Analogue modeling of detachment fault systems and core complexes. Geology 22, 319–322.

Brune, J.N., Ellis, M.A., 1997. Structural features in a brittle-ductile wax model of continetal extension. Lett. to Nat. 387, 67–70.

Brune, S., Autin, J., 2013. The rift to break-up evolution of the Gulf of Aden: Insights from 3D numerical lithospheric-scale modelling. Tectonophysics 507, 65–79. https://doi.org/10.1016/j.tecto.2013.06.029

Brune, S., Corti, G., Ranalli, G., 2017. Controls of inherited lithospheric heterogeneity on rift linkage: Numerical and analog models of interaction between the Kenyan and Ethiopian rifts across the Turkana depression. Tectonics 36, 1767–1786. https://doi.org/10.1002/2017TC004739

Buck, W.R., 1991. Modes of continental lithospheric extension. J. Geophys. Res. Solid Earth 96, 20161–20178. https://doi.org/10.1029/91JB01485

Buck, W.R., Lavier, L.L., Poliakov, A.N.B., 1999. How to make a rift wide. Philos. Trans. R. Soc. A Math. Phys. Eng. Sci. 357, 671–693. https://doi.org/10.1098/rsta.1999.0348

Burke, K., 1977. Aulacogens and continental breakup. Ann. Rev. Earth Planet Sci. 5, 371–396.

Burov, E.B., Watts, A.B., 2006. The long-term strength of continental lithosphere: “jelly sandwich” or “crème brûlée”? GSA Today 16, 4–10.

Chattopadhyay, A., Chakra, M., 2013. Influence of pre-existing pervasive fabrics on fault patterns during orthogonal and oblique rifting: An experimental approach. Mar. Pet. Geol. 39, 74–91. https://doi.org/10.1016/j.marpetgeo.2012.09.009

Chen, W.-P., Molnar, P., 1983. Focal depths of intracontinental and intraplate earthquakes and their implications for the thermal and mechanical properties of the lithosphere. J. Geophys. Res. Solid Earth 88, 4183–4214. https://doi.org/10.1029/JB088iB05p04183

Coney, P.J., 1980. Cordilleran metamorphic core complexes: An overview. Mem. Geol. Soc. Am. 153, 7–31. https://doi.org/10.1130/MEM153-p7

Corti, G., 2009. Continental rift evolution: From rift initiation to incipient break-up in the Main Ethiopian Rift, East Africa. Earth-Science Rev. 96, 1–53. https://doi.org/10.1016/j.earscirev.2009.06.005

Corti, G., Bonini, M., Conticelli, S., Innocenti, F., Manetti, P., Sokoutis, D., 2003. Analogue modelling of continental extension: A review focused on the relations between the patterns of deformation and the presence of magma. Earth-Science Rev. 63, 169–247. https://doi.org/10.1016/S0012-8252(03)00035-7

Dewey, J.F., 1969. Continental margins: a model for conversion of Atlantic type to Andean type. Earth Planet. Sci. Lett. 6, 189–197.

Dewey, J.F., Burke, K., 1974. Hot spots and collisional break-up: Implications for collisional orogeny. Geology 2, 57–60. https://doi.org/10.1130/0091-7613(1974)2<57:HSACBI>2.0.CO;2

Duretz, T., Asti, R., Lagabrielle, Y., Brun, J.P., Jourdon, A., Clerc, C., Corre, B., 2020. Numerical modelling of Cretaceous Pyrenean Rifting: The interaction between mantle exhumation and syn-rift salt tectonics. Basin Res. 32, 652–667. https://doi.org/10.1111/bre.12389

Ebinger, 2005. Continental break-up: The East African perspective. Bullerwell Lect. 46, 2.26-2.21. https://doi.org/10.1111/j.1468-4004.2005.46216.x

Gueydan, F., Leroy, Y.M., Jolivet, L., Agard, P., 2003. Analysis of continental midcrustal strain localization induced by microfracturing and reaction-softening. J. Geophys. Res. Solid Earth 108, 1–18. https://doi.org/10.1029/2001jb000611

Haeser, B. da S., Zalán, P.V., Ferreira, M.A., Petersohn, E., 2014. Revisão litoestratigráfica da Bacia dos Parecis e implicações para a exploração de petróleo, in: Rio Oil & Gas Expo and Conference. Rio de Janeiro, p. 10.

Henza, A.A., Withjack, M.O., Schlische, R.W., 2011. How do the properties of a pre-existing normal-fault population influence fault development during a subsequent phase of extension? J. Struct. Geol. 33, 1312–1324. https://doi.org/10.1016/j.jsg.2011.06.010

Huismans, R.S., Beaumont, C., 2002. Asymmetric lithospheric extension: The role of frictional plastic strain softening inferred from numerical experiments. Geology 30, 211–214.

Keppler, R., Rosas, F.M., Nagel, T.J., 2013. Thin viscous middle-crust and evolving fault distribution during continental rifting: Insights from analog modeling experiments. Tectonophysics 608, 161–175. https://doi.org/10.1016/j.tecto.2013.10.001

Koptev, A., Burov, E., Calais, E., Leroy, S., Gerya, T., Guillou-Frottier, L., Cloetingh, S., 2016. Contrasted continental rifting via plume-craton interaction: Applications to Central East African Rift. Geosci. Front. 7, 221–236. https://doi.org/10.1016/j.gsf.2015.11.002

Koptev, A., Burov, E., Gerya, T., Le Pourhiet, L., Leroy, S., Calais, E., Jolivet, L., 2017. Plume-induced continental rifting and break-up in ultra-slow extension context: Insights from 3D numerical modeling. Tectonophysics 746, 121–137. https://doi.org/10.1016/j.tecto.2017.03.025

Kullberg, J.C., Terrinha, P., Pais, J., Reis, R.P., Legoinha, P., 2006. Arrábida e Sintra: dois exemplos de tectónica pós-rifting da Bacia Lusitaniana, in: Dias, R., Araújo, A., Terrinha, P., Kullberg, J.C. (Eds.), Geologia de Portugal No Contexto Da Ibéria. Universidade de Évora, pp. 369–396.

Lavier, L.L., Manatschal, G., 2006. A mechanism to thin the continental lithosphere at magma-poor margins. Nature 440, 324–328. https://doi.org/10.1038/nature04608

Li, Y., Abbas, A., Li, C.-F., Sun, T., Zlotnik, S., Song, T., Zhang, L., Yao, Z., Yao, Y., 2020. Numerical modeling of failed rifts in the northern South China Sea margin: Implications for continental rifting and breakup. J. Asian Earth Sci. 199, 1–15. https://doi.org/10.1016/j.jseaes.2020.104402

Lister, G.S., Davis, G.A., 1989. The origin of metamorphic core complexes and detachment faults formed during Tertiary continental extension in the northern Colorado River region, U.S.A. J. Struct. Geol. 11, 65–94.

Loureiro, E.M.L., 2016. Caracterização geológico-tectônica da Bacia dos Parecis. Uma interpretação integrada. Universidade do Estado do Rio de Janeiro.

Manatschal, G., Lavier, L., Chenin, P., 2015. The role of inheritance in structuring hyperextended rift systems: Some considerations based on observations and numerical modeling. Gondwana Res. 27, 140–164. https://doi.org/10.1016/j.gr.2014.08.006

Molnar, N., Cruden, A., Betts, P., 2020. The role of inherited crustal and lithospheric architecture during the evolution of the Red Sea: Insights from three dimensional analogue

experiments. Earth Planet. Sci. Lett. 544, 116377. https://doi.org/10.1016/j.epsl.2020.116377

Moresi, L., Dufour, F., Mühlhaus, H.-B., 2003. A Lagrangian integration point finite element method for large deformation modeling of viscoelastic geomaterials. J. Comput. Phys. 184, 476–497.

Moresi, L., Quenette, S., Lemiale, V., Mériaux, C., Appelbe, B., Mühlhaus, H.-B., 2007. Computational approaches to studying non-linear dynamics of the crust and mantle. Phys. Earth Planet. Inter. 163, 69–82. https://doi.org/10.1016/j.pepi.2007.06.009

Mougenot, D., Recq, M., Virlogeux, P., Lepvrier, C., 1986. Seaward extension of the East African Rift. Lett. to Nat. 325, 599–603.

Nagel, T.J., Buck, W.R., 2007. Control of rheological stratification on rifting geometry: A symmetric model resolving the upper plate paradox. Int. J. Earth Sci. 96, 1047–1057. https://doi.org/10.1007/s00531-007-0195-x

Nagel, T.J., Buck, W.R., 2006. Channel flow and the development of parallel-dipping normal faults. J. Geophys. Res. 111, B08407. https://doi.org/10.1029/2005JB004000

Nagel, T.J., Buck, W.R., 2004. Symmetric alternative to asymmetric rifting models. Geology 32, 937–940. https://doi.org/10.1130/G20785.1

Ord, A., Hobbs, B.E., 1989. The strength of the continental crust, detachment zones and the development of plastic instabilities. Tectonophysics 158, 269–289.

Pena dos Reis, R., Pimentel, N., Garcia, A., 2010. A evolução da Bacia Lusitânica (Portugal) e dos sistemas petrolíferos associados. Rev. Electrónica Ciências da Terra 19, 1–4.

Ranalli, G., 1995. Rheology of the Earth, 2nd ed. Chapman & Hall, London.

Siqueira, L.P. de, 1989. Bacia dos Parecis. Bol. Geociências Petrobras 3, 3–16.

Soares, D.M., Alves, T.M., Terrinha, P., 2012. The breakup sequence and associated lithospheric breakup surface: Their significance in the context of rifted continental margins (West Iberia and Newfoundland margins, North Atlantic). Earth Planet. Sci. Lett. 355–356, 311–326. https://doi.org/10.1016/j.epsl.2012.08.036

Tirel, C., Brun, J.-P., Sokoutis, D., 2006. Extension of thickened and hot lithospheres: Inferences from laboratory modeling. J. Geophys. Res. 113, B04403. https://doi.org/10.1029/2005TC001804

Wijns, C., Weinberg, R., Gessner, K., Moresi, L., 2005. Mode of crustal extension determined by rheological layering. Earth Planet. Sci. Lett. 236, 120–134. https://doi.org/10.1016/j.epsl.2005.05.030

Wilson, J.T., 1966. Did the Atlantic close and then re-open? Nature 211, 676–681.

Yoshida, M., Saito, S., Yoshizawa, K., 2020. Dynamics of continental lithosphere extension and passive continental rifting from numerical experiments of visco-elasto-plastic thermo-chemical convection in 2-D Cartesian geometry. Tectonophysics 796, 1–10. https://doi.org/10.1016/j.tecto.2020.228659

Zwaan, F., Corti, G., Keir, D., Sani, F., 2020. A review of tectonic models for the rifted margin of Afar: Implications for continental break-up and passive margin formation. J. African Earth Sci. 164, 1–22. https://doi.org/10.1016/j.jafrearsci.2019.103649

Zwaan, F., Schreurs, G., 2017. How oblique extension and structural inheritance influence rift segment interaction: Insights from 4D analog models. Interpretation 5, SD119–SD138. https://doi.org/10.1190/INT-2016-0063.1

Zwaan, F., Schreurs, G., Buiter, S.J.H., 2019. A systematic comparison of experimental set-ups for modelling extensional tectonics. Solid Earth 10, 1063–1097. https://doi.org/10.5194/se-10-1063-2019

Zwaan, F., Schreurs, G., Naliboff, J., Buiter, S.J.H., 2016. Insights into the effects of oblique extension on continental rift interaction from 3D analogue and numerical models. Tectonophysics 693, 239–260. https://doi.org/10.1016/j.tecto.2016.02.036

# CHAPTER 6. FINAL CONSIDERATIONS

In this research, we aimed to understand the influence of inherited structures in the initial stages of development of parallel to sub-parallel rifts in the context of continental rifting inspired by the example of the development of two sup-parallel grabens in the Parecis Basin – the Colorado and Pimenta Bueno grabens. For this purpose, we have performed and discussed different sets of experiments using the techniques of analogue and numerical modelling. In these experiments, we systematically studied the conditions in which two nearby forming grabens interfered, what were their resulting deformational patterns, how symmetric and asymmetric graben geometries were developed and what were the effects of varying both the distance between the inherited structures and the assumed rheological profiles.

In the analogue models two sets of experiments were performed where the geometric layout of two velocity discontinuities (VDs) was systematically varied in sandbox rifting models. The VDs were used to simulate pre-existing inherited basement heterogeneities in a developing crustal continental rift system. In all the experiments, the extension along the basal VD always led to the formation of an asymmetric and localized rift system. This rift developed independently or interfered with other rifts, depending on the VD initial configuration. In the initial stages of development, two main conjugate faults were developed. One of these faults controlled the evolution of the system acting as a main listric border fault that remained connected to the VD. Also, several antithetic faults formed progressively and migrated towards the depocenter of the grabens. When the VDs were initially in contact or close, one wide symmetric graben was formed (experiments P-00, P-01). In contrast, when the basal VDs were at an initial distance of ≥ 2 cm (scaling to 8 km in nature), two independent rift systems were developed (Experiments P-02 to P-05). The deformation imparted to one of the rifts was independent and did not propagate to the other nearby rift system, as in experiment O-02a, where a brittle sand pack lied directly on top of a rigid basement and the VDs were placed at a distance. In the cases where the VDs were oblique to the moving walls, the faults formed in a segmented way and then connected in longer faults when the deformation increased, as in the case of the oblique and intersecting rift experiments. In nature this type of structures may not

be developed at upper crustal levels in the case of more complex lithospheric rheologies or when there is a ductile layer, in that case, early delocalization may prevail.

In the numerical modelling experiments three sets were developed to test the distance between inherited structures (seeds) in different crustal-type rheological profiles. The model results show that the influence of inherited mechanical weaknesses on continental rift evolution depends on the assumed rheological configuration of the extending crustal segment. Inherited mechanical weaknesses on the base of the upper crust (UC) always anticipate the nucleation of shallow graben structures directly on top of these heterogeneities, where extensional strain is localized. The rifting-seed heterogeneities show a strong mechanical control on the subsequent rift geometry and eventual crustal break-up. The absence of rifting-seeds significantly extends the rifting evolution before the graben nucleation in the UC. The main mechanical control on crustal tensile stress accommodation, in this case, is exerted by the assumed overall rheological configuration on the rifting basement, that determines the way through which deformation is distributed and localized in the brittle UC. When considering inherited rifting-seeds, the resulting rift geometry and evolution cannot be explained only by the possible tectonic interference between early formed grabens, but by the conjugated effect from the inherited mechanical weaknesses and the rheological stratification of the rifting basement in which they are inserted. In a "Crème Brûlée" crustal rheological stratification, the asymmetric rifting mainly results from considering single or separated rift-seeding weaknesses. In the case of a "Jelly Sandwich" rheological stratification the formation of UC symmetric grabens and symmetric rifting are favoured, independent of inter-seed distance. However, these structures can also happen under a "Crème Brûlée" general configuration – as consequence of late graben nucleation or from early-rifting tectonic interference between two nearby hemi-grabens. The evolution of one single rift if favoured by the nucleation of one main graben above a single rifting-seed. It can also result from close inter-graben early tectonic interference or from late graben nucleation in durable over-extended domains under a "Crème Brûlée" rheological arrangement, in the absence of rifting seeds.

Double rifting proved to be a more common result that we anticipated by only considering the number of prescribed rifting-seeds. Despite the rheological stratification it always results from early double graben nucleation and evolution above two separate seeds. It is also strongly favoured by the UC brittle distribution and evolution above two separated seeds. However, it is also strongly favoured by the UC brittle distribution pattern of deformation that arises from a

“Jelly-Sandwich” rheological stratification, which can cause double rifting above only one seed, or even in the absence of any seeds.

The experimental models studied in this research project show that the use of techniques as analogue and numerical modelling are essential for a better understanding of complex geological structures. By performing simple experiments simulating the evolution of certain parts of a determined geological structure we can discuss and understand how similar structures may have evolved at different times in geological history. This research brings new insights about parallel and double-rifting nucleation depending on the existence of basement inherited structures and different rheological profiles, that was not yet very discussed, although the existence of several examples in nature.

In the case of the Pimenta Bueno and Colorado grabens of the Parecis Basin, the structures likely formed as the result of the reactivation of two nearby linear basement structures, eventually inherited from a previous orogenic cycle. In the initial stages of continental rifting, the localization of deformation may be strongly dependent on the existence of basement heterogeneities and their geometry, but also on the crustal-rheological profile. As shown in this research, the case of the Parecis Basin is not an isolated parallel rift case in nature. Similar double/parallel rifting structures at proposed different stages of evolution can be observed and studied through these models for a better understanding on how these structures are developed.

# REFERENCES


Adam, J., Urai, J.L., Wieneke, B., Oncken, O., Pfeiffer, K., Kukowski, N., Lohrmann, J., Hoth, S., van der Zee, W., Schmatz, J., 2005. Shear localisation and strain distribution during tectonic faulting - New insights from granular-flow experiments and high-resolution optical image correlation techniques. J. Struct. Geol. 27, 283–301. https://doi.org/10.1016/j.jsg.2004.08.008

Albuquerque, D.F., França, G.S., Moreira, L.P., Assumpção, M., Bianchi, M., Barros, L.V., Quispe, C.C., Oliveira, M.E., 2017. Crustal structure of the Amazonian Craton and adjacent provinces in Brazil. J. South Am. Earth Sci. 79, 431–442. https://doi.org/10.1016/j.jsames.2017.08.019

Allemand, P., Brun, J.-P., 1991. Width of continental rifts and rheological layering of the lithosphere. Tectonophysics 188, 63–69. https://doi.org/10.1017/cbo9780511975417.004

Allemand, P., Brun, J.P., Davy, P., Van Den Driessche, J., 1989. Symmetry and asymmetry of rifts and mechanism of lithosphere thinning. Bull. - Soc. Geol. Fr. 5, 445–451.

Allken, V., Huismans, R.S., Thieulot, C., 2012. Factors controlling the mode of rift interaction in brittle-ductile coupled systems: A 3D numerical study. Geochemistry Geophys. Geosystems 13, 1–18. https://doi.org/10.1029/2012GC004077

Allken, V., Huismans, R.S., Thieulot, C., 2011. Three-dimensional numerical modeling of upper crustal extensional systems. J. Geophys. Res. 116, 1–15. https://doi.org/10.1029/2011JB008319

Almeida, F.F.M. de, Brito Neves, B.B. De, Dal Ré Carneiro, C., 2000. The origin and evolution of the South American Platform. Earth Sci. Rev. 50, 77–111. https://doi.org/10.1016/S0012-8252(99)00072-0

Almeida, F.F.M. de, Hasui, Y., Brito Neves, B.B. de, Fuck, R.A., 1977. Províncias estruturais brasileiras, in: VIII Simpósio de Geologia Do Norderste. Sociedade Brasileira de Geologia, Campina Grande, PB, pp. 363–391.

Almeida, F.F.M., 1984. Província Tocantins - setor sudoeste, in: Almeida, F.F.M., Hasui, Y. (Eds.), O Pré-Cambriano Do Brasil. Blücher, São Paulo, pp. 265–281.

Almeida, F.F.M., 1978. Tectonic Map of South America, 1:5,000,000. Explanatory note.

Almeida, F.F.M., 1974. Sistema tectônico marginal do Cráton do Guaporé, in: Congresso Brasileiro de Geologia. Porto Alegre, RS, p. 6.

Almeida, F.F.M., 1965. Geologia da Serra da Bodoquema (Mato Grosso). Bol. da Div. Geol. e Mineral. 219, 1–96.

Almeida, F.F.M., 1964. Geologia do centro-oeste mato-grossense. Bol. da Div. Geol. e Mineral. 215, 1–113.

Almeida, F.F.M., Hasui, Y., Brito Neves, B.B., Fuck, R.A., 1981. Brazilian structural provinces: an introduction. Earth Sci. Rev. 17, 1–29. https://doi.org/10.1016/0012-8252(81)90003-9

Alvarenga, C.J.S., Abreu, C.J., Vidotti, R.M., Souza, S.C.R., Vasconcelos, C.S., 2016. Sequências Neoproterozóicas no Sudeste da Bacia dos Parecis: revisão e potencialidades para hidrocarbonetos 1–7.

Alvarenga, C.J.S., Trompette, R., 1992. Glacially influenced sedimentation in the Later Proterozoic of the Paraguay belt (Mato Grosso, Brazil). Palaeogeogr. Palaeoclimatol. Palaeoecol. 92, 85–105. https://doi.org/10.1016/0031-0182(92)90136-S

Alvarenga, C.J.S. de, 1988. Turbiditos e a glaciação do final do Proterozóico superior no Cinturão Paraguai. Rev. Bras. Geociências 18, 323–327. https://doi.org/10.25249/0375-7536.1988323327

Alvarenga, C.J.S. de, 1985. Evidências de fácies turbidíticas grosseiras no Grupo Cuiabá, MT, in: Simpósio de Geologia Do Centro-Oeste. Atas, Goiânia, GO, pp. 256–266.

Alvarenga, C.J.S. de, 1984. Dobramentos da Faixa Paraguai na borda sudeste do Cráton Amazônico, in: Congresso Brasileiro de Geologia. Rio de Janeiro, pp. 3258–3271.

Alvarenga, C.J.S. de, Moura, C.A.V., Gorayeb, P.S. de S., Abreu, F. de A.M. de, 2000. Paraguay and Araguaia Belts, in: Cordani, U.G., Milani, E.J., Thomaz Filho, A., Campos, D.A. (Eds.), Tectonic Evolution of South America. 31st International Geological Congress, Rio de Janeiro, pp. 183–193.

Alvarenga, C.J.S. de, Santos, R. V., Dantas, E.L., 2004. C-O-Sr isotopic stratigraphy of cap carbonates overlying Marinoan-age glacial diamictites in the Paraguay Belt, Brazil. Precambrian Res. 131, 1–21. https://doi.org/10.1016/j.precamres.2003.12.006

Alvarenga, C.J.S. de, Trompette, R., 1993. Evolução tectônica brasiliana da Faixa Paraguai: a

estruturação da região de Cuiabá. Rev. Bras. Geociências 23, 18–30. https://doi.org/10.1590/S0006-87051997000100015

Alvarenga, C.J.S. de, Trompette, R., 1988. Upper Proterozoic glacial environment of the border of Amazonian Cráton and its evolution towards the adjacent Parguay Belt. (Mato Grosso, Brazil), in: Meeting Earth's Glacial Record-Proj. IGCP-UNESCO/UFMT, Cuiabá, MT, pp. 31–44.

Amaral, G., 1974. Geologia pré-cambriana da Região Amazônica. Universidade de São Paulo.

Araújo, H.J.T., Santos Neto, A., Trindade, C.A.H., Pinto, J.C.A., Montalvão, R.M.G., Dourado, T.D.C., Palmeira, R.C.B., Tassinari, G.C.C., 1982. Geologia da Folha SF. 21 Campo Grande. Projeto RADAMBRASIL.

Assumpção, M., Bianchi, M., Julià, J., Dias, F.L., Sand França, G., Nascimento, R., Drouet, S., Pavão, C.G., Albuquerque, D.F., Lopes, A.E.V., 2013. Crustal thickness map of Brazil: Data compilation and main features. J. South Am. Earth Sci. 43, 74–85. https://doi.org/10.1016/j.jsames.2012.12.009

Bahia, R.B.C., 2007. Evolução tectonossedimentar da Bacia dos Parecis - Amazônia. Universidade Federal de Ouro Preto. https://doi.org/10.1016/j.foodqual.2011.09.004

Bahia, R.B.C., Martins-Neto, M.A., Barbosa, M.S.C., Pedreira, A.J., 2007. Análise da evolução tectonossedimentar da Bacia dos Parecis através de métodos potenciais. Rev. Bras. Geociências 37, 639–649. https://doi.org/10.25249/0375-7536.2007374639649

Bahia, Ruy B. C., Martins-Neto, M.A., Barbosa, M.S.C., Pedreira, A.J., 2006. Revisão Estratigráfica Da Bacia Dos Parecis – Amazônia. Rev. Bras. Geociências 36, 692–703. https://doi.org/10.25249/0375-7536.2006364692703

Bahia, R.B.C., Pedreira, A.J., 1996. Depósitos glaciogênicos da Formação Pimenta Bueno ( Carbonífero ) na região de Rolim de Moura, sudeste de Rondônia. A Terra em Rev. 1, 24–29.

Bahia, R.B.C., Quadros, M.L., Pedreira, A.J., 1996. As coberturas sedimentares fanerozóicas da região sudeste de Rondônia, in: Congresso Brasileiro de Geologia. Salvador, BA, pp. 299–302.

Bajolet, F., Replumaz, A., Lainé, R., 2013. Orocline and syntaxes formation during subduction and collision. Tectonics 32, 1529–1546. https://doi.org/10.1002/tect.20087

Balázs, A., Burov, E., Matenco, L., Vogt, K., Francois, T., Cloetingh, S., 2017. Symmetry during the syn-and post-rift evolution of extensional back-arc basins: The role of inherited orogenic structures. Earth Planet. Sci. Lett. 462, 86–98. https://doi.org/10.1016/j.epsl.2017.01.015

Barbosa, O., Andrade Ramos, J.R., 1959. Território do Rio Branco, aspectos principais da geomorfologia, da geologia e das possibilidades minerais da zona setentrional. Bol. da Div. Geol. e Mineral. 196, 1–49.

Barros, A.M., Silva, R.H. da, Cardoso, O.R.F.A., Freire, F.A., Souza Júnior, J.J. de, Rivetti, M., Luz, D.S. da, Palmeira, R.C. de B., Tassinari, C.C.G., 1982. Geologia da Folha SD. 21-Cuiabá. Projeto RADAMBRASIL. Levant. Recur. Natuais 26.

Batezelli, A., Ladeira, F.S.B., 2016. Stratigraphic framework and evolution of the Cretaceous continental sequences of the Bauru, Sanfranciscana, and Parecis basins, Brazil. J. South Am. Earth Sci. 65, 1–24. https://doi.org/10.1016/j.jsames.2015.11.005

Baumgardner, J.R., 1985. Three-dimensional treatment of convective flow in the earth's mantle. J. Stat. Phys. 39, 501–511. https://doi.org/10.1007/BF01008348

Beniest, A., 2017. From continental rifting to conjugate margins : Insights from analogue and numerical modelling. Université Pierre et Marie Curie/IFP Energies nouvelles.

Beniest, A., Koptev, A., Burov, E., 2017. Numerical models for continental break-up: Implications for the South Atlantic. Earth Planet. Sci. Lett. 461, 176–189. https://doi.org/10.1016/j.epsl.2016.12.034

Beniest, A., Willingshofer, E., Sokoutis, D., Sassi, W., 2018. Extending continental lithosphere with lateral strength variations: effects on deformation localization and margin geometries. Front. Earth Sci. 1–11. https://doi.org/10.3389/feart.2018.00148

Bird, P., 1978. Finite elements modeling of lithosphere deformation: the Zagros collision orogeny.

Bonnet, C., Malavieille, J., Mosar, J., 2007. Interactions between tectonics, erosion, and sedimentation during the recent evolution of the Alpine orogen: Analogue modeling insights. Tectonics 26, 1–15. https://doi.org/10.1029/2006TC002048

Boutelier, D.A., Cruden, A.R., 2008. Impact of regional mantle flow on subducting plate geometry and intraplate stress: insights from physical modelling. Geophys. J. Int. 174, 719–732.

Braga, L.F.S., Siqueira, L.P. de, 1996. Three-dimensional gravity modelling of the basement topography beneath Parecis Basin, Brazil, constrained by spectral estimates of depth to magnetic sources, in: 5th Latin America Petroleum Congress. p. 8.

Brun, J.P., 1999. Narrow rifts versus wide rifts: inferences for the mechanics of rifting from laboratory experiments. Philos. Trans. Math. Phys. Eng. Sci. 357, 695–712.

Brun, J.P., Beslier, M.O., 1996. Mantle exhumation at passive margins. Earth Planet. Sci. Lett. 142, 161–173. https://doi.org/10.1016/0012-821x(96)00080-5

Brun, J.P., Sokoutis, D., Van Den Driessche, J., 1994. Analogue modeling of detachment fault systems and core complexes. Geology 22, 319–322.

Brune, J.N., Ellis, M.A., 1997. Structural features in a brittle-ductile wax model of continetal extension. Lett. to Nat. 387, 67–70.

Brune, S., Autin, J., 2013. The rift to break-up evolution of the Gulf of Aden: Insights from 3D numerical lithospheric-scale modelling. Tectonophysics 607, 65–79. https://doi.org/10.1016/j.tecto.2013.06.029

Brune, S., Corti, G., Ranalli, G., 2017. Controls of inherited lithospheric heterogeneity on rift linkage: Numerical and analog models of interaction between the Kenyan and Ethiopian rifts across the Turkana depression. Tectonics 36, 1767–1786. https://doi.org/10.1002/2017TC004739

Buck, W.R., 1991. Modes of continental lithospheric extension. J. Geophys. Res. Solid Earth 96, 20161–20178. https://doi.org/10.1029/91JB01485

Buck, W.R., Lavier, L.L., Poliakov, A.N.B., 1999. How to make a rift wide. Philos. Trans. R. Soc. A Math. Phys. Eng. Sci. 357, 671–693. https://doi.org/10.1098/rsta.1999.0348

Buddensiek, M.L., 2009. Seismic imaging of sandbox models. 1997 SEG Annu. Meet. https://doi.org/doi.org/10.17169/refubium-4670

Burke, K., 1977. Aulacogens and continental breakup. Ann. Rev. Earth Planet Sci. 5, 371–396.

Burov, E.B., Watts, A.B., 2006. The long-term strength of continental lithosphere: “jelly sandwich” or “crème brûlée”? GSA Today 16, 4–10.

Cadell, H.M., 1888. Experimental researches in mountain building. R. Soc. Edinburgh Trans. 35, 337–360.

Chattopadhyay, A., Chakra, M., 2013. Influence of pre-existing pervasive fabrics on fault

patterns during orthogonal and oblique rifting: An experimental approach. Mar. Pet. Geol. 39, 74–91. https://doi.org/10.1016/j.marpetgeo.2012.09.009

Chen, W.-P., Molnar, P., 1983. Focal depths of intracontinental and intraplate earthquakes and their implications for the thermal and mechanical properties of the lithosphere. J. Geophys. Res. Solid Earth 88, 4183–4214. https://doi.org/10.1029/JB088iB05p04183

Clifton, A.E., Schlische, R.W., Withjack, M.O., Ackermann, R. V., 2000. Influence of rift obliquity on fault-population systematics: Results of experimental clay models. J. Struct. Geol. 22, 1491–1509. https://doi.org/10.1016/S0191-8141(00)00043-2

Coney, P.J., 1980. Cordilleran metamorphic core complexes: An overview. Mem. Geol. Soc. Am. 153, 7–31. https://doi.org/10.1130/MEM153-p7

Cordani, U.G., Tassinari, C.C.G., Teixeira, W., Basei, M.A.S., Kawashita, K., 1979. Evolução tectônica da Amazônia com base nos dados geocronológicos, in: Congresso Geológico Chileno. pp. 137–148.

Corrêa, J.A., Correia Filho, F.C.L., Scislewski, G., Neto, C., Cavallon, L.A., Cerqueira, N.L.S., Nogueira, V.L., 1979. Projeto Bodoquena: geologia das regiões centro e oeste de Mato Grosso do Sul. Brasília, DF.

Corti, G., 2009. Continental rift evolution: From rift initiation to incipient break-up in the Main Ethiopian Rift, East Africa. Earth-Science Rev. 96, 1–53. https://doi.org/10.1016/j.earscirev.2009.06.005

Corti, G., Bonini, M., Conticelli, S., Innocenti, F., Manetti, P., Sokoutis, D., 2003. Analogue modelling of continental extension: A review focused on the relations between the patterns of deformation and the presence of magma. Earth-Science Rev. 63, 169–247. https://doi.org/10.1016/S0012-8252(03)00035-7

Corti, G., Bonini, M., Innocenti, F., Manetti, P., Mulugeta, G., 2001. Centrifuge models simulating magma emplacement during oblique rifting. J. Geodyn. 31, 557–576. https://doi.org/10.1016/S0264-3707(01)00032-1

Corti, G., Manetti, P., 2006. Asymmetric rifts due to asymmetric Mohos: An experimental approach. Earth Planet. Sci. Lett. 245, 315–329. https://doi.org/10.1016/j.epsl.2006.02.004

Costa, J.B.S., Hasui, Y., 1997. Evolução Geológica da Amazônia, in: Costa, M.L., Angélica, R.S. (Eds.), Contribuições à Geologia Da Amazônia. SBG-Núcleo Norte, Belém, PA, pp.

15–90.

CPRM. Shapefiles - GeoSGB (website visitado em dezembro, 2020).

Daignières, M., Fremond, M., Friaa, A., 1978. Modèle de type Norton-Hoff généralisé pour l'étude des déformations lithosphériques (example: la collision Himalayenne). Rendus Hebd. des Seances l'Academie des Sci. 268B, 371–374.

Dantas, E.L., Alvarenga, C.J.S. de, Santos, R.V., Pimentel, M.M., 2009. Using Nd isotopes to understand the provenance of sedimentary rocks from a continental margin to a foreland basin in the Neoproterozoic Paraguay Belt, Central Brazil. Precambrian Res. 170, 1–12. https://doi.org/10.1016/j.precamres.2008.11.005

Davaille, A., Limare, A., Touitou, F., Kumagai, I., Vatteville, J., 2011. Anatomy of a laminar starting thermal plume at high Prandtl number. Exp. Fluids 50, 285–300. https://doi.org/10.1007/s00348-010-0924-y

Del'Arco, J.O., Silva, R.H., Tarapanoff, L., Freire, F.A., Pereira, L.G.M., Souza, S.L., Luz, L.G., Palmeira, R.C.B., Tassinari, C.C.G., 1982. Geologia da Folha SE. 21 Corumbá e Parte da Folha SE. 20. Projeto RADAMBRASIL. Levant. Recur. Naturais, 27.

Del Ventisette, C., Gigli, G., Bonini, M., Corti, G., Montanari, D., Santoro, S., Sani, F., Fanti, R., Casagli, N., 2015. Insights from analogue modelling into the deformation mechanism of the Vaiont landslide. Geomorphology 228, 52–59. https://doi.org/10.1016/j.geomorph.2014.08.024

Deng, C., Gawthorpe, R.L., Fossen, H., Finch, E., 2018. How does the orientation of a preexisting basement weakness influence fault development during renewed rifting? Insights from three-dimensional discrete element modeling. Tectonics 37, 2221–2242. https://doi.org/10.1029/2017TC004776

Dewey, J.F., 1969. Continental margins: a model for conversion of Atlantic type to Andean type. Earth Planet. Sci. Lett. 6, 189–197.

Dewey, J.F., Burke, K., 1974. Hot spots and collisional break-up: Implications for collisional orogeny. Geology 2, 57–60. https://doi.org/10.1130/0091-7613(1974)2<57:HSACBI>2.0.CO;2

Dooley, T.P., Schreurs, G., 2012. Analogue modelling of intraplate strike-slip tectonics: A review and new experimental results. Tectonophysics 574–575, 1–71. https://doi.org/10.1016/j.tecto.2012.05.030

Duarte, J.C., Rosas, F.M., Terrinha, P., Gutscher, M.A., Malavieille, J., Silva, S., Matias, L., 2011. Thrust-wrench interference tectonics in the Gulf of Cadiz (Africa-Iberia plate boundary in the North-East Atlantic): Insights from analog models. Mar. Geol. 289, 135–149. https://doi.org/10.1016/j.margeo.2011.09.014

Duarte, J.C., Schellart, W.P., Cruden, A.R., 2013. Three-dimensional dynamic laboratory models of subduction with an overriding plate and variable interplate rheology. Geophys. J. Int. 195, 47–66. https://doi.org/10.1093/gji/ggt257

Duretz, T., Asti, R., Lagabrielle, Y., Brun, J.P., Jourdon, A., Clerc, C., Corre, B., 2020. Numerical modelling of Cretaceous Pyrenean Rifting: The interaction between mantle exhumation and syn-rift salt tectonics. Basin Res. 32, 652–667. https://doi.org/10.1111/bre.12389

Ebinger, 2005. Continental break-up: The East African perspective. Bullerwell Lect. 46, 2.26-2.21. https://doi.org/10.1111/j.1468-4004.2005.46216.x

Faria, H.P.A., 2015. Caracterização de domínios tectono-geofísicos na Bacia dos Parecis com base em dados de métodos potenciais. Universidade de Brasília.

Ferreira, E.O., 1969. Considerações sobre o mapa tectônico do Brasil e sobre a tectônica da Plataforma Brasileira, in: Congresso Brasileiro de Geologia. Salvador, BA, p. 2.

Figueiredo, A.J.A., Olivatti, O., 1974. Relatório final integrado: Projeto Alto Guaporé. Goiânia, GO.

Gerya, T., 2019. Introduction numerical geodynamic modelling , 2nd editio. ed. Cambridge.

Gomes, A.S., Rosas, F.M., Duarte, J.C., Schellart, W.P., Almeida, J., Tomás, R., Strak, V., 2019. Analogue modelling of brittle shear zone propagation across upper crustal morpho-rheological heterogeneities. J. Struct. Geol. 126, 175–197. https://doi.org/10.1016/j.jsg.2019.06.004

Gomes, C.J.S., 2013. Investigating new materials in the context of analog-physical models. J. Struct. Geol. 46, 158–166. https://doi.org/10.1016/j.jsg.2012.09.013

Gomes, C.J.S., Caldeira, J.N. de M., 2011. As propriedades friccionais de areias de quartzo (natural e colorida): Medidas efetuadas em experimentos físico-analógicos e em um ring-shear tester. Rev. Esc. Minas 64, 289–298. https://doi.org/10.1590/S0370-44672011000300006

Gueydan, F., Leroy, Y.M., Jolivet, L., Agard, P., 2003. Analysis of continental midcrustal strain localization induced by microfracturing and reaction-softening. J. Geophys. Res. Solid Earth 108, 1–18. https://doi.org/10.1029/2001jb000611

Haeser, B. da S., 2013. Bacia dos Parecis, in: Brasil 12ª Rodada Licitações de Petróleo e Gás. Rio de Janeiro.

Haeser, B. da S., Zalán, P.V., Ferreira, M.A., Petersohn, E., 2014. Revisão litoestratigráfica da Bacia dos Parecis e implicações para a exploração de petróleo, in: Rio Oil & Gas Expo and Conference. Rio de Janeiro, p. 10.

Hasui, Y., Haralyi, N.L.E., Schobbenhaus, C., 1984. Elementos geofísicos e geológicos da Região Amazônica: subsídios para o modelo geotectônico. II Symp. Amaz.

Henza, A.A., Withjack, M.O., Schlische, R.W., 2011. How do the properties of a pre-existing normal-fault population influence fault development during a subsequent phase of extension? J. Struct. Geol. 33, 1312–1324. https://doi.org/10.1016/j.jsg.2011.06.010

Henza, A.A., Withjack, M.O., Schlische, R.W., 2010. Normal-fault development during two phases of non-coaxial extension: An experimental study. J. Struct. Geol. 32, 1656–1667. https://doi.org/10.1016/j.jsg.2009.07.007

Hubbert, M.K., 1951. Mechanical basis for certain familiar geologic structures. Bull. Geol. Soc. Am. 62, 355–372. https://doi.org/10.1130/0016-7606(1951)62

Hubbert, M.K., 1937. Theory of scale models as applied to the study of geologic structures. Geol. Soc. Am. Bull. 48, 1459–1520. https://doi.org/10.1130/GSAB-48-1459

Huismans, R.S., Beaumont, C., 2002. Asymmetric lithospheric extension: The role of frictional plastic strain softening inferred from numerical experiments. Geology 30, 211–214.

Keep, M., McClay, K.R., 1997. Analogue modelling of multiphase rift systems. Tectonophysics 273, 239–270. https://doi.org/10.1016/S0040-1951(96)00272-7

Keppler, R., Rosas, F.M., Nagel, T.J., 2013. Thin viscous middle-crust and evolving fault distribution during continental rifting: Insights from analog modeling experiments. Tectonophysics 608, 161–175. https://doi.org/10.1016/j.tecto.2013.10.001

Kingston, D.R., Dishroon, C.P., Williams, P.A., 1983. Global Basin Classification System. Am. Assoc. Pet. Geol. Bull. 67, 2175–2193. https://doi.org/10.1306/ad460936-16f7-11d7-8645000102c1865d

Klinkmüller, M., Schreurs, G., Rosenau, M., Kemnitz, H., 2016. Properties of granular analogue model materials: A community wide survey. Tectonophysics 684, 23–38. https://doi.org/10.1016/j.tecto.2016.01.017

Koptev, A., Burov, E., Calais, E., Leroy, S., Gerya, T., Guillou-Frottier, L., Cloetingh, S., 2016. Contrasted continental rifting via plume-craton interaction: Applications to Central East African Rift. Geosci. Front. 7, 221–236. https://doi.org/10.1016/j.gsf.2015.11.002

Koptev, A., Burov, E., Gerya, T., Le Pourhiet, L., Leroy, S., Calais, E., Jolivet, L., 2017. Plume-induced continental rifting and break-up in ultra-slow extension context: Insights from 3D numerical modeling. Tectonophysics 746, 121–137. https://doi.org/10.1016/j.tecto.2017.03.025

Koyi, H., 1997. Analogue modelling: from a qualitative to a quantitative technique - a historical outline. J. Pet. Geol. 20 (2), 223–238.

Krawczyk, C.M., Buddensiek, M.-L., Oncken, O., Kukowski, N., 2013. Seismic imaging of sandbox experiments-laboratory hardware setup and first reflection seismic sections. Solid Earth 4, 93–104. https://doi.org/10.5194/se-4-93-2013

Kroonenberg, S.B., 1982. A Grenvillian granulite belt in the Colombian Andes and its relation to the Guiana Shield. Geol. en Mijnb. 61, 325–333.

Kullberg, J.C., Terrinha, P., Pais, J., Reis, R.P., Legoinha, P., 2006. Arrábida e Sintra: dois exemplos de tectónica pós-rifting da Bacia Lusitaniana, in: Dias, R., Araújo, A., Terrinha, P., Kullberg, J.C. (Eds.), Geologia de Portugal No Contexto Da Ibéria. Universidade de Évora, pp. 369–396.

Lavier, L.L., Manatschal, G., 2006. A mechanism to thin the continental lithosphere at magma-poor margins. Nature 440, 324–328. https://doi.org/10.1038/nature04608

Li, Y., Abbas, A., Li, C.-F., Sun, T., Zlotnik, S., Song, T., Zhang, L., Yao, Z., Yao, Y., 2020. Numerical modeling of failed rifts in the northern South China Sea margin: Implications for continental rifting and breakup. J. Asian Earth Sci. 199, 1–15. https://doi.org/10.1016/j.jseaes.2020.104402

Lister, G.S., Davis, G.A., 1989. The origin of metamorphic core complexes and detachment faults formed during Tertiary continental extension in the northern Colorado River region, U.S.A. J. Struct. Geol. 11, 65–94.

Lohrmann, J., Kukowski, N., Adam, J., Oncken, O., 2003. The impact of analogue material

properties on the geometry, kinematics, and dynamics of convergent sand wedges. J. Struct. Geol. 25, 1691–1711. https://doi.org/10.1016/S0191-8141(03)00005-1

Loureiro, E.M.L., 2016. Caracterização geológico-tectônica da Bacia dos Parecis. Uma interpretação integrada. Universidade do Estado do Rio de Janeiro.

Loureiro, E.M.L., Menezes, P.T.L., Zalán, P. V., Heilbron, M., 2017. Tectonic framework of Parecis Basin: a seismic-gravity integrated interpretation, in: 15th International Congress of the Brazilian Gephysical Society. Rio de Janeiro. https://doi.org/10.1190/sbgf2017-094

Machetel, P., Rabinowicz, M., Bernardet, P., 1986. Three-dimensional convection in spherical shells. Geophys. Astrophys. Fluid Dyn. 37, 57–84. https://doi.org/10.1080/03091928608210091

Manatschal, G., Lavier, L., Chenin, P., 2015. The role of inheritance in structuring hyperextended rift systems: Some considerations based on observations and numerical modeling. Gondwana Res. 27, 140–164. https://doi.org/10.1016/j.gr.2014.08.006

Mandl, G., 1988. Mechanics of tectonic faulting. Elsevier.

Matsumoto, T., Tomoda, Y., 1983. Numerical-simulation of the initiation of subduction at the fracture-zone, J. Phys. Earth.

McClay, K.R., 1990. Extensional fault systems in sedimentary basins: a review of analogue model studies. Mar. Pet. Geol. 7, 206–233. https://doi.org/10.1016/0264-8172(90)90001-W

McClay, K.R., Dooley, T., Gloaguen, R., Whitehouse, P., Khalil, S., 2001. Analogue modelling of extensional fault architectures: comparisons with natural rift fault systems, in: PESA Eastern Australasian Basins Symposium. Petroleum Exploration Society of Australia (PESA), Melbourne Victoria.

McClay, K.R., White, M.J., 1995. Analogue modelling of orthogonal and oblique rifting. Mar. Pet. Geol. 12, 137–151. https://doi.org/10.1016/0264-8172(95)92835-K

McClay, K.R., Whitehouse, P.S., 2004. Analog modeling of doubly vergent thrust wedges. AAPG Mem. 184–206. https://doi.org/10.1306/m82813c10

McKenzie, D., 1978. Some remarks on the development of sedimentary basins. Earth Planet. Sci. Lett. 40, 25–32. https://doi.org/10.1016/0012-821X(78)90071-7

Mériaux, C.A., Mériaux, A.-S., Schellart, W.P., Duarte, J.C., Duarte, S.S., Chen, Z., 2016.

Mantle plumes in the vicinity of subduction zones. Earth Planet. Sci. Lett. 454, 166–177. https://doi.org/10.1016/j.epsl.2016.09.001

Minear, J.W., Toksöz, M.N., 1970. Thermal regime of a downgoing slab and new global tectonics. J. Geophys. Res. 75, 1397–1419. https://doi.org/10.1029/JB075i008p01397

Molnar, N., Cruden, A., Betts, P., 2020. The role of inherited crustal and lithospheric architecture during the evolution of the Red Sea: Insights from three dimensional analogue experiments. Earth Planet. Sci. Lett. 544, 116377. https://doi.org/10.1016/j.epsl.2020.116377

Molnar, N.E., Cruden, A.R., Betts, P.G., 2019. Interactions between propagating rifts and linear weaknesses in the lower crust. Geosphere 15, 1617–1640. https://doi.org/10.1130/GES02119.1

Moresi, L., Dufour, F., Mühlhaus, H.-B., 2003. A Lagrangian integration point finite element method for large deformation modeling of viscoelastic geomaterials. J. Comput. Phys. 184, 476–497.

Moresi, L., Quenette, S., Lemiale, V., Mériaux, C., Appelbe, B., Mühlhaus, H.-B., 2007. Computational approaches to studying non-linear dynamics of the crust and mantle. Phys. Earth Planet. Inter. 163, 69–82. https://doi.org/10.1016/j.pepi.2007.06.009

Moresi, L.N., 2013. Underworld: What we set out to do, How far did we get, What did we Learn ? (Invited). AGUFM 2013, T33E-01.

Moresi, L.N., Giordani, J., Mansour, J., Knepley, M., 2018. The Underworld renovation project using PETScDS, in: American Geophysical Union - Fall Meeting. AGU.

Moresi, L.N., Mansour, J., Giordani, J., Farrington, R., Kaluza, O., Quenette, S., Woodcock, R., Squire, G., Moresi, L.N., Mansour, J., Giordani, J., Farrington, R., Kaluza, O., Quenette, S., Woodcock, R., Squire, G., 2017. Underworld - Bringing a Research Code to the Classroom. Am. Geophys. Union - Fall Meet. 2017, ED41B-0283.

Mougenot, D., Recq, M., Virlogeux, P., Lepvrier, C., 1986. Seaward extension of the East African Rift. Lett. to Nat. 325, 599–603.

Nagel, T.J., Buck, W.R., 2007. Control of rheological stratification on rifting geometry: A symmetric model resolving the upper plate paradox. Int. J. Earth Sci. 96, 1047–1057. https://doi.org/10.1007/s00531-007-0195-x

Nagel, T.J., Buck, W.R., 2006. Channel flow and the development of parallel-dipping normal faults. J. Geophys. Res. 111, B08407. https://doi.org/10.1029/2005JB004000

Nagel, T.J., Buck, W.R., 2004. Symmetric alternative to asymmetric rifting models. Geology 32, 937–940. https://doi.org/10.1130/G20785.1

Naylor, M.A., Laroque, J.M., Gauthier, B.D.M., 1994. Understanding extensional tectonics: insights from sandbox models, in: Geodynamic Evolution of Sedimentary Basins, International Symposium. Moscow, pp. 69–83.

Nogueira, V.L., Oliveira, C.C., 1978. Relatório final 1: Projeto Bonito Aquidauana. Goiânia, GO.

Oliva, L.A., Olivatti, O., Ribeiro Filho, W., Schobbenhaus Filho, C., 1979. Carta geológica do Brasil ao milionésimo: Folha SD21 Cuiabá.

Oliveira, M.E., Alves da Silva, F.C., 2016. A importância da estratigrafia mecânica no desenvolvimento de falhas e juntas em contexto de bacias sedimentares : contribuição de modelos experimentais. Geol. USP - Ser. Cient. 16, 39–55. https://doi.org/10.11606/issn.2316-9095.v16i3p39-55

Ord, A., Hobbs, B.E., 1989. The strength of the continental crust, detachment zones and the development of plastic instabilities. Tectonophysics 158, 269–289.

Panien, M., Schreurs, G., Pfiffner, A., 2006. Mechanical behaviour of granular materials used in analogue modelling: insights from grain characterisation, ring-shear tests and analogue experiments. J. Struct. Geol. 28, 1710–1724. https://doi.org/10.1016/j.jsg.2006.05.004

Pena dos Reis, R., Pimentel, N., Garcia, A., 2010. A evolução da Bacia Lusitânica (Portugal) e dos sistemas petrolíferos associados. Rev. Electrónica Ciências da Terra 19, 1–4.

Priem, H.N.A., Kroonenberg, S.B., Boelrijk, N.A.I.M., Hebeda, E.H., 1989. Rb-Sr and K-Ar evidence for the presence of a 1.6 Ga basement underlying the 1.2 Ga Garzón-Santa Marta granulite belt in the Colombian Andes. Precambrian Res. 42, 315–324. https://doi.org/10.1016/0301-9268(89)90016-8

Quenette, S., Moresi, L., Sunter, P., Hodkinson, L., Lo, A., Hassan, R., Appelbe, B., Turnbull, R., 2005. From StGermain to Underworld: Enabling Community-based code Development in Geodynamics, in: American Geophysical Union, Fall Meeting 2005. p. 1187.

Quenette, S., Xi, Y.F., Mansour, J., 2015. Underworld-GT Applied to Guangdong, a Tool to

Explore the Geothermal Potential of the Crust. J. Earth Sci. 26, 78–88. https://doi.org/10.1007/s12583-015-0517-z

Quenette, S.M., Moresi, L.N., Abramson, D., Quenette, S.M., Moresi, L.N., Abramson, D., 2013. Underworld results as a triple (shopping list, posterior, priors). AGUFM 2013, T31C-2525.

Quenette, S.M., O'Neill, C., Moresi, L.N., Danis, C.R., Mansour, J., Quenette, S.M., O'Neill, C., Moresi, L.N., Danis, C.R., Mansour, J., 2011. Underworld and multi-basin heat flow. AGUFM 2011, H51C-1218.

Ranalli, G., 2001. Experimental tectonics : from Sir James Hall to the present. J. Geodyn. 32, 65–76.

Ranalli, G., 1995. Rheology of the Earth, 2nd ed. Chapman & Hall, London.

Rauch, M., 2013. The Oligocene-miocene tectonic evolution of the northern outer carpathian fold-and-thrust belt: Insights from compression-and-rotation analogue modelling experiments. Geol. Mag. 150, 1062–1084. https://doi.org/10.1017/S0016756813000320

Ribeiro Filho, W., Figueiredo, A.J.A., 1974. Reconhecimento geológico da região oeste de Mato Grosso, in: Congresso Brasileiro de Geologia. Porto Alegre, p. 8.

Ribeiro Filho, W., Luz, J.S., Abreu Filho, W., 1975. Relatório final: Projeto Serra Azul. Goiânia, GO.

Rosas, F.M., Duarte, J.C., Almeida, P., Schellart, W.P., Riel, N., Terrinha, P., 2017. Analogue modelling of thrust systems: Passive vs. active hanging wall strain accommodation and sharp vs. smooth fault-ramp geometries. J. Struct. Geol. 99, 45–69. https://doi.org/10.1016/j.jsg.2017.05.002

Rossi, D., Storti, F., 2003. New artificial granular materials for analogue laboratory experiments: Aluminium and siliceous microspheres. J. Struct. Geol. 25, 1893–1899. https://doi.org/10.1016/S0191-8141(03)00041-5

Rowan, M.G., Peel, F.J., Vendeville, B.C., Gaullier, V., 2012. Salt tectonics at passive margins: Geology versus models - Discussion. Mar. Pet. Geol. 37, 184–194. https://doi.org/10.1016/j.marpetgeo.2012.04.007

Rubert, R.R., Pimentel Mizusaki, A.M., Martinelli, A.G., 2019. Mesozoic tectonic in the deposition and evolution of Cretaceous sedimentary packages of the Parecis Basin, center-

western Brazil. J. South Am. Earth Sci. 93, 140–154. https://doi.org/10.1016/j.jsames.2019.05.002

Rubert, R.R., Pimentel Mizusaki, A.M., Martinelli, A.G., Urban, C., 2017. Paleoenvironmental reconstruction and evolution of an Upper Cretaceous lacustrine-fluvial-deltaic sequence in the Parecis Basin, Brazil. J. South 80, 512–528. https://doi.org/10.1016/j.jsames.2017.10.013

Santos, H.S., Flexor, J.M., 2013. Estudo da Bacia dos Parecis a partir da integração de dados gravimétricos, magnéticos e magnetotelúticos. Geociências USP 32, 411–428.

Santos, J.O.S., 2003. Geotectônica dos Escudos das Guianas e Brasil-Central, in: Bizzi, L.A., Schobbenhaus, C., Vidotti, R.M., Gonçalves, J.H. (Eds.), Geologia, Tectônica e Recursos Minerais Do Brasil. Brasília, pp. 169–226.

Santos, J.O.S., Hartmann, L.A., Gaudette, H.E., Groves, D.I., Mcnaughton, N.J., Fletcher, I.R., 2000. A new understanding of the Provinces of the Amazon Craton based on integration of field mapping and U-Pb and Sm-Nd geochronology. Gondwana Res. 453–488.

Scandolara, J.E., Correa, R.T., Fuck, R.A., Souza, V.S., Rodrigues, J.B., Ribeiro, P.S.E., Frasca, A.A.S., Saboia, A.M., Lacerda Filho, J. V., 2017. Paleo-Mesoproterozoic arc-accretion along the southwestern margin of the Amazonian craton: The Juruena accretionary orogen and possible implications for Columbia supercontinent. J. South Am. Earth Sci. 73, 223–247. https://doi.org/10.1016/j.jsames.2016.12.005

Schellart, W.P., 2004. Kinematics of subduction and subduction-induced flow in the upper mantle. J. Geophys. Res. Solid Earth 109, 1–19. https://doi.org/10.1029/2004JB002970

Schellart, W.P., 2002. Analogue modelling of large-scale tectonic processes: An introduction. J. Virtual Explor. 7. https://doi.org/10.3809/jvirtex.2002.00045

Schellart, W.P., 2000. Shear test results for cohesion and friction coefficients for different granular materials: scaling implications for their usage in analogue modelling. Tectonophysics 324, 1–16. https://doi.org/10.1016/S0040-1951(00)00111-6

Schellart, W.P., Nieuwland, D.A., 2003. 3D evolution of a pop-up structure above a double basement strike-slip fault: Some insights from analogue modelling. Geol. Soc. Spec. Publ. 212, 169–179. https://doi.org/10.1144/GSL.SP.2003.212.01.11

Schellart, W.P., Strak, V., 2016. A review of analogue modelling of geodynamic processes: Approaches, scaling, materials and quantification, with an application to subduction

experiments. J. Geodyn. 100, 7–32. https://doi.org/10.1016/j.jog.2016.03.009

Schmatz, J., Vrolijk, P.J., Urai, J.L., 2010. Clay smear in normal fault zones - The effect of multilayers and clay cementation in water-saturated model experiments. J. Struct. Geol. 32, 1834–1849. https://doi.org/10.1016/j.jsg.2009.12.006

Schobbenhaus, C., Brito Neves, B.B. de, 2003. A Geologia do Brasil no Contexto da Plataforma Sul-Americana, in: Bizzi, L.A., Schobbenhaus, C., Vidotti, R.M., Gonçalves, J.H. (Eds.), Geologia, Tectônica e Recursos Minerais Do Brasil. CPRM, Brasília, pp. 5–54.

Schobbenhaus Filho, C., Campos, D.A., Derze, G.R., Asmus, H.E., 1984. Geologia do Brasil. Texto explicatico do mapa geológico e da área adjacente incluindo depósitos minerais. Brasília, DF.

Schobbenhaus Filho, C., Campos, D.A., Derze, G.R., Asmus, H.E., 1981. Mapa geológico do Brasil e da área oceânica adjacente incluindo depósitos minerais 1/2,500,000.

Schobbenhaus Filho, C., Oliva, L.A., 1979. Carta geológica do Brasil ao milionésimo: Folha SE2J Corumbá.

Schrank, C.E., Boutelier, D.A., Cruden, A.R., 2008. The analogue shear zone: From rheology to associated geometry. J. Struct. Geol. 30, 177–193. https://doi.org/10.1016/j.jsg.2007.11.002

Schreurs, G., Buiter, S.J.H., Boutelier, D., Corti, G., Costa, E., Cruden, A.R., Daniel, J.M., Hoth, S., Koyi, H.A., Kukowski, N., Lohrmann, J., Ravaglia, A., Schlische, R.W., Withjack, M.O., Yamada, Y., Cavozzi, C., Del Ventisette, C., Elder Brady, J.A., Hoffmann-Rothe, A., Mengus, J.M., Montanari, D., Nilforoushan, F., 2006. Analogue benchmarks of shortening and extension experiments. Geol. Soc. Spec. Publ. 253, 1–27. https://doi.org/10.1144/GSL.SP.2006.253.01.01

Sherlock, D.H., Evans, B.J., 2001. The development of seismic reflection sandbox modeling. Am. Assoc. Pet. Geol. Bull. 85, 1645–1659.

Silva, A.J.P. da, Lopes, R. da C., Vasconcelos, A.M., Bahia, R.B.C., 2003. Bacias sedimentares Paleozóicas e Meso-Cenozóicas interiores, in: Bizzi, L.A., Schobbenahus, C., Vidotti, R.M., Gonçalves, J.H. (Eds.), Geologia, Tectônica e Recursos Minerais Do Brasil. CPRM - Seviço Geológico do Brasil, Brasília, pp. 55–85.

Silva, M.F. da, 2007. Aerogeofísica, litogeoquímica e geologia na caracterização do rifte intracontinental da Faixa Paraguai. Univ. Brasília. Universidade de Brasília.

Siqueira, L.P. de, 1989. Bacia dos Parecis. Bol. Geociências Petrobras 3, 3–16.

Soares, D.M., Alves, T.M., Terrinha, P., 2012. The breakup sequence and associated lithospheric breakup surface: Their significance in the context of rifted continental margins (West Iberia and Newfoundland margins, North Atlantic). Earth Planet. Sci. Lett. 355–356, 311–326. https://doi.org/10.1016/j.epsl.2012.08.036

Souza, S.C. dos R. de, 2015. Revisão estratigráfica das unidades superiores da Faixa Paraguai norte: litoestratigrafia, quimioestratigrafia (C e Sr) e geogronologia (U-Pb). Mato Grosso, Brasil. Universidade de Brasília.

Stegman, D.R., Freeman, J., Schellart, W.P., Moresi, L., May, D., 2006. Influence of trench width on subduction hinge retreat rates in 3-D models of slab rollback. Geochemistry, Geophys. Geosystems 7, n/a-n/a. https://doi.org/10.1029/2005GC001056

Suszczynski, E.F., 1970. La geologie et la tectonique de la Plataforme Amazonienne. Geol. Rundschau 59, 1232–1253.

Szatmari, P., Aires, J.R., 1987. Experimentos com modelagem ficica de processos tectônicos no centro de pesquisas da Petrobras. Bol. geociências da PETROBRAS 1, 13–24.

Tassinari, C.C.G., 1996. O mapa geocronológico do Cráton Amazônico no Brasil: Revisão dos dados isotópicos.

Tassinari, C.C.G., Bettencourt, J.S., Geraldes, M.C., Macambira, M.J.B., Lafon, J.M., 2000. The Amazonian Craton, in: Cordani, U.G., Milani, E.J., Thomaz Filho, A., Campos, D.A. (Eds.), Tectonic Evolution of South America. 31st International Geological Congress, Rio de Janeiro, pp. 41–95.

Tassinari, C.C.G., Cordani, U.G., Nutman, A.P., Van Schmus, W.R., Bettencourt, J.S., Taylor, P.N., 1996. Geochronological systematics on basement rocks from the Río Negro-Juruena Province (Amazonian Craton) and tectonic implications. Int. Geol. Rev. 38, 161–175. https://doi.org/10.1080/00206819709465329

Tassinari, C.C.G., Macambira, M.J.B., 2004. A evolução tectônica do Cráton Amazônico, in: Mantesso-Neto, V., Bartorelli, A., Carneiro, C.D.R., Brito-Neves, B.B. de (Eds.), Geologia Do Continente Sul-Americano: Evolução Da Obra de Fernando Flávio Marques de Almeida. Beca, São Paulo, pp. 471–486.

Tassinari, C.C.G., Macambira, M.J.B., 1999. Geochronological provinces of the Amazonian Craton. Episodes 22, 174–182. https://doi.org/10.1080/00206819709465329

Tavares, F.M., Trouw, R.A.J., da Silva, C.M.G., Justo, A.P., Oliveira, J.K.M., 2018. The multistage tectonic evolution of the northeastern Carajás Province, Amazonian Craton, Brazil: Revealing complex structural patterns. J. South Am. Earth Sci. 88, 238–252. https://doi.org/10.1016/j.jsames.2018.08.024

Teixeira, W., Tassinari, C.C.G., Cordani, U.G., Kawashita, K., 1989. A review of the geochronology of the Amazonian Craton: Tectonic implications. Precambrian Res. 42, 213–227. https://doi.org/10.1016/0301-9268(89)90012-0

Tirel, C., Brun, J.-P., Sokoutis, D., 2006. Extension of thickened and hot lithospheres: Inferences from laboratory modeling. J. Geophys. Res. 113, B04403. https://doi.org/10.1029/2005TC001804

Torrance, K.E., Turcotte, D.L., 1971. Thermal convection with large viscosity variations. J. Fluid Mech. 47, 113–125. https://doi.org/10.1017/S002211207100096X

Tron, V., Brun, J.P., 1991. Experiments on oblique rifting in brittle-ductile systems. Tectonophysics 188, 71–84. https://doi.org/10.1016/0040-1951(91)90315-J

van Gent, H.W., Holland, M., Urai, J.L., Loosveld, R., 2010. Evolution of fault zones in carbonates with mechanical stratigraphy - Insights from scale models using layered cohesive powder. J. Struct. Geol. 32, 1375–1391. https://doi.org/10.1016/j.jsg.2009.05.006

Vasconcelos, C.S., Morales, I.V.F., Figueiredo, M.F., 2014. Revisão da estratigrafia da Bacia dos Parecis-Alto Xingu, in: 47º Congresso Brasileiro de Geologia. Salvador, p. 1.

Vendeville, B., Cobbold, P.R., Davy, P., Brun, J.P., Choukroune, P., 1987. Physical models of extensional tectonics at various scales. Geol. Soc. Spec. Publ. 28, 95–107. https://doi.org/10.1144/GSL.SP.1987.028.01.08

Vidotti, R.M., Abreu, C.J., Alvarenga, C.J.S., Vasconcelos, C.S., 2016. Bacia dos Parecis e sua porção dobrada (Faixa Paraguai) registrada em seção magnetotelúrica. Rio Oil Gas Expo Conf. 1–6.

Vilela, P.C., Leggieri, R.F., Castro, N.O. de, Fernandes, R.F., Cardoso, R. de A., D'Almeida, K.S., Souza, M.F.F. de, 2020. Caracterização do limite Paleozoico-Neoproterizoico da Bacia dos Parecis, in: Rio Oil & Gas Expo and Conference. Rio de Janeiro, p. 9.

Warsitzka, M., Kley, J., Kukowski, N., 2013. Salt diapirism driven by differential loading - Some insights from analogue modelling. Tectonophysics 591, 83–97.

https://doi.org/10.1016/j.tecto.2011.11.018

Wernicke, B., 1985. Uniform-sense normal simple shear of the continental lithosphere. Can. J. Earth Sci. 22, 108–125. https://doi.org/10.1139/e85-009

Wijns, C., Weinberg, R., Gessner, K., Moresi, L., 2005. Mode of crustal extension determined by rheological layering. Earth Planet. Sci. Lett. 236, 120–134. https://doi.org/10.1016/j.epsl.2005.05.030

Willis, B., 1893. The mechanics of Appalachian structure. US Geol. Surv. 13th Annu. Rep. 211–282.

Wilson, J.T., 1966. Did the Atlantic close and then re-open? Nature 211, 676–681.

Withjack, M.O., Jamison, W.R., 1986. Deformation produced by oblique rifting. Tectonophysics 126, 99–124. https://doi.org/10.1016/0040-1951(86)90222-2

Yoshida, M., Saito, S., Yoshizawa, K., 2020. Dynamics of continental lithosphere extension and passive continental rifting from numerical experiments of visco-elasto-plastic thermo-chemical convection in 2-D Cartesian geometry. Tectonophysics 796, 1–10. https://doi.org/10.1016/j.tecto.2020.228659

Zwaan, F., Corti, G., Keir, D., Sani, F., 2020. A review of tectonic models for the rifted margin of Afar: Implications for continental break-up and passive margin formation. J. African Earth Sci. 164, 1–22. https://doi.org/10.1016/j.jafrearsci.2019.103649

Zwaan, F., Schreurs, G., 2017. How oblique extension and structural inheritance influence rift segment interaction: Insights from 4D analog models. Interpretation 5, SD119–SD138. https://doi.org/10.1190/INT-2016-0063.1

Zwaan, F., Schreurs, G., Buiter, S.H., 2019. A systematic comparison of experimental set-ups for modelling extensional tectonics. Solid Earth 10, 1063–1097. https://doi.org/10.5194/se-2018-96

Zwaan, F., Schreurs, G., Naliboff, J., Buiter, S.J.H., 2016. Insights into the effects of oblique extension on continental rift interaction from 3D analogue and numerical models. Tectonophysics 693, 239–260. https://doi.org/10.1016/j.tecto.2016.02.036

# ATTACHEMENTS

## A.1. Conference proceedings

1. “Evolution of sub-parallel grabens: insights from analogue modelling” – Oliveira et al., 2019 – Presented at EGU General Assembly, Vienna, Austria.

2. “Interfering sub-parallel rift grabens: insights from combined analogue and numerical models” – Oliveira et al., 2019 – Presented at AGU Fall Meeting, San Francisco, CA, United States of America.

## A.2. Participation in other research projects

1. “Results from interpolation of Vp/Vs data for the brazilian territory” – França et al., 2016 – Presented at 2nd TIDES Training School, Sesimbra, Portugal.

2. “Crustal structure of the Amazonian Craton and adjacent provinces in Brazil” – Albuquerque et al., 2017 – in Journal of South American Earth Sciences, Elsevier.

3. “Sismicidade Induzida por Reservatório no Brasil” – Sayão et al. 2017 – Presented in II Simpósio Brasileiro de Sismologia, João Pessoa, PB, Brazil.

4. “Banco de dados espaciais de sismicidade induzida por reservatório” – Sayão et al. 2018 – Presented at 49º Congresso Brasileiro de Geologia, Rio de Janeiro, RJ, Brazil.

## A.3. Additional analogue experiments (developed in LME, UFRN)

### A.3.1. Test experiment PAR-I-01

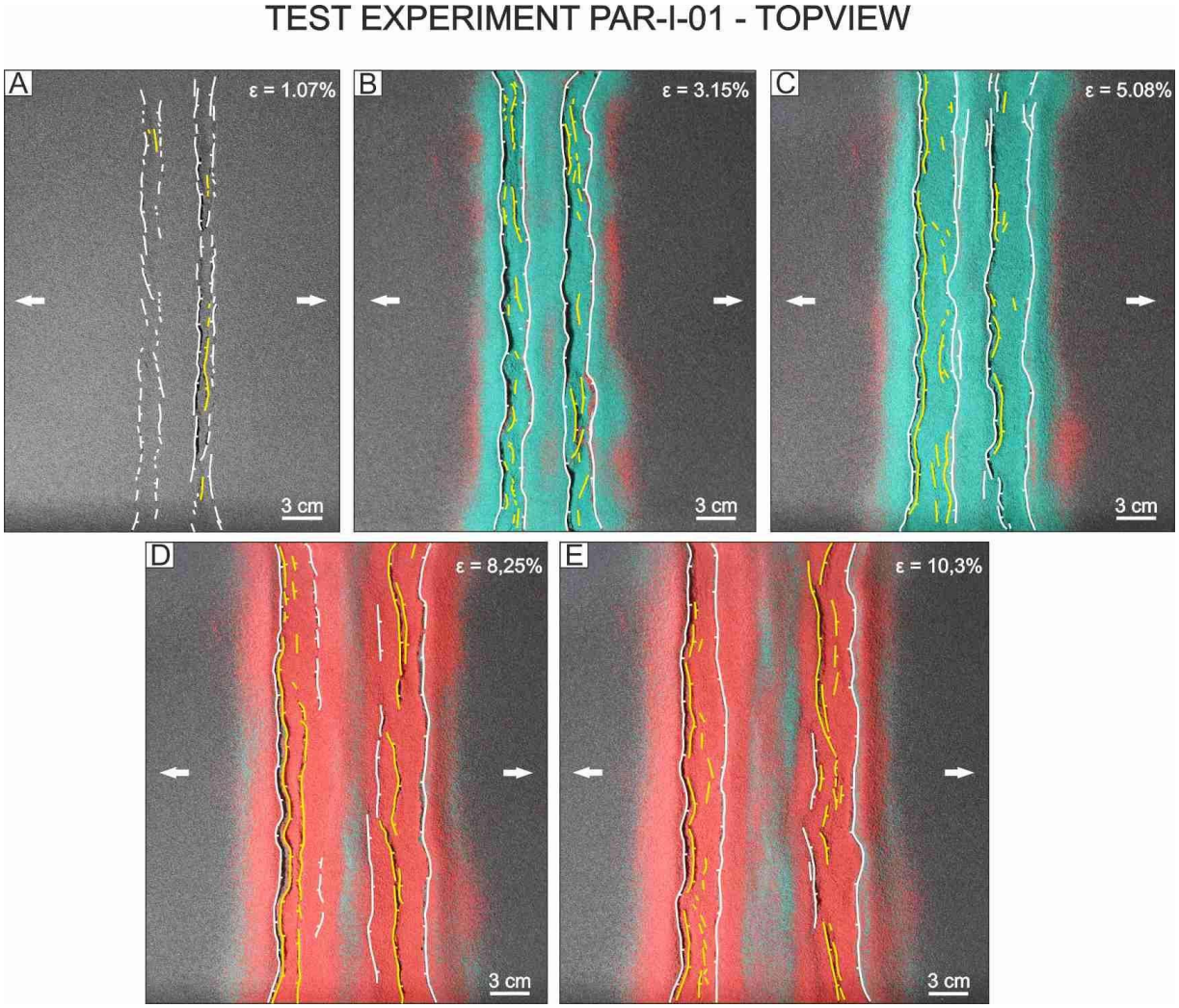


**A.3.1.1**. Topview evolution of the test experiment PAR-I-01. In this test the initial distance between VDs was of 3.5 cm. The sand pack was 2.5 cm thick with a mixture of quartz sand (80%) and gypsum powder layers (20%) with colour sand layers. Syntectonic deposition was considered in this case. The main faults are interpreted in the figure (border faults in white). There is the formation of two grabens orthogonal to the extension direction with a middle horst, and the formation of new faults inside the grabens. The faults present segmented geometries mainly due to the rheological contrast between layers.

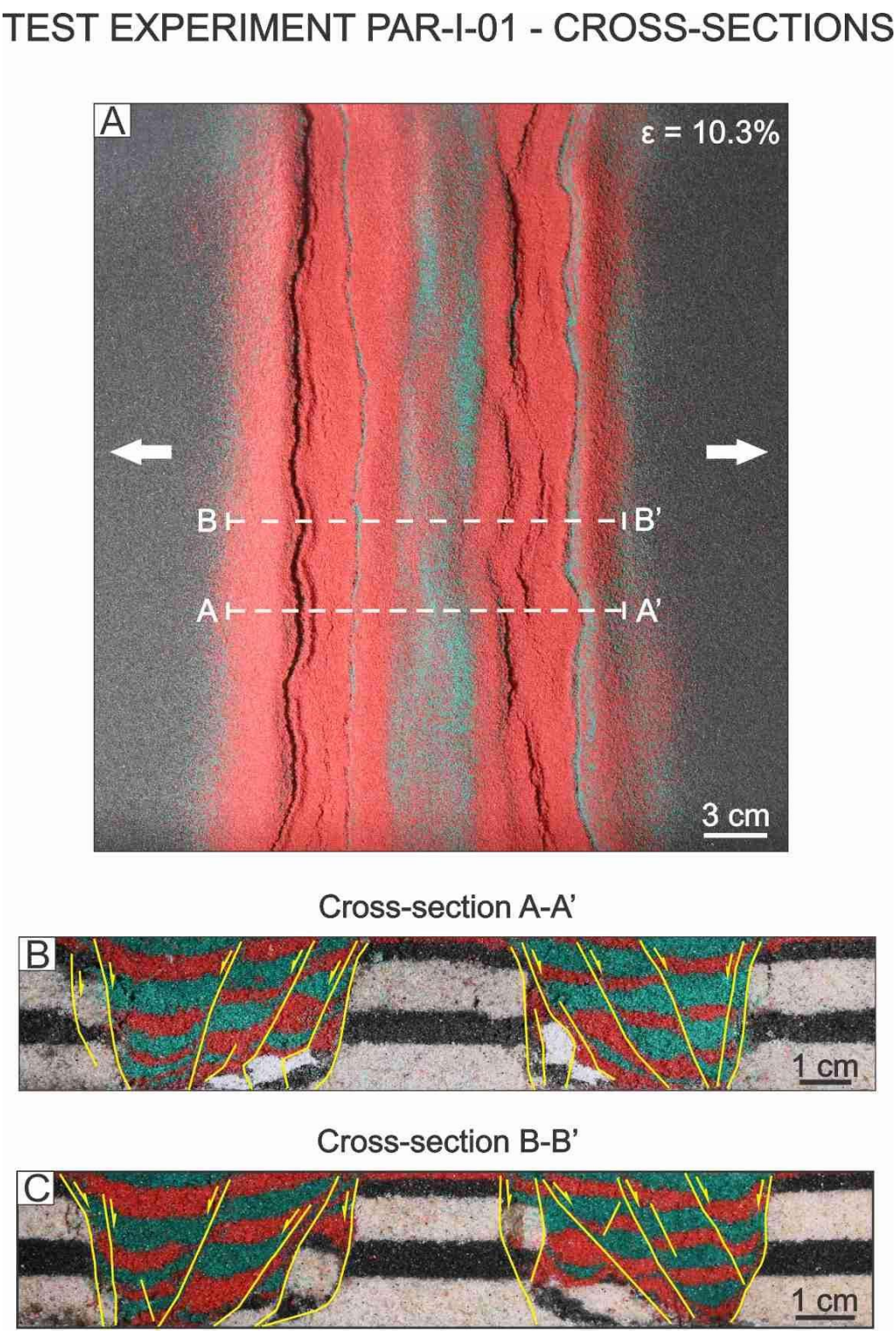


**A.3.1.2.** Final cross-sections of the test experiment PAR-I-01. This experiment was tested by using an initial distance between VDs of 3.5 cm. The sand pack was 2.5 cm thick with a mixture of quartz sand (80%) and powder plaster (20%) layers with colour sand layers. Syntectonic deposition was considered in this case (represented by the red and green layers inside the grabens). Two grabens with a middle horst are observed. The main faults are interpreted in the figure. The geometries of the faults vary depending on the rheological contrast between the different layers. The grabens are infilled with syntectonic deposition.

## A.3.2. Test experiment PAR-I-02

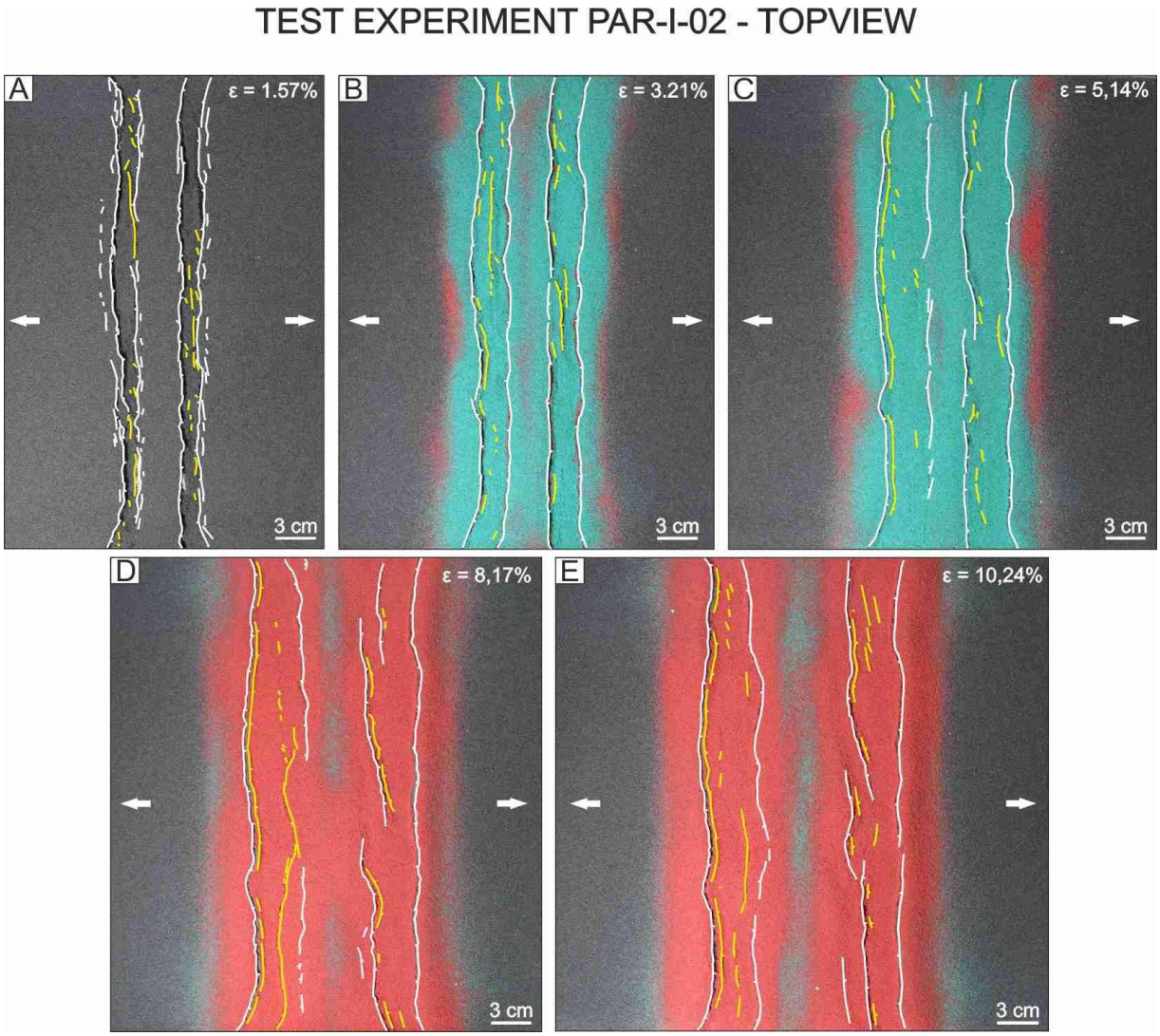


**A.3.2.1.** Topview evolution of the test experiment PAR-I-02. In this test the initial distance between VDs was of 3.5 cm. A styrofoam block ~0.5 cm was placed in the base of the box to induce the formation of a middle horst. The sand pack was 2.5 cm thick with a mixture of quartz sand (80%) and gypsum powder layers (20%) with colour sand layers. Syntectonic deposition was considered in this case. The main faults are interpreted in the figure (border faults in white). There is the formation of two grabens orthogonal to the extension direction with a middle horst, and the formation of new faults inside the grabens. The faults present segmented geometries mainly due to the rheological contrast between layers.

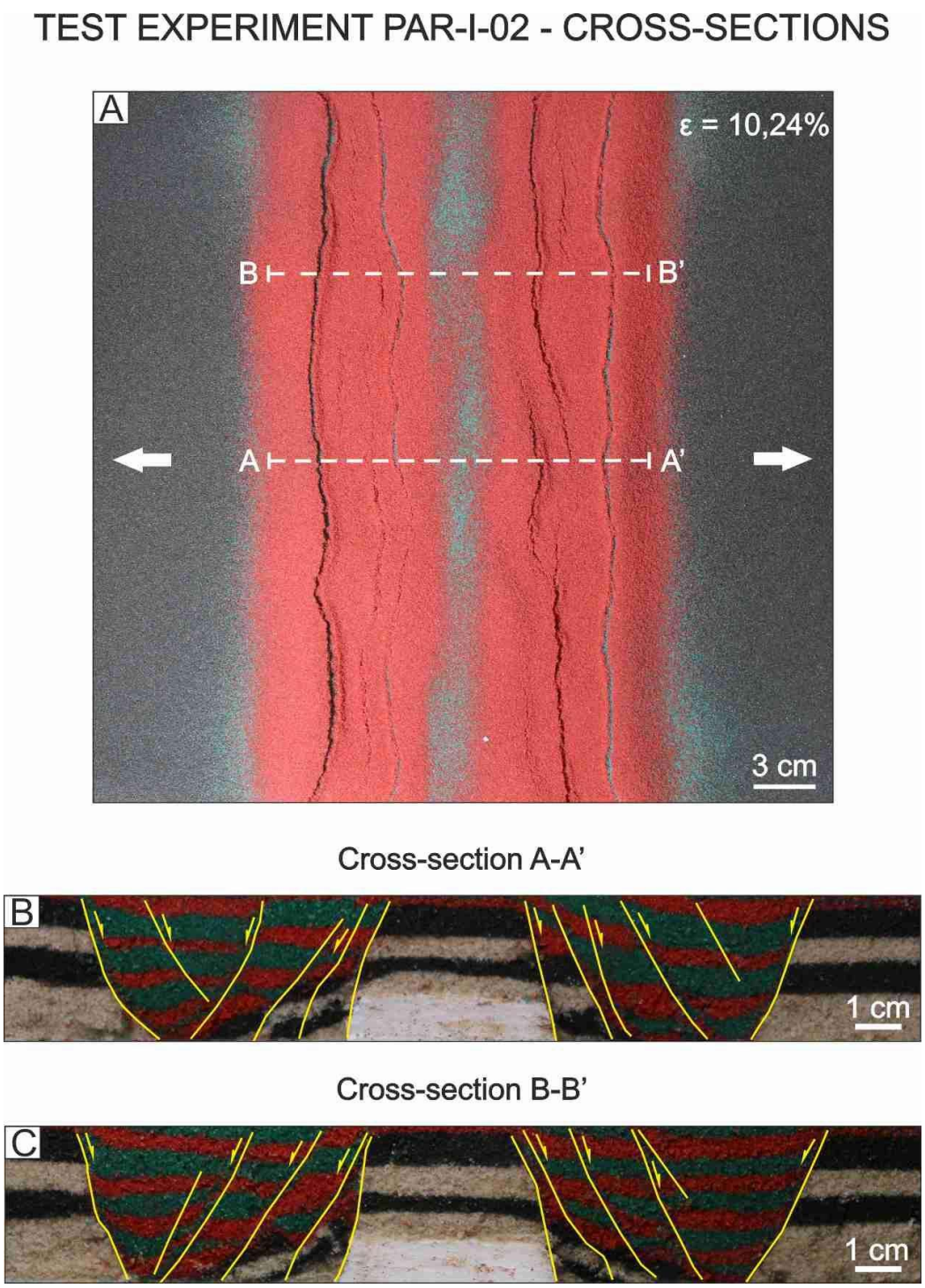


**A.3.2.2.** Final cross-sections of the test experiment PAR-I-02. This experiment was tested by using an initial distance between VDs of 3.5 cm. The sand pack was 2.5 cm thick with a mixture of quartz sand (80%) and powder plaster (20%) layers with colour sand layers. A styrofoam block was placed at the base of the sandbox to induce the formation of the middle horst. Syntectonic deposition was considered in this case (represented by the red and green layers inside the grabens). Two grabens with a middle horst are observed. The main faults are interpreted in the figure. The geometries of the faults vary depending on the rheological contrast between the different layers. The grabens are infilled with syntectonic deposition.

## A.3.3. Test experiment PAR-II-01

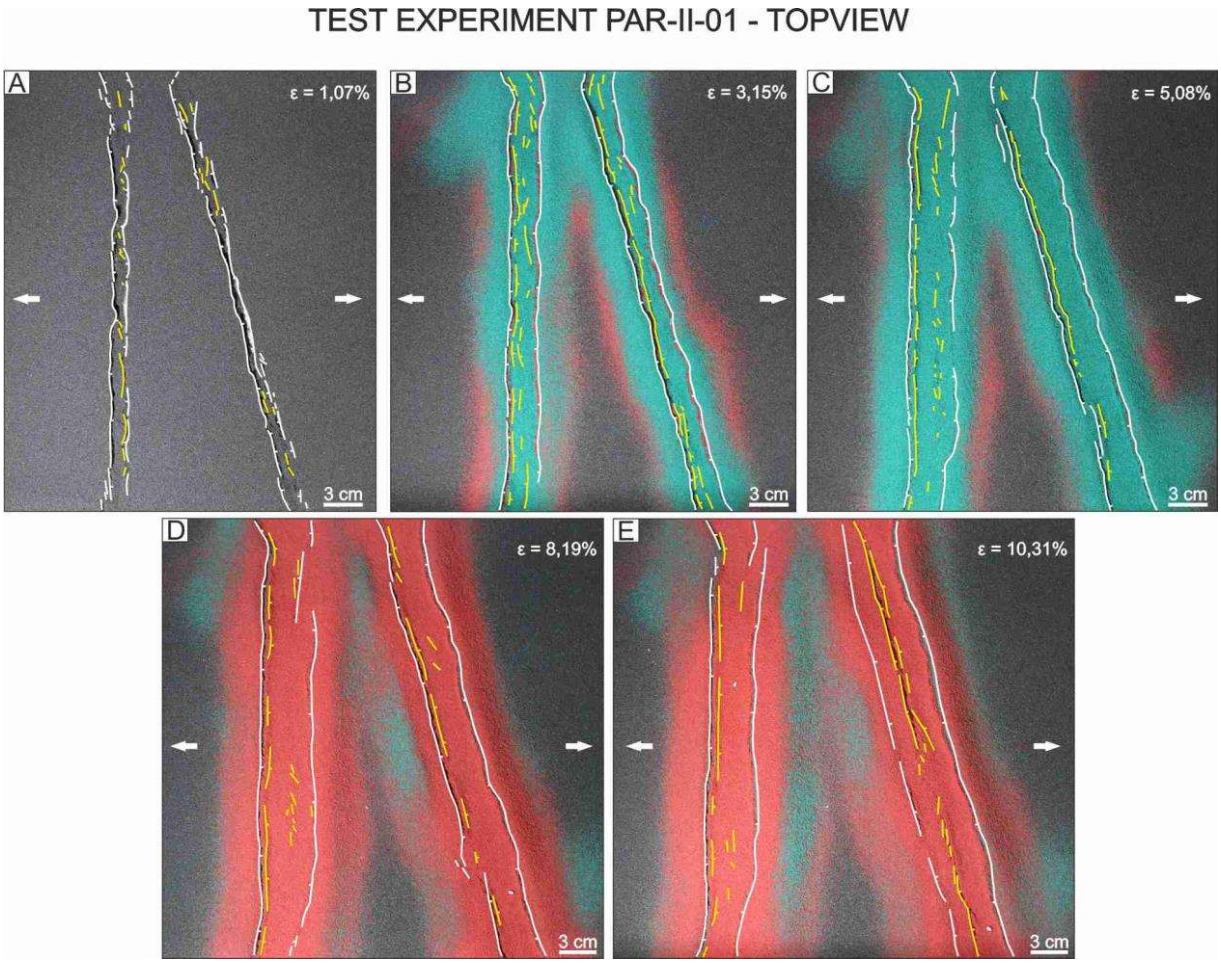


**A.3.3.1.** Topview evolution of the test experiment PAR-II-01. In this test the VDs were placed one orthogonal to the extension direction and the other oblique to the extension direction with an angle of 15º. The sand pack was 2.5 cm thick with a mixture of quartz sand (80%) and gypsum powder layers (20%) with colour sand layers. Syntectonic deposition was considered in this case. The main faults are interpreted in the figure (border faults in white). There is the formation of two grabens one orthogonal and one oblique to the extension direction and one middle horst. The faults present segmented geometries mainly due to the rheological contrast between layers.

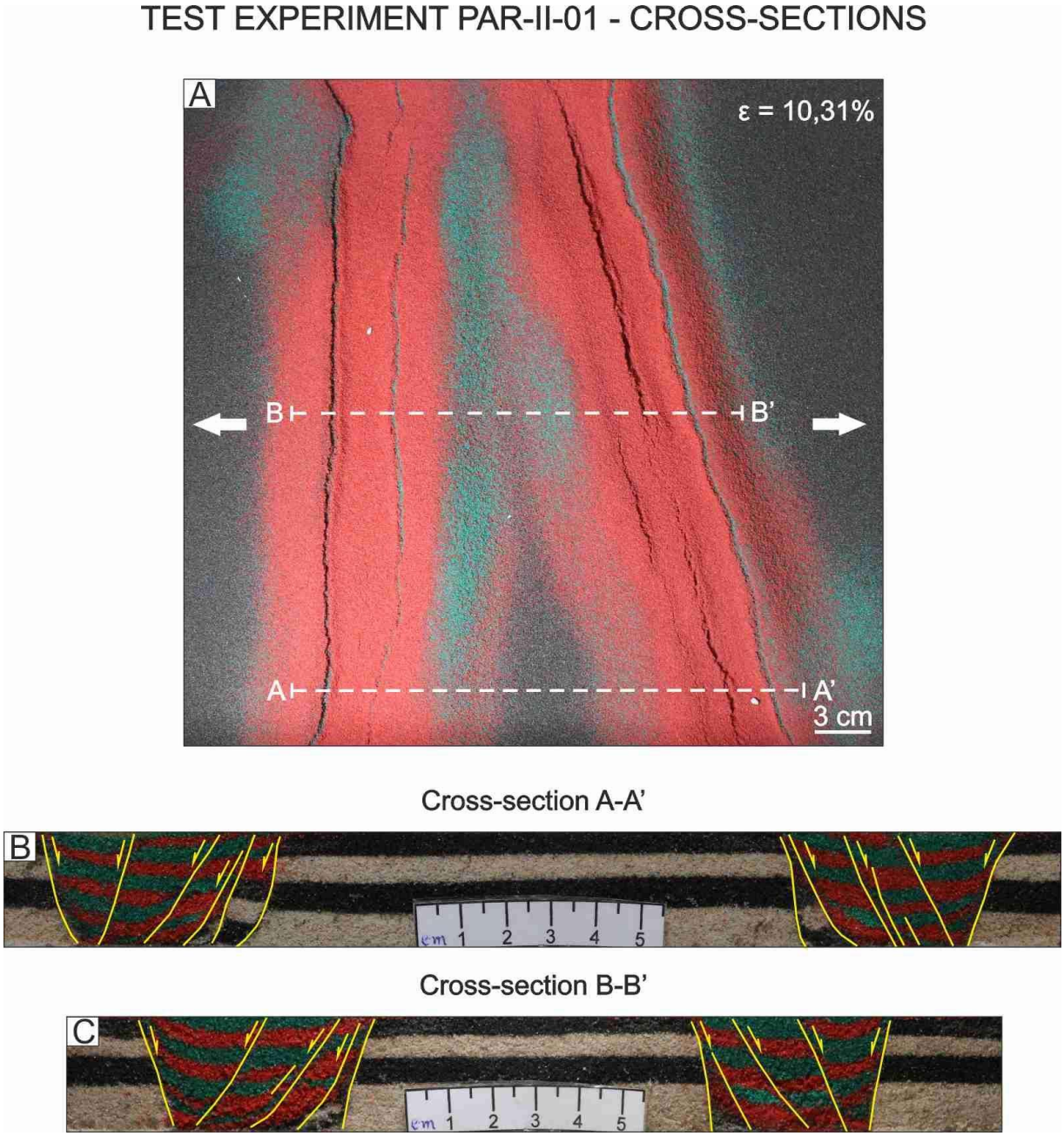


**A.3.3.2.** Final cross-sections of the test experiment PAR-II-01. In this experiment an orthogonal and one oblique (15º) VD were placed at the base of sandbox. A 2.5 cm sand pack with a mixture of quartz sand (80%) and powder plaster (20%) layers and colour sand layers. Syntectonic deposition was considered in this case (represented by the red and green layers inside the grabens). Two grabens with a middle horst are observed. The main faults are interpreted in the figure. The geometries of the faults vary depending on the rheological contrast between the different layers. The grabens are infilled with syntectonic deposition.

## A.3.4. Test Experiment PAR-II-02

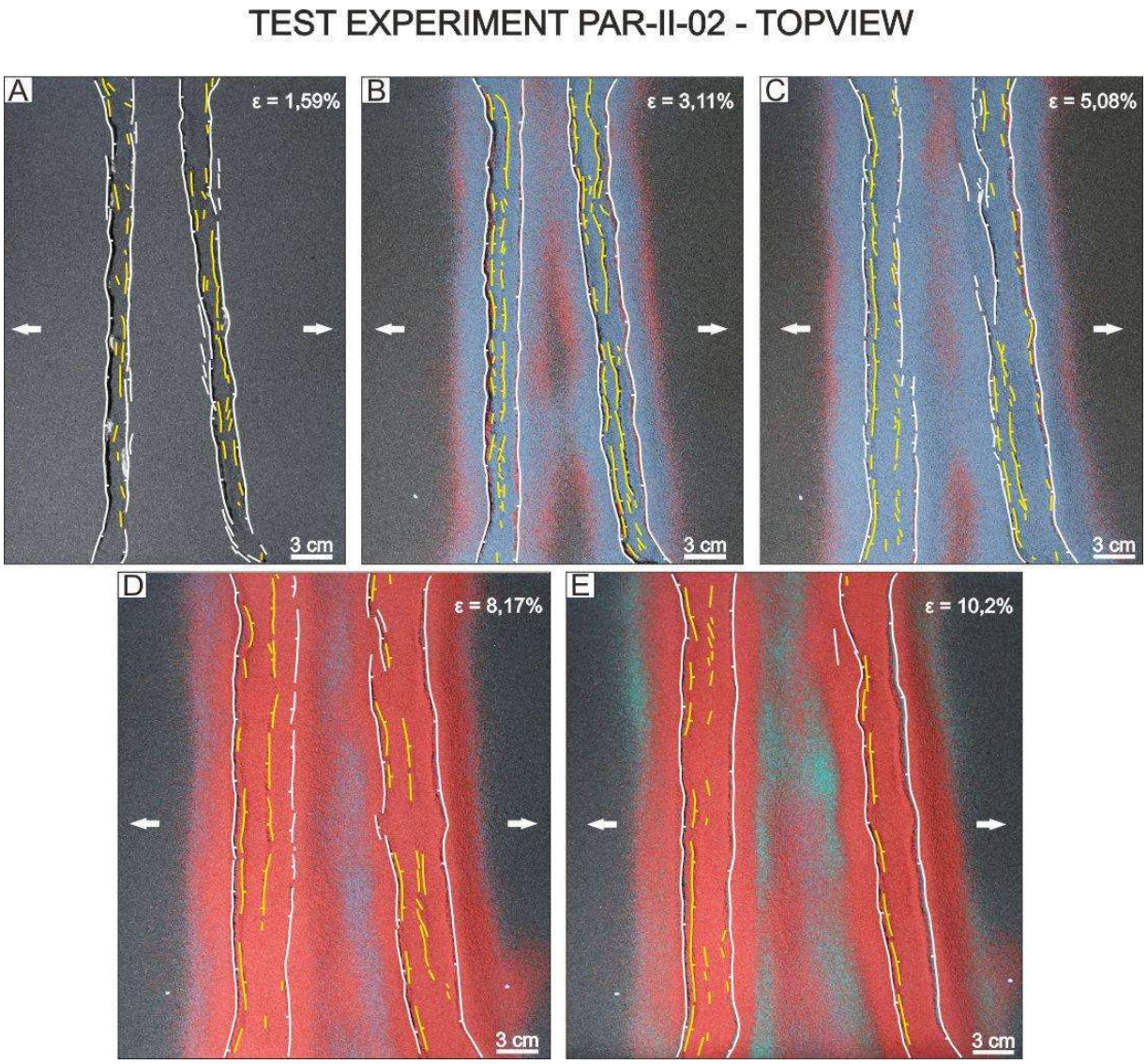


**A.3.4.1.** Topview evolution of the test experiment PAR-II-02. In this test the VDs were placed one orthogonal to the extension direction and the other oblique to the extension direction with an angle of 5º and with a styrofoam block at the base of the sandbox to induce the formation of a middle horst. The sand pack was 2.5 cm thick with a mixture of quartz sand (80%) and gypsum powder layers (20%) with colour sand layers. Syntectonic deposition was considered in this case. The main faults are interpreted in the figure (border faults in white). There is the formation of two grabens one orthogonal and one oblique to the extension direction and one middle horst. The faults present segmented geometries mainly due to the rheological contrast between layers.

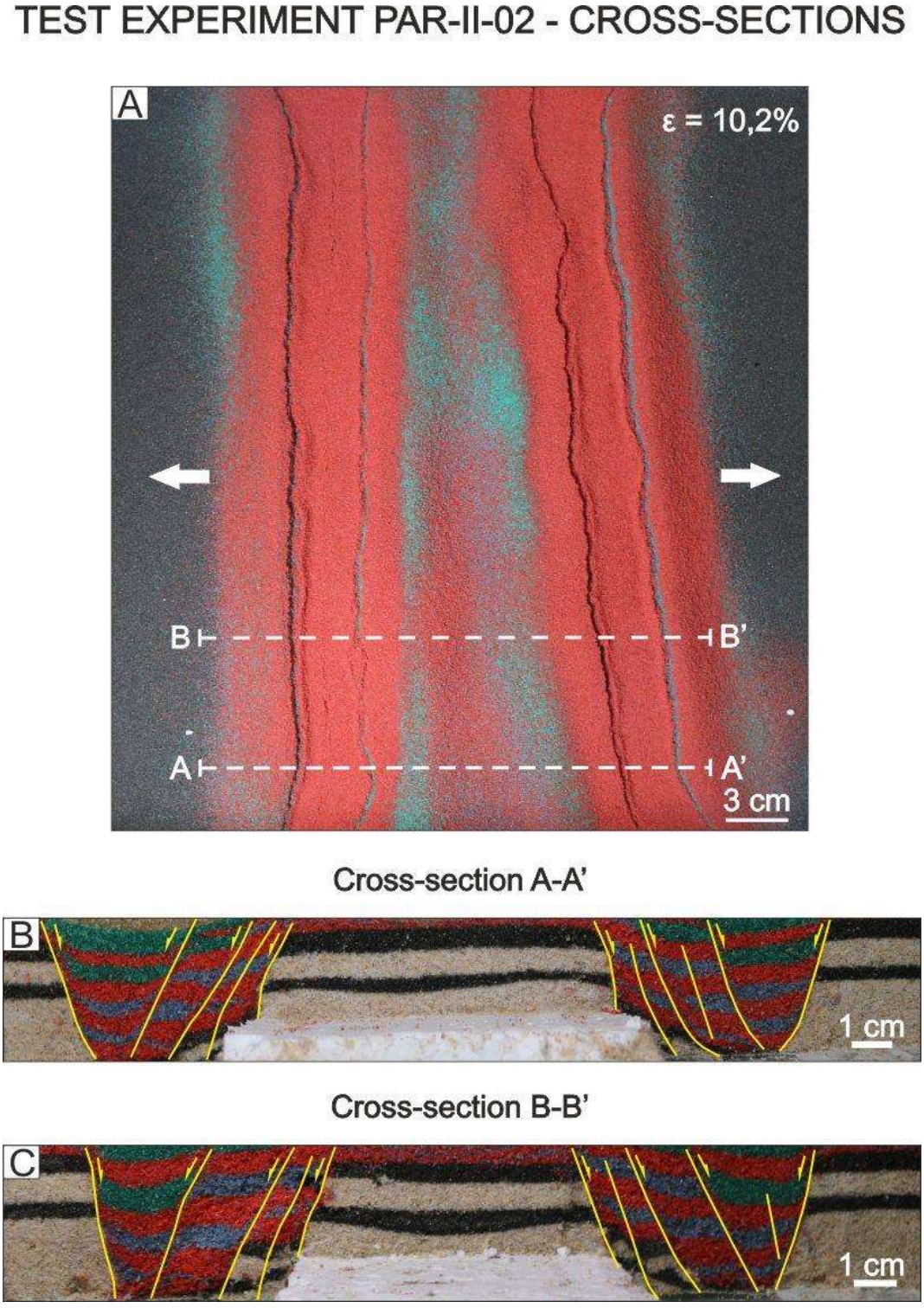


**A.3.4.2.** Final cross-sections of the test experiment PAR-II-02. In this experiment an orthogonal and one oblique (5º) VD were placed at the base of sandbox. A 2.5 cm sand pack with a mixture of quartz sand (80%) and powder plaster (20%) layers and colour sand layers. A styrofoam block was placed at the base of the sandbox to induce the formation of the middle horst. Syntectonic deposition was considered in this case (represented by the red and green layers inside the grabens). Two grabens with a middle horst are observed. The main faults are interpreted in the figure. The geometries of the faults vary depending on the rheological contrast between the different layers. The grabens are infilled with syntectonic deposition.